2020-06

TRADE STUDY OF COMMERCIAL SOFTWARE-DEFINED RADIO TECHNOLOGIES FOR SMALL SATELLITE GROUND STATION NETWORK COMMAND AND CONTROL APPLICATIONS

Wood, Samuel H.

Monterey, CA; Naval Postgraduate School

NAVAL POSTGRADUATE SCHOOL

MONTEREY, CALIFORNIA

THESIS

TRADE STUDY OF COMMERCIAL SOFTWARE-DEFINED RADIO TECHNOLOGIES FOR SMALL SATELLITE GROUND STATION NETWORK COMMAND AND CONTROL APPLICATIONS

by

Samuel H. Wood

June 2020

Thesis Advisor:	Giovanni Minelli
Co-Advisor:	Anthony Canan
Second Reader:	Michael Matthews, Northrop Grumman Innovation Systems

THIS PAGE INTENTIONALLY LEFT BLANK

REPORT DOCUMENTATION PAGE	*Form Approved OMB No. 0704-0188*

1. AGENCY USE ONLY *(Leave blank)*	**2. REPORT DATE** June 2020	**3. REPORT TYPE AND DATES COVERED** Master's thesis

4. TITLE AND SUBTITLE
TRADE STUDY OF COMMERCIAL SOFTWARE-DEFINED RADIO TECHNOLOGIES FOR SMALL SATELLITE GROUND STATION NETWORK COMMAND AND CONTROL APPLICATIONS

5. FUNDING NUMBERS

6. AUTHOR(S) Samuel H. Wood

7. PERFORMING ORGANIZATION NAME(S) AND ADDRESS(ES)
Naval Postgraduate School
Monterey, CA 93943-5000

8. PERFORMING ORGANIZATION REPORT NUMBER

9. SPONSORING / MONITORING AGENCY NAME(S) AND ADDRESS(ES)
N/A

10. SPONSORING / MONITORING AGENCY REPORT NUMBER

11. SUPPLEMENTARY NOTES The views expressed in this thesis are those of the author and do not reflect the official policy or position of the Department of Defense or the U.S. Government.

12a. DISTRIBUTION / AVAILABILITY STATEMENT
Approved for public release. Distribution is unlimited.

12b. DISTRIBUTION CODE
A

13. ABSTRACT (maximum 200 words)

The Mobile CubeSat Command and Control (MC3) ground station network headquartered at the Naval Postgraduate School monitors and controls small satellites in support of various U.S. government, Department of Defense, public university, and commercial partner missions. In order to conduct the necessary Command and Control functions with the on-orbit satellites, MC3-networked ground stations utilize the baseline NI USRP-2292 software-defined radio (SDR) to transmit and receive command messages through ultra-high frequency and S-band RF signals. Two alternative high-end commercial systems have been advertised to provide superior performance and functionality to that of the baseline USRP devices. This thesis documents the trade study performed between the baseline NI USRP-2922, the Ettus Research USRP B205mini-i, the Kratos RT Logic quantumRadio, and the AMERGINT satTRAC system. The study investigated and evaluated the performance, functionality, and suitability of these SDR technologies for implementation in the MC3 ground station network. The results were analyzed and compared for applicability to other comparable university stations, commercial networks, and government applications. The research culminated in a characterization of these four SDR devices, a description of their suitability in the MC3 network, and a comparative analysis of their operational functionality and any limitations.

14. SUBJECT TERMS	**15. NUMBER OF PAGES**
software-defined radio, SDR, Mobile CubeSat Command and Control, MC3, CubeSat, ground station, radio study, small-satellite, space, ultra high frequency, S-band, digital-IF, transceiver	149
	16. PRICE CODE

17. SECURITY CLASSIFICATION OF REPORT	**18. SECURITY CLASSIFICATION OF THIS PAGE**	**19. SECURITY CLASSIFICATION OF ABSTRACT**	**20. LIMITATION OF ABSTRACT**
Unclassified	Unclassified	Unclassified	UU

NSN 7540-01-280-5500 Standard Form 298 (Rev. 2-89)
Prescribed by ANSI Std. 239-18

THIS PAGE INTENTIONALLY LEFT BLANK

Approved for public release. Distribution is unlimited.

TRADE STUDY OF COMMERCIAL SOFTWARE-DEFINED RADIO TECHNOLOGIES FOR SMALL SATELLITE GROUND STATION NETWORK COMMAND AND CONTROL APPLICATIONS

Samuel H. Wood
Captain, United States Air Force
BS, Rutgers University, 2012

Submitted in partial fulfillment of the
requirements for the degrees of

**MASTER OF SCIENCE IN SYSTEMS TECHNOLOGY
(COMMAND, CONTROL, AND COMMUNICATIONS)**

and

MASTER OF SCIENCE IN SPACE SYSTEMS OPERATIONS

from the

**NAVAL POSTGRADUATE SCHOOL
June 2020**

Approved by: Giovanni Minelli
Advisor

Anthony Canan
Co-Advisor

Michael Matthews
Second Reader

Thomas J. Housel
Chair, Department of Information Sciences

James H. Newman
Chair, Space Systems Academic Group

THIS PAGE INTENTIONALLY LEFT BLANK

ABSTRACT

The Mobile CubeSat Command and Control (MC3) ground station network headquartered at the Naval Postgraduate School monitors and controls small satellites in support of various U.S. government, Department of Defense (DoD), public university, and commercial partner missions. In order to conduct the necessary Command and Control functions with the on-orbit satellites, MC3-networked ground stations utilize the baseline NI USRP-2292 software-defined radio (SDR) to transmit and receive command messages through ultra-high frequency and S-band RF signals. Two alternative high-end commercial systems have been advertised to provide superior performance and functionality to that of the baseline USRP devices. This thesis documents the trade study performed between the baseline NI USRP-2922, the Ettus Research USRP B205mini-i, the Kratos RT Logic quantumRadio, and the AMERGINT satTRAC system. The study investigated and evaluated the performance, functionality, and suitability of these SDR technologies for implementation in the MC3 ground station network. The results were analyzed and compared for applicability to other comparable university stations, commercial networks, and government applications. The research culminated in a characterization of these four SDR devices, a description of their suitability in the MC3 network, and a comparative analysis of their operational functionality and any limitations.

THIS PAGE INTENTIONALLY LEFT BLANK

TABLE OF CONTENTS

THIS PAGE INTENTIONALLY LEFT BLANK

LIST OF FIGURES

LIST OF TABLES

THIS PAGE INTENTIONALLY LEFT BLANK

LIST OF ACRONYMS AND ABBREVIATIONS

1GbE	One Gigabit Ethernet
1U	One unit
A/D	Analog-to-digital
ADC	Analog-to-digital converter
AGC	Automatic gain control
BER	Bit error rate
bps	bits per second
C2	Command and control
CCSDS	Consultative Committee for Space Data Systems
COTS	Commercial off-the-shelf
CRC	Cyclical redundancy codes
DAC	Digital-to-analog converter
dB	Decibel
dBc	Decibel below carrier
DoD	Department of Defense
DSP	Digital signal processor
DUT	Device under test
EMS	Electromagnetic Spectrum
FEC	Forward error correction
GUI	Graphical user interface
Hz	Hertz
ICD	Interface Control Document
IF	Intermediate Frequency
ITU	International Telecommunication Union
LEO	Low-earth orbit
LNA	Low-noise amplifier
MC3	Mobile CubeSat Command and Control
MHz	Megahertz
NI	National Instruments
NPS	Naval Postgraduate School

PN	Pseudorandom Noise
PSK	Phase-shift keying
QPSK	Quadrature Phase Shift Keying
RF	Radio frequency
RFBE	RF back end
RFFE	RF front end
RFSoC	RF System-on-chip
RUS	Radio(s) under study
Rx	Receive
SATRN	Satellite Agile Transmit and Receive Network
SDR	Software-defined radio
SFDR	Spurious free dynamic range
SNR	Signal-to-noise ratio
SOC	Satellite Operations Center
SSAG	Space Systems Academic Group
SWaP	Size, weight, and power
SwD	Software Devices
TT&C	Telemetry, tracking, and command
Tx	Transmit
UHF	Ultra-High Frequency
USG	United States Government
USRP	Universal Software Radio Peripheral
VRT	VITA 49 Radio Transport

ACKNOWLEDGMENTS

I would thank to thank my thesis advisors, Dr. Giovanni Minelli and Dr. Mustafa Canan, for their support and guidance during my education and research. I would also like to thank my second reader and mentor, Dr. Michael Matthews, for the countless hours of instruction and patience he provided to a mechanical engineer trying to learn about digital communication systems. A special thanks also to Mr. David Rigmaiden for his unwavering support and assistance with all of the laboratory equipment he so expertly manages. Also, I am grateful to Mr. Noah Weitz, who helped me work through various networking issues well above my understanding. I would also like to thank all my professors and military colleagues for their encouragement and friendship throughout this process. I have learned a tremendous amount while pursuing my degree at NPS about space, command and control, C4I technologies, and the joint-services as a whole.

My time at NPS has been a blessing, and I am so lucky that the USAF gave me the opportunity to learn alongside many impressive servicemen and servicewomen, and government civilians. I will always cherish this experience and know that I am a better engineer and military officer because of the many lessons I have learned during my time here.

Above all, I would be remiss not to acknowledge the unending support and assistance provided by my wife, my two sons, and the rest of my family who encouraged me along the way. I could not have possibly completed my degree and research without their love and understanding during this process.

THIS PAGE INTENTIONALLY LEFT BLANK

I. INTRODUCTION

The purpose of this thesis was to investigate, characterize, and comparatively analyze two commercial off-the-shelf (COTS) software-defined radio (SDR) systems against two baseline devices for implementation in the Mobile CubeSat Command and Control (MC3) ground station network, comparable small satellite ground stations, and other potential command and control (C2) applications. The results of this research will provide MC3 and other stakeholders with a comparative characterization of the four SDR systems which will inform future acquisitions and implementation of these technologies.

The software-defined radios under study (RUS) were the USRP-2922, USRP B205mini-i, Kratos RT Logic quantumRadio, and the AMERGINT satTRAC system. Experimentation and analysis evaluated the receiver performance of each RUS and characterized the functionality, interoperability, suitability, and supportability of each SDR system. The costs of these systems also factored in the analysis for comparison. These results were documented, analyzed, and compared to evaluate their applicability for the uses described above.

Before this study was conducted, there was a lack of detailed information available to effectively compare the functional characteristics of these four SDR systems in order to select the optimal solution for a consumer's given application. Product specifications provided by the contractor to consumers are often inconsistent, incomplete, and may not characterize the functional performance of the system. The results and analysis contained in this study will better inform stakeholders about the benefits, shortfalls, and associated costs of these RUS, providing the ability to leverage this information to acquire and implement the specific hardware that best fits their given mission.

A. SMALL SATELLITE GROUND STATIONS

Satellite ground stations transmit radio frequency (RF) signals from antennas on Earth to conduct telemetry, tracking, and command (TT&C) communications with satellites orbiting in space. Most of these satellites can be categorized as small satellites, weighing less than 500 kg and residing in a low-earth orbit (LEO), which is defined as any

orbit measuring less than 3000 km from the Earth's surface [1]. Traditionally these RF communications have been transmitted using dedicated hardware systems that are designed to communicate with a single satellite and with a singular waveform and in a narrow, predefined frequency range. The advent of flexible SDR technologies has enabled ground stations to support communications with many diverse satellites at different frequencies and through different waveform parameters without necessitating additional, dedicated hardware. These technologies provide ground stations the ability to use the same SDR device to transmit and receive completely different waveforms over multiple frequency ranges. A single SDR device has the potential to communicate with many satellites and support multiple missions, thereby reducing the requisite logistical and hardware footprint associated with using separate and dedicated radio systems to conduct C2 communications. This is an especially important capability as the number of satellites in orbit continues to grow rapidly and each new satellite will need ground segments to support them. Satellite ground station engineers will need to find creative solutions to support the growing number of customers operating within different areas of the RF spectrum, utilizing unique, dissimilar waveforms, and with differing data rate requirements. The solution of building separate, dedicated hardware stations for each satellite system may be impractical, especially given the often-limited budgets and modest workspaces that are typically available to operators of small-satellite missions. Future small satellite ground stations will need to incorporate flexible hardware like SDR technologies that are able to accommodate numerous satellites at a reduced logistical footprint, minimize potential points of failure by supporting multiple missions with fewer devices, and above all assure reliable and effective C2 operations.

B. CUBESATS

CubeSats are a specific class of small satellite, weighing between 10 and 100 kg, with a standard size and form factor [2]. The CubeSat standard was originally jointly developed in 1999 by the California Polytechnic State University at San Luis Obispo and Stanford University to promote collaboration for education and space exploration [2]. The standard designates a "one unit" or "1U" volume of 10×10×10 cm definition, scalable to

2, 3, 6, or even 12U, that was adopted to provide a common design platform for educational institutions, government organizations, other scientific platforms, and the commercial industry [2]. The CubeSat class of satellite is particularly popular due to the reduced manufacturing time required compared to other larger and more sophisticated satellites and their relatively low production costs on the order of approximately $50K as opposed to the hundreds of millions of dollars spent on large satellite acquisition programs [3]. These advantages empower CubeSat designers to accept more design risk with reduced financial consequences to deploy less mature, but more innovative technologies in a limited capability or as a proof of concept.

Because of their size, sophistication, and intended missions, CubeSats have a shorter life expectancy than larger classes of satellites, on the order of one year as opposed to five to ten years or more. Because these satellites are much smaller and cheaper than large government satellites, the designers must make design trade-offs including reduced on-board fuel for station-keeping and less sophisticated and redundant electronics. This condensed mission time reduces the associated service life and reliability requirements of flight components and allows CubeSat designers to iterate their designs more frequently to incorporate current and emerging technologies. The cycle time for major Department of Defense (DoD) acquisition programs averages approximately seven years, and the resulting systems can be constrained by component selections that may have been determined during the early stages of design and many years before a launch and operations [4]. The abbreviated mission durations of CubeSats also allows designers to select cheaper, COTS components as opposed to expensive, high-reliability parts, resulting in a more cost-effective product.

An advantage of the industry-accepted standard CubeSat framework is that many small-satellite designers and engineers are working to solve similar problems within these common design parameters, which invites collaboration and cooperation within the CubeSat community. The common standard has enabled previously stove-piped projects to share their work and combine efforts to advance technologies in the field. Since the standard's development in 1999, the CubeSat market has developed into its own flourishing industry, full of stakeholders from the government, private industry, and academia, who

collaborate through scientific experiments, technology demonstrations, and potential mission concepts [2]. The potential applications for the quick reaction capability of CubeSat development and deployment are also particularly attractive to some DoD organizations that are searching for solutions to augment and supplement their current space systems with more dispersed and resilient architectures.

C. MOBILE CUBESAT COMMAND AND CONTROL (MC3) GROUND STATION NETWORK

The MC3 ground station network is a DoD-directed endeavor headquartered at the Naval Postgraduate School (NPS) in Monterey, California. Initially fielded in 2012, the network was established as an attempt to build on common-use infrastructure supporting a wide range of experimental and operational missions for its stakeholders, including numerous U.S. government (USG) organizations, other universities, foreign partners, and commercial-industry partner missions [5]. The MC3 architecture leverages predominantly low-cost, flexible, COTS hardware when feasible to provide a reliable but cost-effective ground segment solution that can be proliferated reasonably at other locations [5]. This networked ground station architecture currently utilizes the USRP-2922 SDR to transmit and receive RF messages with small satellites and, along with the USRP B205mini-i, for many laboratory applications to conduct testing and integration activities in support of its missions and other related academic research.

In addition to the main Satellite Operations Center (SOC) operated by the Space Systems Academic Group (SSAG) at NPS, there are nine additional active ground stations that are part of the MC3 network. These nine geographically-separated stations along with three international collaborators form an integrated ground station network in support of a diverse small-satellite operations community [5]. Each participating ground station consists of a low-cost SDR terminal that provides bent-pipe access to satellite operators from any networked location with an internet connection [5]. Transmissions to on-orbit satellites are managed by the Satellite Agile Transmit and Receive Network (SATRN), which is a USG-owned software product that has been tailored for MC3 to provide secure bent-pipe communications between operators and their satellites [5].

Traditionally, whenever a small satellite was launched into orbit, a dedicated ground station was constructed to conduct TT&C communications with the satellite bus and payload. These C2 communications were constrained by the limited amounts of time the satellite was accessible due to orbital parameters, usually only a few times a day when the satellite would be orbiting overhead the footprint of that one ground station. The duration and frequency of these accesses were also dependent on the inclination of the satellite's orbit and the geographic location of the ground station. The MC3 network has been working to connect these geographically separated, and often cost-constrained, ground stations together into an integrated control network that shares its resources and provides more operational availability to the satellite operators [5]. The cooperating ground stations of the MC3 network can collaboratively support numerous small-satellite users and provide more opportunities for access to its stakeholders due to their numbers and their dispersed geographic locations. The satellite communications on this network are enabled by common, commercially available SDR technologies and controlled through the integrated networked architecture.

The participation of these ground stations is mutually beneficial to all relevant parties because the integrated network offers more access to any participating satellite while also expanding the overall resources and capability of the MC3 network. These benefits are provided to the participating satellite operator without the requirement to acquire ground stations or additional hardware and the requisite technical support to ensure reliable operations. In turn, the partner ground stations represent additional nodes that contribute resources to the network, which provides redundancy and increases the amount of opportunities for access to its users. Future goals of MC3 include the continued expansion of the network through additional ground station partners, thereby bolstering the capability of the network and providing additional reliable C2 capacity to more small-satellite operators. This effort will continue to promote scientific cooperation and will advance the capabilities of the small-satellite industry and community, spurring further innovation, research, and technological development.

D. SOFTWARE-DEFINED RADIO (SDR)

An SDR can be described as a device used to exchange digital information between two points, also referred to as a radio, in which software defines or controls some or all the physical layer functions of the communication system [7]. An essential characteristic of SDR technology is the ability to be flexible and support different frequencies and waveforms, and this is accomplished through modifications made in the software or firmware of the device, without modifying or augmenting the associated hardware [7].

The growing implementation of flexible SDR technologies has revolutionized modern communication networks, especially small satellite ground stations, and how their hardware architectures are being designed and implemented [8]. Currently, SDR systems are employed for a variety of applications, including basic radio communications, radio frequency (RF) detection and identification, remote-sensing, and satellite TT&C and payload operations [8]. Basic forms of SDR have been operational in military and commercial platforms for decades, but greater acceptance and incremental technological improvements have resulted in increased adoption due to increased system performance, improved ease-of-use, and decreased costs [8]. This has made SDR systems an attractive hardware solution as part of many users' architectures [8]. Because many of the system parameters are manipulated through software, SDR systems provide hardware architectures a unique flexibility in how they can operate and for what functions or missions. This flexible capability can be employed to combine missions that previously required separate hardware systems into a single device capable of supporting multiple missions. Ideally, this could result in cost savings for ground station system operators, who would need fewer separate and dedicated hardware devices to support multiple satellite missions. This could also lead to improved operational reliability due to less disaggregated points of failure and fewer standalone systems to repair and maintain.

E. METHODOLOGY

The research, experimentation, and analysis of this thesis include the evaluation and verification of manufacturer-provided documentation, laboratory measurements of received RF signal waveforms, and the investigation of the digital baseband processing

performance of each SDR. The performance evaluation encompasses specified parameters by the manufacturers as well as unpublished parameters that may be critical to small-satellite operators. The comparative analysis also includes a description of each system's software interfaces and details the functionality and ease-of-use by the operator. The level of manufacturer support and cost were also considered in the conclusions of the analysis. Experimentation was designed for this thesis to consistently evaluate the four SDR systems and characterize their applicability for utilization in MC3 and other comparable small satellite ground station missions.

F. OVERVIEW

This thesis is organized into five chapters plus additional appendices. Chapter II covers background material relevant to this thesis including digital communication theory, radio receiver architectures, a description of SDR technologies, the MC3 mission and baseline architecture, and a description of the four RUS. Chapter III describes critical radio characteristics that were evaluated during this research and describes the experiments designed to investigate those characteristics. It also provides a compilation of available radio specifications gathered about the four RUS. Chapter IV discusses the results uncovered during experimentation as well as the analysis of the findings. Chapter V contains the conclusions of the trade study and identifies potential additional work to be completed in future research.

THIS PAGE INTENTIONALLY LEFT BLANK

II. BACKGROUND

The MC3 SOC currently utilizes SDR technologies in its small satellite ground station to conduct TT&C communications with multiple on-orbit satellites as well as for laboratory applications like testing and verification activities. The research, testing, and analyses performed for this thesis were conducted to characterize the capabilities of the baseline SDR systems currently in use, as well as two commercially available systems, to determine if the baseline systems provide the best value to the MC3 and the DoD. Comparison of the test results and the corresponding analyses will advise the SSAG, the MC3 network operators and other stakeholders about the capabilities and functionality of the four RUS. This research will enable future users to make informed hardware selection decisions regarding these SDR systems.

A. DIGITAL COMMUNICATIONS

Communication systems are designed to convey information with messages, either analog or digital, that facilitate the transfer of data between a source and destination [9]. The primary task of any communication system is to reproduce information at the destination that reasonably represents what was generated at the source after passing through its transmission channel [9]. The transmission channel is the physical medium between the source and destination and contains various sources of noise, interference, and distortion [9]. These effects need to be considered and compensated for in order to communicate effectively between the source and destination. Figure 1 illustrates the primary elements in any communication system, regardless if the messages are being transmitted as analog or digital messages between the information source and its destination.

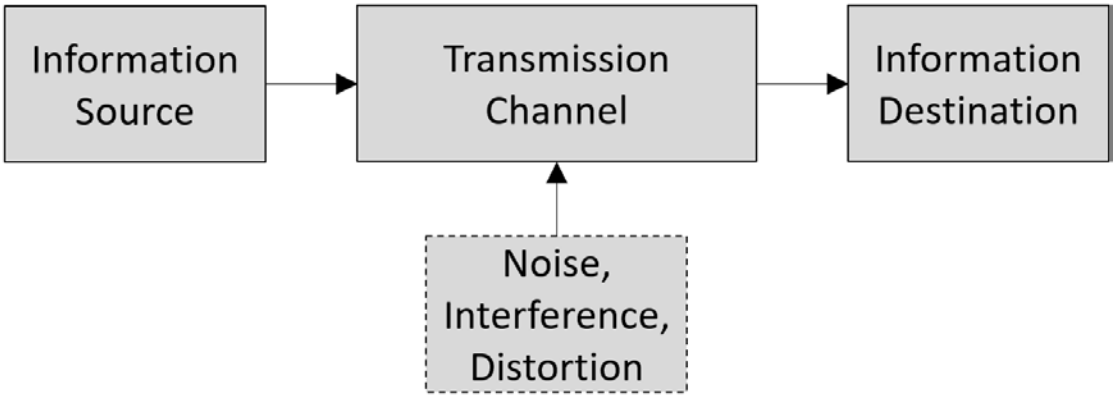

Figure 1. Elements of an example communication system. Adapted from [9].

Analog messages are physical quantities, like RF waves, that are usually continuous and vary with time [9]. Digital messages can be described as discrete electrical signals that represent transmitted information using a predefined set of symbols, like a 1 or 0 in binary code [9].

1. Digital Radio Communications

Digital radio communication systems are designed to operate through various electronic components employed to transmit and receive the messages between a source and destination. In order to receive the transmitted information, a digital communication system uses electronic components to sample, quantize, and digitize the received analog RF waveforms and convert them into discrete electrical signals. These electrical signals are then decoded into digital messages that can be processed and further manipulated. In order to transmit information this process is reversed, and digital messages are transformed into coded electrical signals that are constructed into analog waveform transmissions that are then propagated from an antenna.

During digital radio transmissions messages generated by the source are efficiently converted into a sequence of binary digits through a process called source encoding [10]. The sequence of binary digits or information sequence produced by the source encoder is then fed to a channel encoder, which adds redundancy into the sequence [10]. This redundancy assists the receiver to overcome or mitigate the effects of noise and other interference that will be experienced in the transmission channel [10]. These added

redundancies include techniques like forward error correction (FEC), cyclical redundancy codes (CRC), parity checks, and other coding schemes that are designed to overcome losses that occurred during transmission. These signal coding operations are performed at the source prior to transmission to improve the reliability, fidelity, and resiliency of information transfer, and to improve the probability that the intended message is successfully interpreted at the destination [9], [10].

After passing through a channel encoder, the information sequence is then manipulated by a digital modulator, which serves as the interface to the communication channel by mapping the digital binary data onto analog signal waveforms [10]. The process of mapping digital information content onto analog signals for transmission over a communication channel is referred to as digital modulation [10]. The modulation scheme selected for this process will determine the power required to transmit a given amount of information between the source and destination, as well as the spectral efficiency of the information exchange on the communication link [1]. Modulators employ various forms of data modulation techniques including amplitude modulation, frequency modulation, and phase-shift keying (PSK) modulation to encode different numbers of bits onto an analog RF carrier signal [1]. Each of these schemes involve manipulating the carrier signal in a predefined way such that the digital data can be transferred through encoded analog waveforms and received and interpreted at the destination.

Once the information has been modulated onto an analog RF carrier, it is then ready to be propagated by an antenna toward the destination receiver. The medium through which the message is transmitted to the receiver, referred to as the transmission or communication channel, introduces various sources of distortion such as additive thermal noise from electronic devices, atmospheric disturbances, and other natural and man-made interference [10]. The contributions from these sources must be accounted for in order to ensure an acceptable signal-to-noise ratio (SNR) of the signal that will be detected by a receiver. SNR is a power measurement expressed as the ratio of the signal of interest being transmitted relative to the noise present in the received spectrum [9]. Figure 2 is a block diagram representation of a digital communication transmission and reception process between an information source and destination.

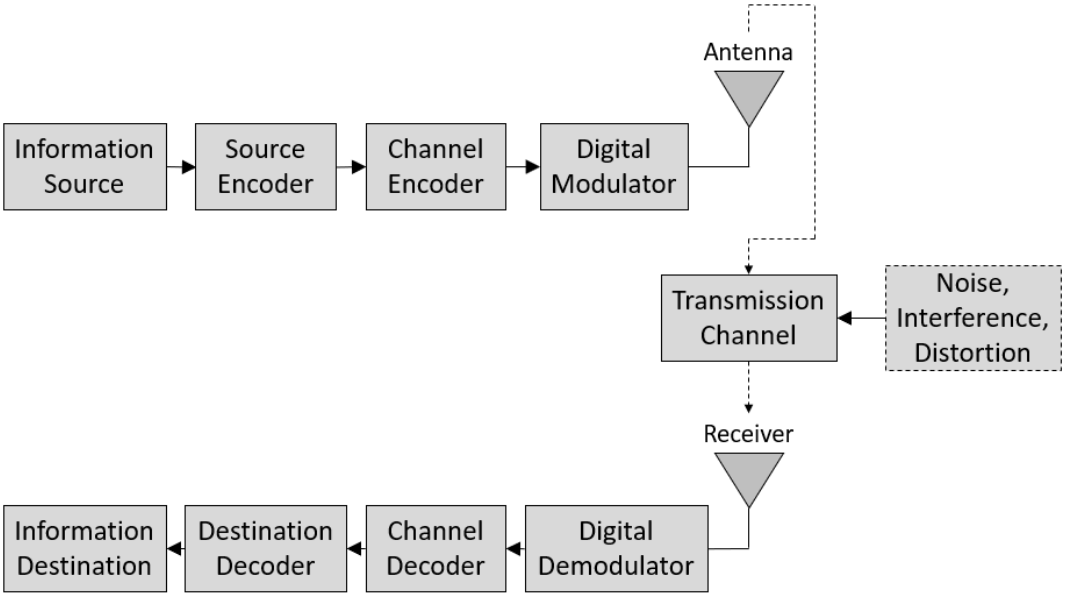

Figure 2. Components in a digital communication system. Adapted from [10].

Modern digital radio communication systems execute this described process with various electronic components that transform received analog signals into discrete digital signals. This digital information is then decoded, processed, and encoded again before being transmitted in analog form.

The signal reception process begins when electromagnetic waves impinge on an antenna and are converted into electrical signals [7]. These typically weak electrical signals are then manipulated by an RF front end (RFFE), where the ambient noise from the transmission channel is filtered out before the signal is amplified to a level capable of further processing and interpretation [7]. This process is particularly important because the signal produced by the RFFE contains the maximum possible SNR before further manipulation by the rest of the radio's components [7]. Amplification inside the RFFE is usually accomplished by low-noise amplifiers (LNA), which are designed to provide high voltage gain while contributing minimal thermal noise, which maximizes the SNR of the weak signal detected by the receiver [11]. An LNA produces a much cleaner signal than typical power amplifiers that are generally used for other applications like increasing the power level of a signal right before transmission [11]. The amplified signal out of the LNA

is then mixed with a complex sinusoidal waveform that is typically generated by a local oscillator inside the RFFE. This mixing process ultimately results in another signal that retains the detailed information of the original waveform but is shifted down to a lower carrier frequency [11], [12]. Depending on how the radio system has been designed, the replicated lower-frequency signal has been mixed down to either an intermediate frequency (IF) or to baseband frequency. A baseband signal can be described as one in which the carrier frequency is located close to zero Hertz (Hz) [8]. IF signals exist at a predefined frequency marginally above baseband, typically around 70 or 1200 MHz, but are below the received carrier frequency before mixing [8]. The signal of interest is then passed through a low-pass filter before furthering processing to remove the harmonic images created during the mixing process. Figure 3 is a block diagram illustration of components that sense, amplify, and down-convert received signals, to baseband or IF, and filters them before further processing by the radio system.

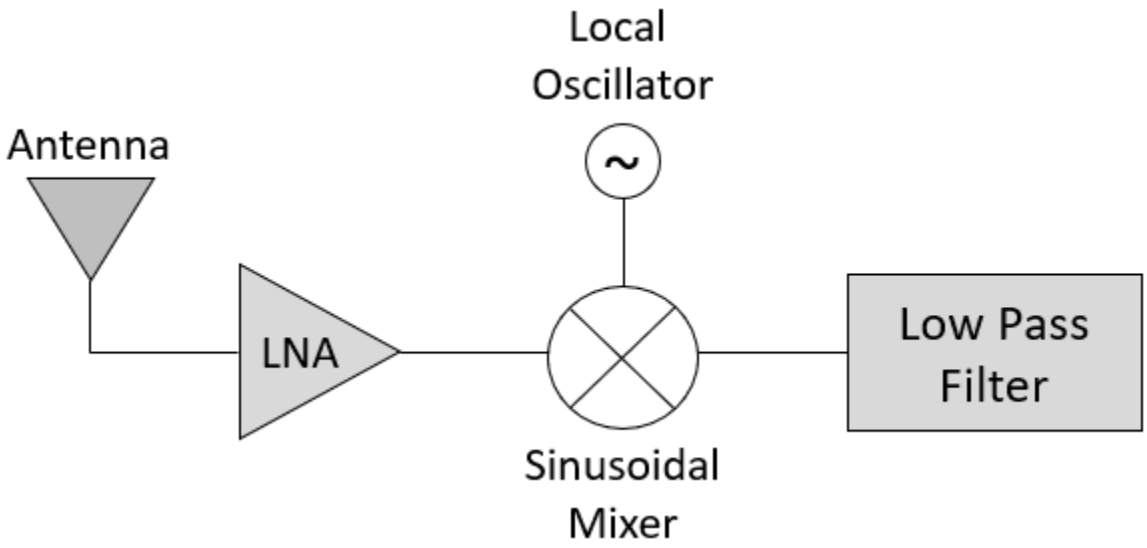

Figure 3. Diagram of LNA amplification, mixing, and frequency translation. Adapted from [10].

After the signal has been low-pass filtered, it is fed into an analog-to-digital converter (ADC), also referred to as a digitizer, which transforms the continuous-time analog signal into a discrete-time digital signal through sampling and quantization [13],

[14]. The sampled values during digitization are compared to known quantization thresholds, producing estimates of the digital bits in words that represent the analog waveforms that have been captured [14]. The digital representation of the analog signal after sampling retains the critical parameters that defined the original waveform [7]. However, some of the signal information is lost during this process due to finite precision and other physical limitations of the hardware used to perform the digitization [7].

The reverse process to digital modulation is referred to as demodulation and involves the activities by which digital information is reconstructed or recreated from modulated analog signals previously captured and digitized by a receiver [1], [10]. At the destination, a digital demodulator processes the received RF signals and converts the waveforms back into a digital sequence of information that represents an estimation of the original data transmission [10]. The digital signal output from the ADC is demodulated into a known format, like binary, which can be interpreted and further manipulated by a digital signal processor (DSP). DSPs are employed to extract the information contained in the digitized electric signal and output a stream of data bits which are often further translated into data packets, voice, video, etc. [7]. The exact role and function of the DSP varies between SDR systems but often include activities like recognizing the offsets introduced in signal acquisition, compensating for Doppler frequency effects, tracking and demodulation of the received signal, decoding of the various redundancies or coding, and deciphering any encryption incorporated during transmission [7]. Using previous knowledge of the coding scheme and any redundancy contained in the received data, the sequence of numbers is then passed through decoders which attempt to reconstruct the message that was previously encoded at the source [10].

The signal reception process performed by modern digital radio systems involves the acquisition of analog signal waveforms, the conversion into electrical signals, and the demodulation and decoding of the signals into digital information streams. Figure 4 depicts this reception and analog-to-digital (A/D) transformation in a block diagram form, where a signal enters through a receive antenna, is down-converted, converted into a digital signal, demodulated, decoded, and passed to a DSP for further processing.

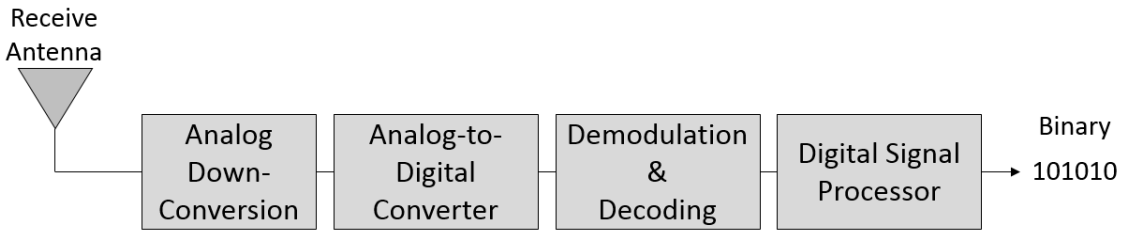

Figure 4. Digital radio receive path. Adapted from [11].

Once the transmitted message has been received, deciphered, and interpreted at the destination, the process can then be reversed in order to transmit messages as analog responses or commands to the source of the original transmissions.

Transmissions from digital radio communication systems are conducted through words and symbols made of bits, and the associated data rates are measured and often described in bits per second (bps) [1]. The bit error rate (BER) of a communications link is a probability measure that describes the number of transmitted information bits that have been received successfully without errors between a source and destination [1]. The BER increases as the SNR decreases, like when the signal of interest is corrupted by the presence of interference or noise. The BER also varies as a function of SNR per bit or E_b/N_0, which is the ratio of energy per bit (E_b) over the noise per hertz of bandwidth (N_0) [14]. In any digital communication system, a required BER is specified, and is a function of SNR modified by the bit rate of the transmission, as well as the effective bandwidth of the receiver as described in Equation 1 [14].

$$\frac{E_b}{N_0} = SNR \times \frac{bandwidth}{bit\ rate} \quad (1)$$

Equation 1. E_b/N_0 described as a function of SNR, bit rate, and effective receiver bandwidth. Source: [14].

There are multiple radio architectures in existence that accomplish these digital communication processes in different ways depending on the methods and components selected during design. Each unique radio architecture design is a combination of the

various hardware and software trade-offs made during development that affect the cost, complexity, performance, flexibility, form factor, and size, weight, and power (SWaP) of the digital communication system. Ultimately, a well-designed digital radio can be an effective communication system, but it must first overcome the fundamental physical limitations of bandwidth and noise, which are inevitable with electronic components and with any information transmission by electrical means [9].

2. Sampling Theory

Sampling is the process of converting continuous-time signals into discrete-time signals by taking measurements of the continuous analog signal at discretely defined intervals in order to create digital information. [13]. The reverse process of converting digital discrete-time signals into a continuous analog signal is referred to as reconstruction, although this process is not always successful at representing the original signal [13]. The fidelity and accuracy of signal reconstruction are driven by the method utilized to perform the sampling functions as well as the electronic components chosen to perform the tasks. The Nyquist sampling theorem describes that the captured spectrum of a signal during sampling can be reconstructed without losing any information, as long it is sampled at a rate (f_s) greater than twice its bandwidth (B) [13].

$$f_s \geq 2B \tag{2}$$

Equation 2. Equation stating that sampling frequency must be at least twice the bandwidth in order to successfully reconstruct signal being sampled. Source: [13].

The decision regarding how a system samples a received signal is an important design consideration in the development of a digital radio communication system. The higher the sampling rate, the more samples of information will be captured about the original signal. This frequency, or sampling rate, also determines the highest input frequency response, referred to as the system bandwidth, that can be captured and preserved digitally [14]. The system bandwidth, or usable frequency response, describes the ability of a receiver to follow signal variations occurring across the RF spectrum [9]. Every digital radio communication system has a finite bandwidth that limits the rate of signal variations that can be stored and processed through the system [9]. Ideally this

bandwidth needs to be wide enough to accommodate the entire portion of spectrum containing the signals of interest, but as the amount of bandwidth increases, so does the amount information to be processed as well as the amount of noise that is present [9].

Additional data points acquired during sampling provide more information about the captured spectrum and can result in a more accurate and precise representation of the original signal during reconstruction. However, sampling at very high rates consumes more power, computation, and storage, which drives unnecessary requirements for a communication system. Sampling above a certain rate may also be unnecessary to estimate the parameters necessary to perform the essential functions of the communication system. On the other hand, undersampling at a rate less than twice the bandwidth results in a phenomenon referred to as aliasing, whereby information about the original signal is truncated and incomplete and will not result in successful reconstruction of the original signal [13]. A representation of proper sampling (top) and this aliasing phenomenon (bottom) is depicted in Figure 5.

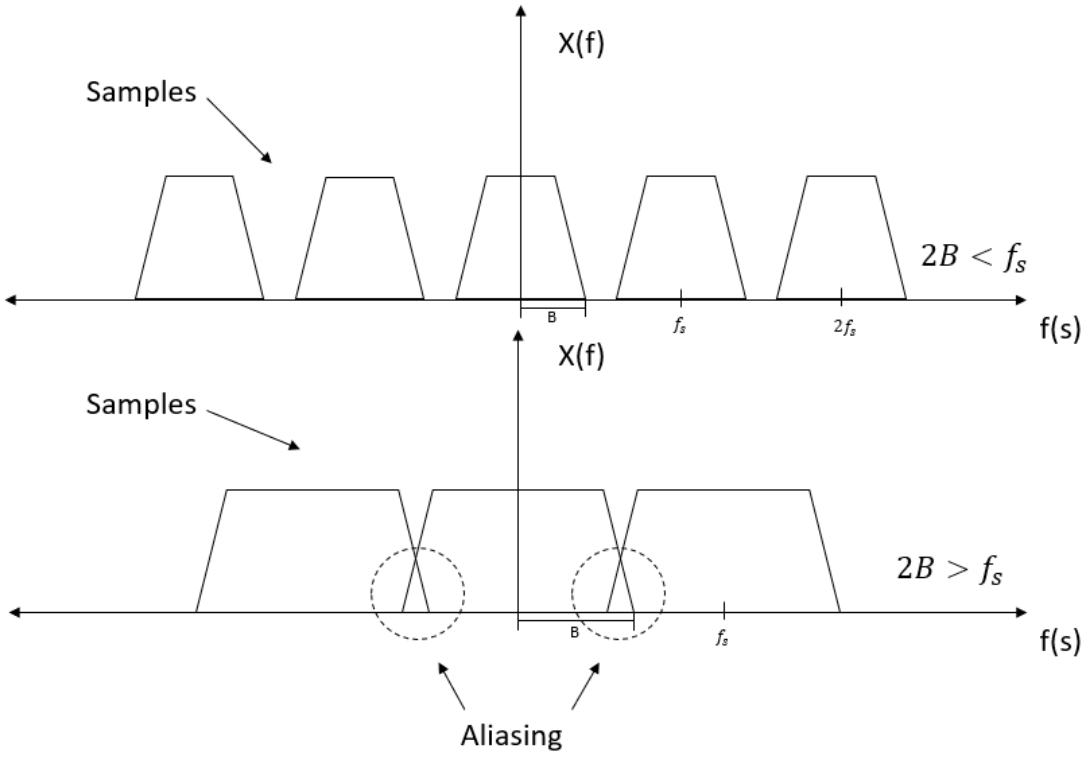

Figure 5. Example of proper sampling (top) and the aliasing of signals due to undersampling. Adapted from [13].

When aliasing occurs, the information captured through sampling of a signal is inadequate because portions of sampled spectrum overlap with other parts of the signal of interest, resulting in substantial errors during reconstruction [9]. This can be avoided by sampling at a higher rate to ensure that all the information is captured within a given sample.

Quantization is the process of converting analog samples and their captured portions of the spectrum into a discrete digital representation [13]. The number of quantization threshold values utilized during digitization is designated as the bit resolution of the ADC. During the process of digitizing a received analog signal the digital representation of the analog signal information is limited by the finite precision and sampling rate of the ADC [7]. This precision is quantified through an ADC's bit resolution, which determines how many digital bits will be used to represent the analog signal in digital form. The bit resolution is important because once an analog signal has been digitized, the

accuracy of its reconstruction is limited to the resolution by which it has been quantized [14]. The number of bits per sample governs the precision of the digital word, which also affects the SNR and dynamic range of the reconstructed signal [14]. The dynamic range is defined as a measure describing the range of signals that can be successfully reconstructed in the presence of the smallest and largest signal present [14]. The greater the bit resolution of an ADC, the more precise representation of the signal which is propagated through the rest of the digital system. A signal sampled with insufficient bit resolution can degrade the ability of a digital communications system to discern a signal of interest from the entire received spectrum. It would also reduce the accuracy of the reconstructed signals before transmission.

B. RADIO RECEIVER ARCHITECTURES

It is a challenging task to design a digital radio communication system that is both efficient and flexible. Many design characteristics of commercially available systems are driven by cost-benefit decisions made regarding the receiver architecture. The exact balance of functionality and performance involved in RF design is both an art and a science of generating, manipulating, and interpreting the electromagnetic spectrum (EMS) in a way that allows for the reliable transfer of meaningful information between two circuits that have no direct electrical connection [11]. The ideal radio system would be able to take advantage of the programmability and flexibility of SDR technologies, while still being able to produce clean, precise, and accurate signals while receiving a myriad of incoming signals over an infinite spectrum [7]. In reality, trade-offs are made during the system design process, which account for the differences in cost, performance, and reliability of commercially available systems.

One of the main considerations when designing a digital radio is the amount of noise that is generated by the internal electronic components. Noise is an unavoidable reality in the EMS and with the hardware designed to manipulate it, but certain radio components and architectures inherently produce more noise. For example, there are two fundamental types of amplifiers utilized in RF systems, power amplifiers and LNAs [11]. By design these components generate very different levels of noise that may have

cascading consequences in radio design. High-gain, power amplifiers amplify noise and out-of-channel harmonics that have the potential to interfere with other nearby systems. The EMS is intrinsically noisy so an ideal SDR would generate very little of its own internal noise that could degrade the SNR and the probability of successful transfer of information between a source and destination.

Radio system architectures can be categorically divided into two designated functional areas: the RF front end (RFFE), which is responsible for the transmission and reception of signals, and the RF back end (RFBE), which encompasses the signal processing functionality [12]. A graphical representation of these areas and their components can be found in Figure 6.

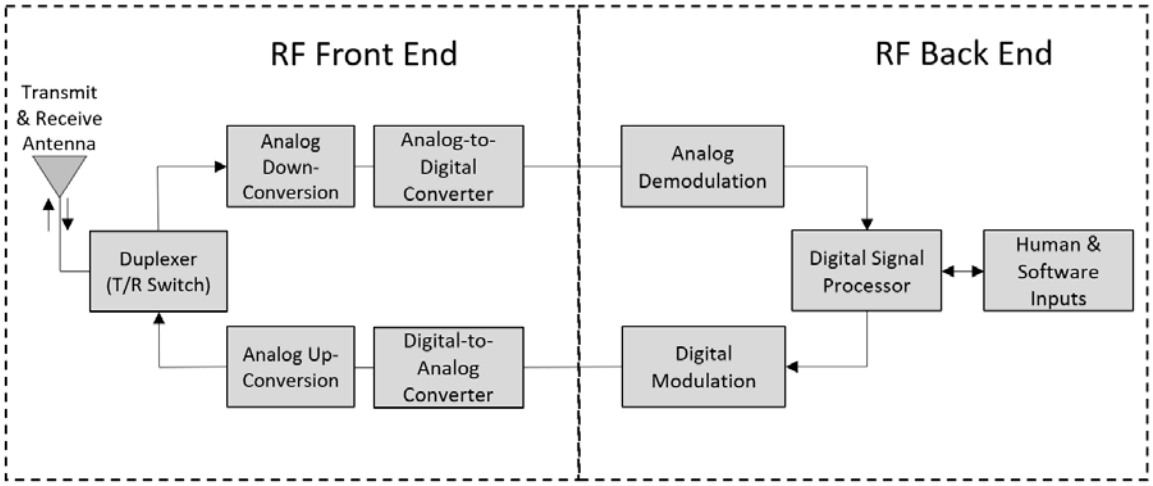

Figure 6. Depiction of example SDR architecture and the RFFE and RFBE functional areas. Adapted from [12].

Architectural decisions by an RF engineer on how the radio will perform the functions of the RFFE and RFBE, either through software or hardware means, will affect the overall performance, parameters, and characteristics of the system. Some of the most important design considerations for an SDR include the desired transmit power, the receiver input sensitivity, the maximum power of the expected input signal, the sensitivity of the power control, and the effects of potential spurious emissions that are created by the various electronic components [12].

A typical radio receiver must perform carrier-frequency tuning to capture a desired signal of interest, filtering to separate the signal from any others received with it, and the requisite amplification to compensate for the losses experienced during the transmission [9]. The basic function of a digital radio receiver is to capture this analog, low-power, RF signal and down-convert it into a complex baseband signal which retains the information of the original waveform [12]. During this process, the power of the received signal at an antenna is amplified to an adequate level such that the signal can be more easily deciphered, demodulated, and digitally represented before manipulation by the DSP. While transporting through a digital system, the power of the signal of interest must remain sufficiently greater than the noise power in order to maintain an acceptable SNR and to produce the desired BER performance of the modulation scheme being utilized [12].

When discussing potential receiver architectures as an aspect of an overall SDR design, the primary distinction between several options is the method and number of stages implemented to down-convert a received analog signal into digital baseband data [12]. Direct conversion receivers perform this translation in one step, while super-heterodyne receivers employ two or more down-conversions to shift the signal to baseband [12]. In general, the complexity of an architecture increases with the number of times the received signal is incrementally down-converted into baseband, but each additional step allows for greater filtering of the unwanted images created during the mixing process [12]. It is the responsibility of the RF engineer designing a radio receiver to weigh the advantages and disadvantages involved with the various receiver architectures and to select the appropriate design that will adequately meet the requirements for the system.

1. Direct Conversion Receiver

A direct conversion, or homodyne, receiver architecture transforms received signals from their original RF frequency immediately down to baseband. A diagram of a direct conversion receiver architecture is pictured in Figure 7. It consists of an LNA to amplify the weak received signal, a bandpass filter to capture only the frequency band of interest, a complex sinusoidal mixer to down-convert the signal to baseband, and a low pass or baseband filter to remove the unwanted images created during the mixing process.

The output of this architecture is an analog baseband signal, and in a digital communication system this signal is then passed through an ADC before demodulation, decoding, and further processing by a DSP.

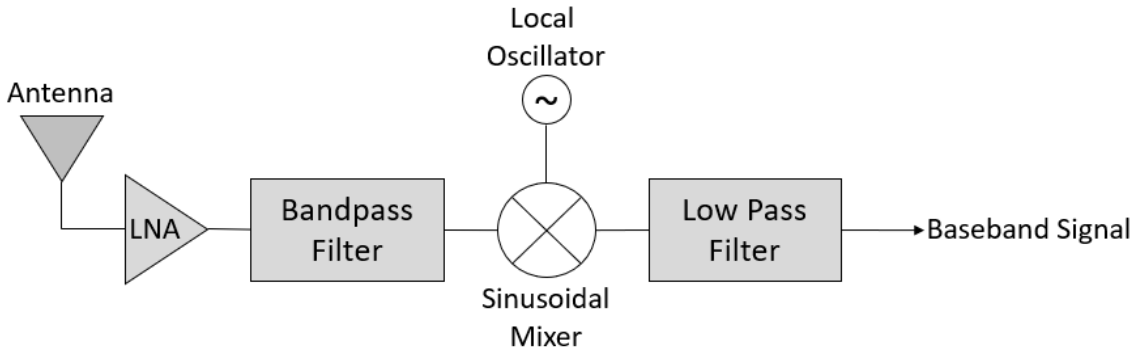

Figure 7. Example direct conversion receiver architecture. Adapted from [12].

This architecture offers advantages due to its overall low complexity, simple filtering requirements, and easier harmonic image signal suppression [12]. However, the mixers involved in down-converting the received signals need to be balanced and capable of operating over a wide frequency spectrum in order to capture a range of potential signals [12]. An analog device called a local oscillator is also required to ensure that the signals produced by the mixer are balanced in both phase and amplitude [12]. The existence of this oscillator generates signal leakage through the mixer and LNA from the antenna that can be reflected back into the receiver spectrum [12]. These artifacts result in unwanted noise in the receiver and transmitted signals that degrade the overall SNR and reduce the fidelity of the communications. This architecture may be the easiest and cheapest way to digitally process analog signals but depending on the mission the limitations may reduce the overall performance of the radio to an unacceptable level.

2. Super-Heterodyne Receiver

A super-heterodyne receiver architecture differs from a direct conversion architecture because in this design the received signal is initially down-converted to an IF and filtered again before being translated down to baseband. The objective of converting a

received analog signal into digital baseband can be accomplished through different means and methods through a variety of components. This includes down-converting a signal multiple times and digitizing the signal at different points of the process. These translations can be performed by analog components like RF mixers and filters as well as through the processing of a digitized signal by a DSP. Figure 8 depicts a super-heterodyne receiver architecture where an analog signal is mixed and down-converted to an IF before passing through an ADC and being digitized into Digital-IF. Once the signal exists in digital form it can be further manipulated and down-converted, but without creating the unwanted images that are created by analog mixing [12].

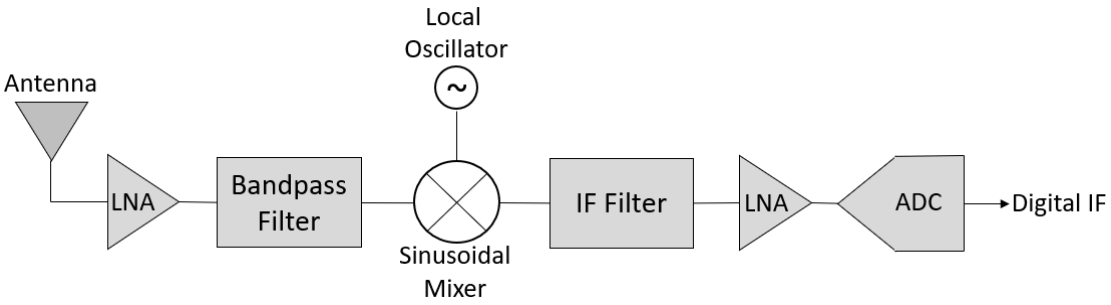

Figure 8. Example of a super-heterodyne receiver architecture. Adapted from [12].

This heterodyne architecture allows for good RF selectivity due to the presence of preselect and channel filters and allows the input gain to be distributed over several amplifiers at different points, unlike with a direct conversion architecture [12]. Also, the existence of multiple filters operating in various frequency bands limits the amplification of internal noise during the process [12]. Furthermore, the down-conversion from a real to a complex signal is performed at a single and fixed IF frequency as opposed to a direct conversion architecture which is required to accommodate a wide range of frequencies. This allows the local oscillator to be dedicated to that IF frequency, which produces less noise interference than components designed to operate over a wider frequency range [12]. The disadvantages of this architecture include the added complexity and required components, including the potential requirement of multiple oscillators and specialized IF

filters, which may add significant cost and SWaP requirements to the system [12]. The additional electronic components also represent more potential points of failure which reduce the overall system reliability and complicate potential troubleshooting. The precision of the signal reconstruction before transmission is still limited to the resolution of the signal when it was digitized by the ADC. However, the use of an ADC with sufficient bit-resolution should capture enough spectral information of the signal at a low IF to result in successful reconstruction without significant information loss.

C. SOFTWARE-DEFINED RADIO

An SDR can be defined as a radio where the digitization of the received signal is performed at some stage downstream from the antenna [12]. This digitization typically occurs after the signal has passed through some form of wideband filtering to capture the spectrum containing the desired carrier frequency, low-noise amplification of the weak received signal, and a down-conversion to a lower frequency in subsequent stages [12]. The stages of down-conversion to baseband can be accomplished through analog mixers, executed digitally inside a DSP, or a combination of both [12]. These activities are conducted during reception before a reverse process is performed for the transmission digitization and analog propagation [12].

In modern SDR systems, an ADC is employed to translate the received analog signal into a digital signal, either as Digital-IF (intermediate frequency) or digital baseband. Once the signal has been digitized, information from the original carrier signal is demodulated, decoded, and processed by a DSP [8]. The capability and functionality of the DSP determines many of the critical characteristics of the SDR, as opposed to the legacy hardware approach where each unique radio interface or frequency band utilized would be constructed around a dedicated set of specific applications or the implementation of integrated circuits [12]. These legacy radio interfaces and circuits were hard coded and fixed at the time of design or manufacturing, which limited the flexibility of the radio system unlike with reprogrammable SDR systems [12].

In an SDR system, software is utilized to create digital messages which are modulated back onto a carrier wave through a digital-to-analog converter (DAC) before

being transmitted as an analog RF signal. The software associated with an SDR communication system defines parameters of the receiver, transmitter, and how signals are processed and created, allowing the user to change many characteristics that would be impossible with legacy radio systems. In order to perform similar parametric changes to what is altered through software in an SDR, these legacy radio systems would require hardware modifications. The main distinction of the term "SDR" from other modern systems that may be software-controlled is that with an SDR, different waveforms can be received and supported by modifying the software or firmware inside a system without a change in hardware [7]. This is a distinction from a strictly software-controlled system, where just the processing functions of the radio may be executed through software [7]. This combination of flexible, digital RFFE and signal processing in software has led to the birth and widespread adoption of SDR and the replacement of traditional, inflexible radio systems [13].

These characteristics allow SDR systems to perform multiband and multimode communications, which means they can transmit and receive in several frequency bands and operate in various modes including different modulation techniques and signal waveforms [12]. These advantages of adaptability, reconfigurability, and multifunctionality encompassing modes of operation, RF bands, and waveforms have led to the replacement of traditional radio technologies in many commercial, civil, and military applications [12]. More specifically, the software functionality of SDR offers the ability to tune parameters of the radio to address potential interoperability issues, achieve higher performance like reduced BER, greater spectral efficiency, and the adaptability to intelligently compensate for unforeseen variations in the operational environment [12]. As SDR systems, and the components used to create them, continue to mature and develop, they will continue to provide more flexibility to users and allow them to support more missions and over larger frequency ranges and parameters.

A block diagram example of an ideal SDR is pictured in Figure 9 and consists of only microprocessors, an ADC, DAC, transmitter and receiver. The ideal SDR would be capable of transmitting and receiving all possible signals, regardless of the frequency, modulation type, power level, or available bandwidth [12]. Figure 9 depicts how with an

ideal SDR, messages are mapped to the desired waveform inside a microprocessor and the digital samples are then converted directly into an analog RF signal by a DAC and passed to the antenna for transmission [7]. The transmitted signal is then propagated through the transmission or communication channel to the receiver, sampled and digitized by an ADC, and finally ingested by another microprocessor [7]. The description of an ideal SDR in Figure 9 does not include a dedicated RFFE like a typical radio system previously described or a generic DSP block. This is because an ideal SDR would not require RF band selection, and all signal conditioning and manipulation would be performed on the digitized spectrum inside of the microprocessors [7].

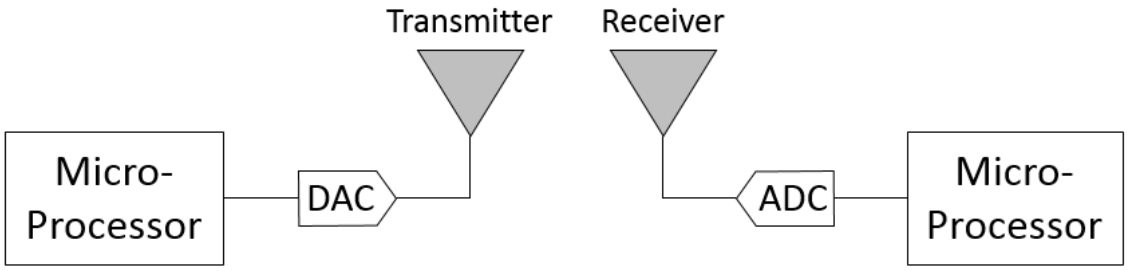

Figure 9. Block diagram depiction of an ideal SDR. Adapted from [7].

The selection of the desired RF band and the desired frequency matching the signal of interest are key features of a typical RFFE because most antennas are limited to certain frequency ranges driven by their size and geometric design [7]. However, an ideal SDR system would digitize the entire received spectrum, eliminating the need for specialized antennas and their appropriate filters, which are usually electromechanical devices that are difficult to tune dynamically [7]. While the creation of an ideal SDR system may not be physically possible with the hardware components available today, modern SDR technologies offer many advantages and flexibility over legacy analog radio systems.

D. MC3 MISSIONS AND ARCHITECTURE

The networked MC3 ground stations utilize predesignated RF channels to conduct TT&C communications with the satellites in LEO. These frequency channels reside in the Ultra-High Frequency (UHF) and S-Band frequency ranges, which are specific portions of

the EMS officially designated by the International Telecommunication Union (ITU) [6]. A list of approved and supported frequency ranges utilized by the MC3 network appears in Table 1. UHF is defined by the ITU as the frequencies between 300 MHz and 3000 MHz, while S-Band is the range between 2000 MHz and 4000 MHz [6].

Table 1. MC3 operational frequency ranges. Adapted from [5].

Band	Frequencies	Designator
UHF uplink	449.75 - 450.25 MHz	12K5F1D 43K0F1D
UHF downlink	902 - 928 MHz	115KG1D
S-band uplink	2025 - 2110 MHz	2M00G2D 2M45G1D
S-band downlink	2200 - 2290 MHz	1M60G1D 2M00G2D 2M45G1D

The MC3 ground stations also support a wide range of waveforms, protocols, and data rates by leveraging SDR systems along with open-source and commercially available applications such as GNU Radio, MATLAB, and LabView [5]. The use of these applications is another example of flexible and cost-efficient operations that enable the MC3 network to support numerous customers with a limited hardware footprint through dynamic software that can manage many different mission sets.

Typical C2 communications conducted by MC3 through SDR technologies include TT&C and health status checks with the multiple small satellites that are accessible through the network. The USRP-2922 SDR, which is the baseline hardware used for MC3's operational communications and is prevalent across the small-satellite community, is also utilized in the lab for testing purposes including integration testing with future satellite systems. Other similar USRP devices, like the B205mini-i, are also used in the lab for testing and research purposes.

E. RADIO UNDER STUDY (RUS) OVERVIEW

The research of this thesis focused on the experimentation and comparative analysis between the four radios under study (RUS). The RUS include two baseline Universal Software Radio Peripheral (USRP) systems, the USRP-2922 and the B205mini-i, which represent common hardware that has been used in many operational applications with small satellite ground stations and in academic settings like the SSAG at NPS. The other two RUS, the Kratos SpectralNet and qRadio and the AMERGINT satTRAC system, are two purportedly high-end commercial satellite communication systems that have not been thoroughly evaluated or well characterized by the MC3 program and its user community. Investigation and comparative analysis of the four RUS will provide the SDR stakeholders more insight into the performance and characteristics of these systems. This will help inform potential customers about the suitability of these RUS for their desired applications.

Each of the four RUS is comprised of a hardware and software element employed together to perform the signal transmission, reception, and processing functions of an SDR. Each SDR system includes a front-end hardware RF transceiver component that transmits and receives the analog RF signals. The RFFE also performs the ADC, DAC, up/down mixing, and sampling functions. The back-end software components of each system are responsible for tuning the desired parameters of RFFE as well for performing the digital processing functions on the baseband signals, to include modulation/demodulation, encoding/decoding, etc. The two high-end commercial SDR include their own dedicated proprietary software that is required to operate the systems. The baseline USRP devices can be operated either by using software available for purchase from the manufacturer National Instruments called LabVIEW, commercial products like Simulink from MathWorks, or with the free and open-source development toolkit called GNU Radio [15], [16]. GNU Radio was used to operate the USRP radios during this research.

The experimentation, evaluation, and analysis performed for this thesis investigated both the hardware and software components of these radio systems individually as well as how they performed together as a cohesive system. From this point forward, the various SDR systems will be referred to as their combination of hardware and software components by the designations RUS-1:4.

1. National Instruments (NI) USRP-2922 (RUS-1)

RUS-1 is the National Instruments (NI) USRP-2922 tunable RF transceiver, advertised to perform high-speed ADC and DAC for streaming baseband signals to a host computer over an Ethernet connection [15]. The USRP-2922 device is essentially a combination of the Ettus Research USRP N210 peripheral hardware device equipped with a 40 MHz bandwidth, SBX USRP RF Daughterboard [17], [18]. The SBX transceiver implements a direct conversion RF receiver architecture, meaning that it mixes incoming signals immediately down to baseband for digital processing.

Figure 10. Picture of NI USRP-2922 device. Source: [15].

During experimentation RUS-1 was linked with a Linux-based computer through a standard one gigabit Ethernet (1GbE) connection. On the host computer, Ettus Research's Universal Hardware Driver (UHD) was used to manage the baseband data flow and control messaging between the USRP device and the computer where it was being manipulated. The UHD code enabled the connected USRP device to function as either a 'source' or 'sink' block inside GNU Radio flowgraphs that were developed for this experimentation. A 'source' block designated that the USRP device was acting as a transmitter, while a 'sink' block designated that it was acting as a receiver. The GNU Radio flowgraphs

represented the RFBE of the SDR device and performed the desired signal processing functions necessary to conduct the experiments.

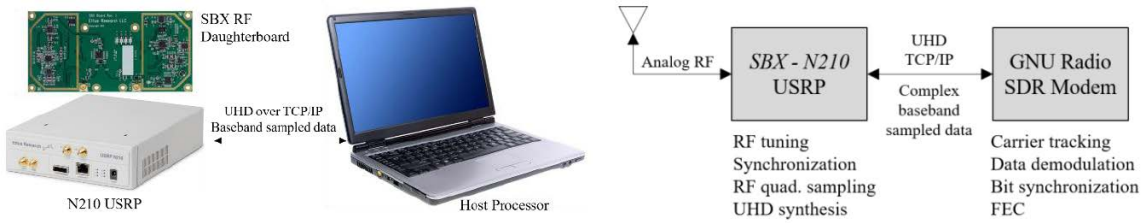

Figure 11. Depiction of RUS-1 system components used during research and experimentation. Source: [19].

The USRP-2922 is the baseline SDR hardware currently deployed in all the ground stations conducting small-satellite communications in the MC3 network. The USRP-2922 hardware is also widely employed throughout academia, private industry, and the small-satellite community because of its low cost, low complexity, flexible interfaces, and ease-of-use [19]. RUS-1 represents an operational baseline reference radio for this study because of the widespread use of this device and the considerable amount user experience associated with it.

2. Ettus USRP B205mini-i (RUS-2)

RUS-2 is the Ettus Research USRP B205mini-i device. It is marketed as an RF system-on-chip (RFSoC), meaning that the device integrates the complex baseband data processing and RFFE transceiver functions onto a single integrated circuit. This differs from RUS-1, which employs two separate hardware components connected together to perform the same functions. This integration of radio functions inside RUS-2 results in an SDR device roughly the size of a credit card [18]. The RFFE of RUS-2 is comprised of the Analog Devices AD9364 transceiver chip and is bus-powered by a high-speed USB3.0 connection which is used to stream data to a connected host computer [18]. The AD9364 transceiver chip is designed with the same direct conversion architecture as the SBX in RUS-1 and translates analog signals directly down to baseband before any digital processing by its RFBE.

Figure 12. Picture of USRP B205mini-i device. Source: [18].

As with RUS-1, the Ettus Research UHD software was utilized to control the SDR through GNU Radio models during experimentation. The GNU Radio flowgraphs used with RUS-2 during experimentation were identical to those used with RUS-1 other than the name of the source or sink block which designated which USRP hardware was connected to the host computer.

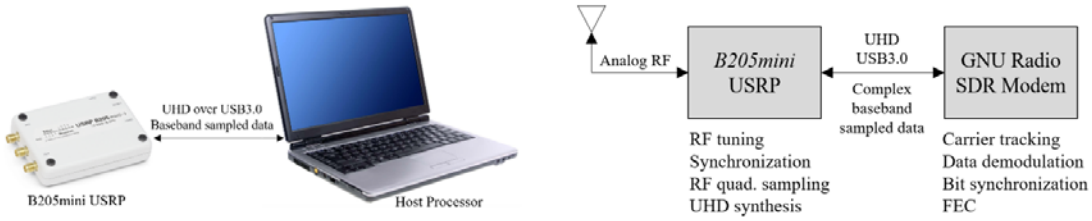

Figure 13. RUS-2 system components used during research and experimentation. Source: [19].

The B205mini is used throughout the SSAG small-satellite laboratory for various academic and operational testing purposes. Much like RUS-1, RUS-2 is a small and low-cost SDR which shares the common GNU Radio RFBE. The integrated RFSoC technology of the Analog Devices AD9364 chip represents another reference baseline for the family

of devices commonly used throughout industry, academia, and the satellite communications community [19].

3. Kratos SpectralNet Lite Digitizer and quantumRadio SDR (RUS-3)

RUS-3 is the system comprised of the SpectralNet Lite Digitizer and quantumRadio (qRadio) SDR produced by Kratos. The original manufacturer acquired by Kratos was known as RT Logic. The SpectralNet Lite Digitizer functions as the system's RFFE transceiver and interfaces with the qRadio signal processor through Digital-IF waveforms [20]. The SpectralNet Lite Digitizer also employs Analog Digital's RFSoC AD9364 chip to perform direct down-conversion of received analog signals into Digital-IF. Figure 14 is an annotated picture of the SpectralNet Lite front plate from the manufacturer's quickStart Guide describing the external interfaces on the digitizer.

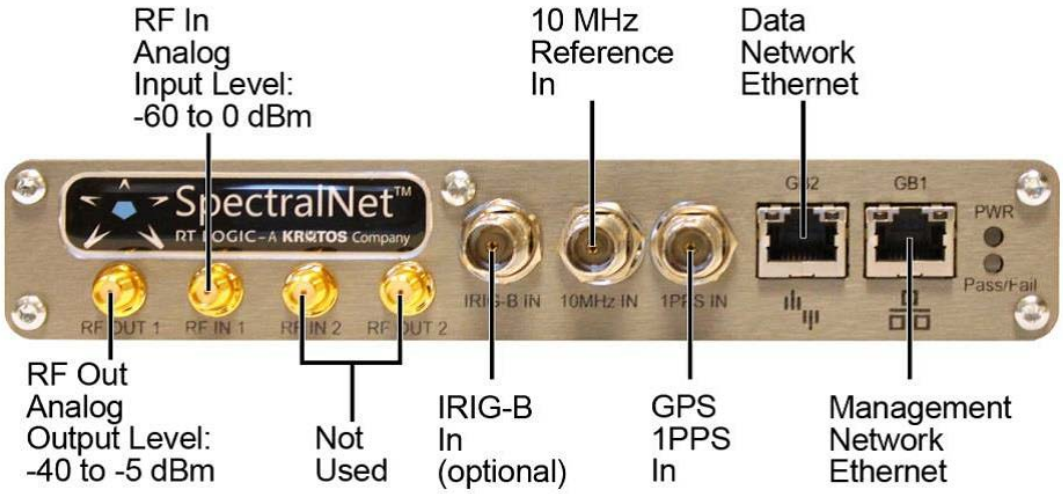

Figure 14. SpectralNet Lite Front Plate from manufacturer's quickStart Guide. Source: [20].

The Digital-IF waveforms transferred between SpectralNet and qRadio are formatted in the open-standard VITA-49 protocol as a packetized data stream [20]. The packets are transported via ethernet cable through a 1GbE interface [20]. Figure 15 illustrates how the waveforms are packetized and communicated to and from the qRadio

before and after DAC/ADC processing. More information regarding the VITA-49 protocol can be found in Appendix C.

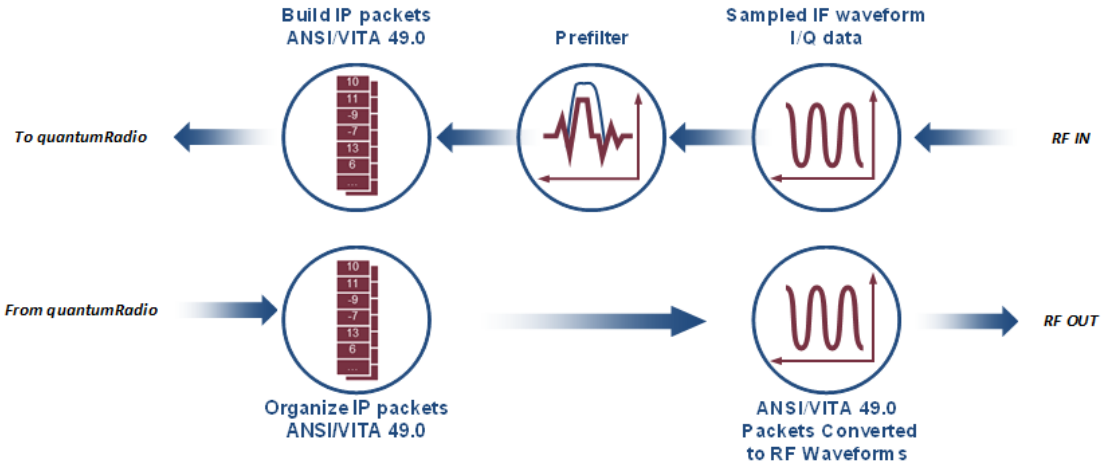

Figure 15. Overview of SpectralNet Lite VITA-49 Packetization as described by RUS-3 manufacturer. Source: [20].

The manufacture-provided SpectralNet graphical user interface (GUI) was utilized to operate the digitizer hardware. A separate qRadio GUI was utilized to operate the qRadio SDR processor. The qRadio SDR is the RFBE that employs digital receiver and modulator technologies to perform signal processing functions such as carrier tracking, data modulation and demodulation, bit synchronization, and digital processing of independently tunable frequencies between the system's operating range with adjustable data rates [20]. The qRadio signal processing software runs on a Dell R440 server and is accessible through manufactured provided VMware software. These hardware components and their connections are pictured in Figure 16.

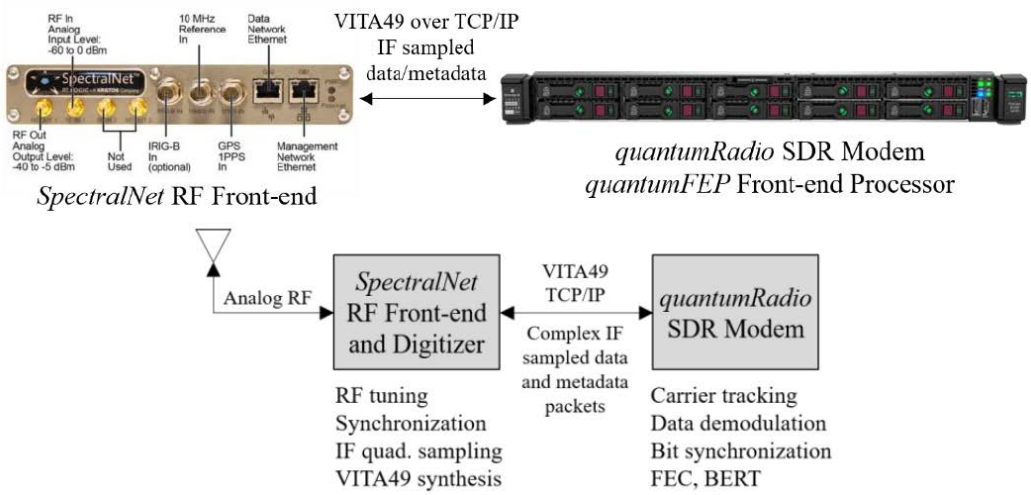

Figure 16. RUS-3 system components used during research and experimentation. Source: [19].

Unlike the open-source software used to control the USRP devices RUS-1 and RUS-2, RUS-3 is operated with two pieces of proprietary software provided by the manufacturer Kratos. The SpectralNet Digitizer graphical GUI, pictured on the left side of Figure 17, is used to set the analog input and output RF and power parameters for the digitizer. The qRadio SDR GUI, pictured on the right side of Figure 17, is used to define the desired transmit and receive RFFE parameters of the radio which are communicated to and from the SpectralNet through Digital-IF. This is accomplished through the use of various software modules that define the signal processing characteristics of the uplink and downlink signals which correspond to the information flowing through the SpectralNet 'RF OUT' and 'RF IN' ports. The qRadio software also reports various metrics and allows data files to be recorded of signals at different points in the transmit and receive chains.

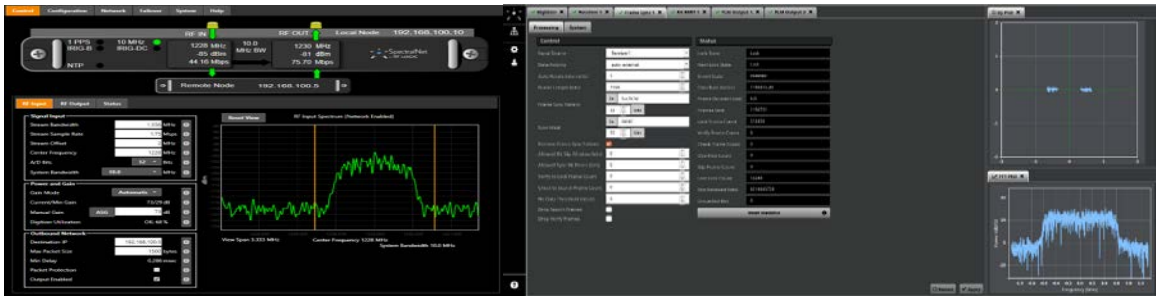

Figure 17. Snapshots of SpectralNet (left) and qRadio (right) Software GUI's.

To transmit analog RF signals from RUS-3, outgoing baseband data is fed to the 'Modulator' module from one of the qRadio command input modules or from a Pseudorandom Noise (PN) generator. Parameters including modulation type, sample rate, and filter type can be adjusted through this module as pictured on the left side of Figure 18. The 'Digitizer' module, pictured on the right of Figure 18, is used to select the 'Modulator' as the desired input source and to enable the transmit channel of the radio.

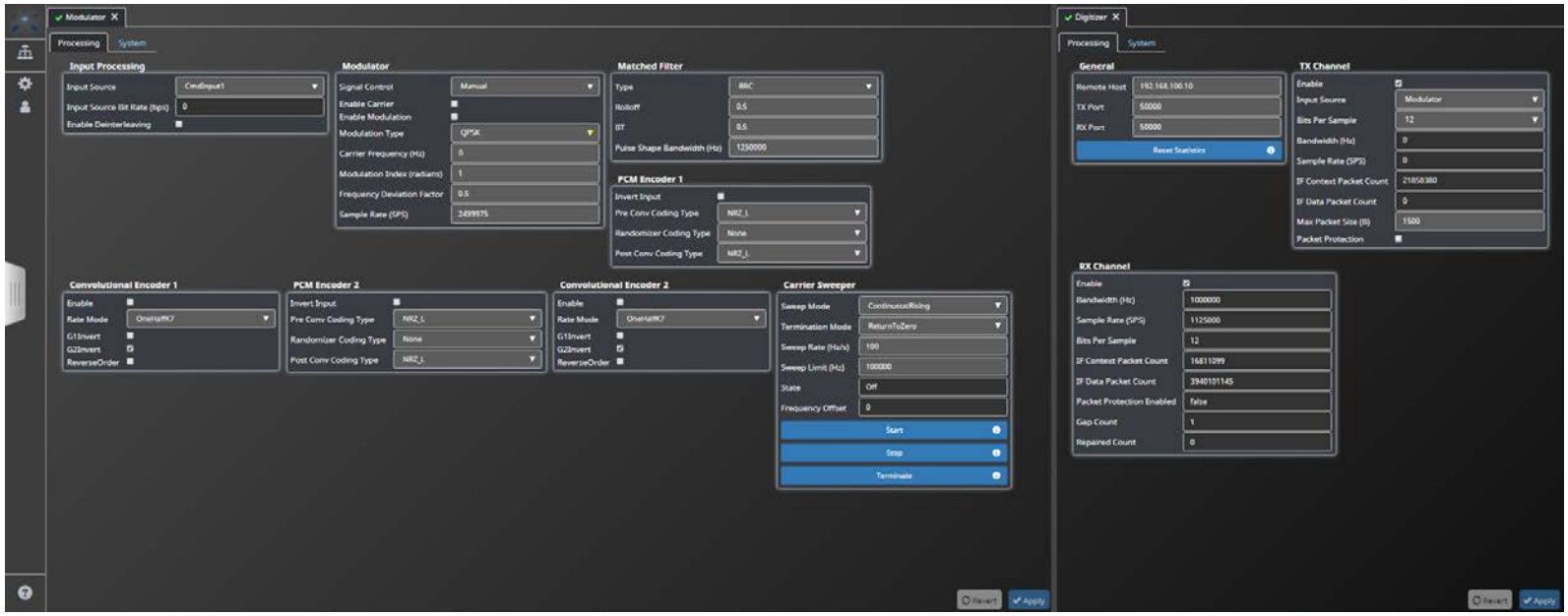

Figure 18. Snapshot of qRadio SDR GUI containing example parameters set inside the system's uplink modules.

The parameters defined within these uplink modules are included in the baseband Digital-IF packets which are generated from the qRadio and transferred to the SpectralNet Lite device for DAC and RF transmission. The ‘RF Output’ tab inside the SpectralNet Digitizer GUI is utilized to set the desired carrier frequency and output power of the analog signal. This directs the digitizer to perform DAC and up-conversion of the baseband Digital-IF constructed by the parameters set in the qRadio SDR GUI. An example of the ‘RF Output’ tab of the SpectralNet Digitizer GUI is depicted in Figure 19.

Figure 19. Snapshot of RF Output tab from SpectralNet Digitizer GUI.

To receive RF signals with RUS-3, the ‘RF Input’ tab of the SpectralNet Digitizer GUI is utilized to tune the center frequency and instantaneous bandwidth of the RFFE to match the signal of interest as pictured in Figure 20. The GUI reports the sensed signal power of RF energy present in the designated input spectrum as well as the data rate at which Digital-IF is being transferred over the network to the qRadio. The device by default automatically controls the input gain to attempt to amplify received signals to the maximize the utilization of the digitizer close to its full-scale dynamic range without causing saturation or clipping of the transmitted signals. This ensures the maximum possible

resolution during sampling and ADC. If desired, the automatic gain control (AGC) can be turned off and gain can be adjusted manually.

Figure 20. Snapshot of RF Input tab from SpectralNet Digitizer GUI.

Inside the qRadio SDR GUI, the ‘Digitizer’ module is used to enable the receive channel of the radio, and the input source is set to ‘Digitizer’ inside of the ‘Receiver’ module. The expected modulation type and data rate of the signal of interest are also defined in the ‘Receiver’ module as pictured in the center of Figure 21. Given this information, the GUI reports in real-time the derived symbol processing rate as well as the amount of frequency offset measured from the designated carrier frequency in the SpectralNet Digitizer GUI. The ‘Receiver’ module also reports the receiver SNR as well as the current status of the carrier lock and symbol lock onto the signal of interest. The ‘Frame Sync’ module, as depicted on the right of Figure 21, can be programmed to sync onto a defined frame length in bits with or without the presence of a frame sync pattern. Once a successful lock is achieved inside the ‘Frame Sync’ module, the received bits can be passed off to one of the available decoders inside the software. The qRadio allows for bits to be captured and recorded from the ‘Receiver’, ‘Frame Sync’, or any of the available decoder modules and can be saved as binary data files onto the host computer.

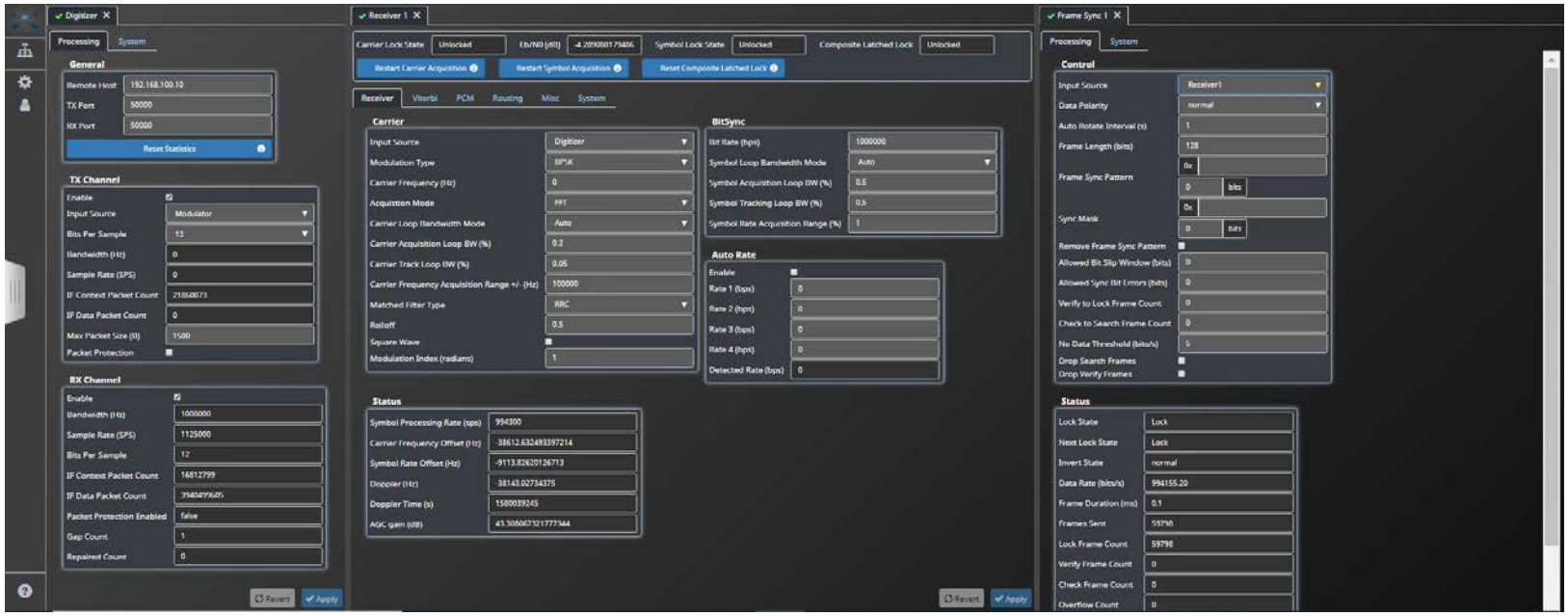

Figure 21. Snapshot of qRadio SDR GUI containing example downlink modules.

The Kratos quantum product line, which includes the SpectralNet Lite and qRadio SDR contained in RUS-3, is advertised as a robust small satellite ground system developed by leveraging the contractor's, "proven experience in RF and C2 solutions" [21]. The hardware and software packages are marketed as high-end commercial products developed by an experienced and reliable contractor and suitable for all types of small satellite missions. Because of these claims and moderate price, RUS-3 is presumed to be a superior product to RUS-1 and RUS-2, and is expected to provide more performance and value to the customer. This claim was investigated through the research and experimentation of this thesis.

4. AMERGINT satTRAC System (RUS-4)

RUS-4 is the AMERGINT satTRAC system, which is comprised of satTRAC Signal Converter RFFE and a software-defined baseband modem RFBE operated on a Dell R740 server. These components interface with each other through a standard 1GbE connection using the VITA-49 protocol as annotated in Figure 22.

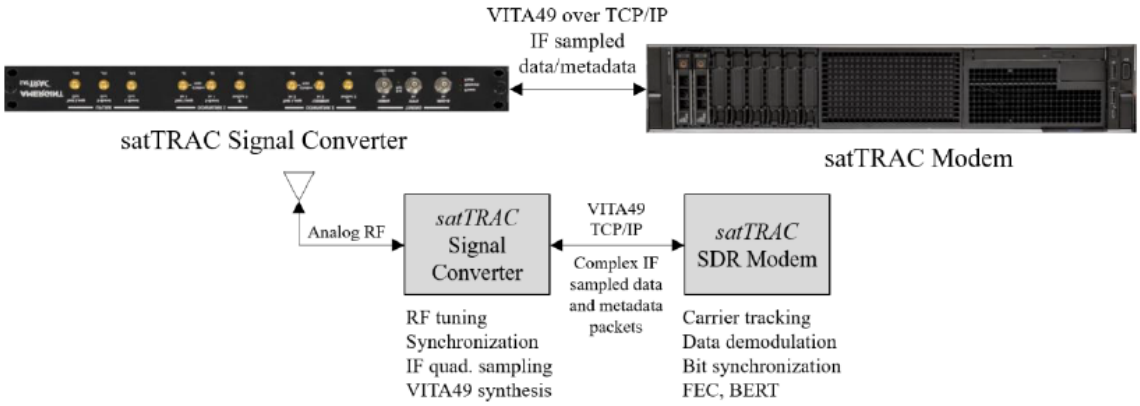

Figure 22. RUS-4 system components used during research and experimentation. Source: [19].

The satTRAC Signal Converter of RUS-4 pictured in Figure 23 performs the analog transceiver functions for the radio. The Signal Converter hardware is accessed and

manipulated through the operation of the satTRAC software component which conditions, filters, down-converts, samples, and decimates analog signals into Digital-IF [23].

Figure 23. Annotated picture of the satTRAC Signal Converter front plate of RUS-4. Source: [22].

Unlike the other SDR receivers in the study, the satTRAC radio uses discrete components to employ a heterodyne receiver architecture, down-converting received RF signals into a 70 MHz IF before digital sampling. The samples are then digitally translated down to baseband, a process that does not create analog images that could negatively affect the received SNR. A block diagram depiction of the entire transmit and receive chain is depicted in Figure 24.

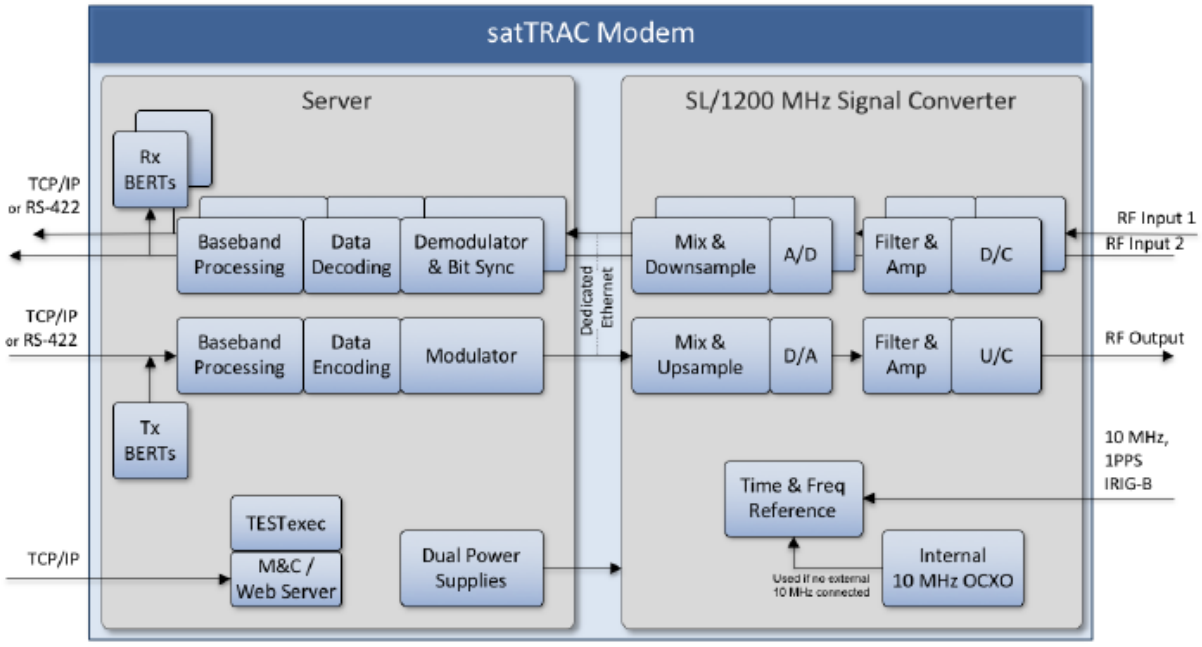

Figure 24. Functional block diagram of the AMERGINT satTRAC system. Source: [22].

The satTRAC server, hosted on a Dell PowerEdge rack-mount server performs all the digital signal processing associated with modulation, demodulation, and baseband data processing through the contractor's softFEP applications, a part of AMERGINT's SOFTLINK Product Architecture [22]. The applications can be accessed through the softFEP GUI pictured in Figure 25 which provides a 'Modem Overview' that reports the status of some of the top-level parameters of the SDR. Programmable values like receiver tuning frequency, demodulation type, expected data rate, etc. can be adjusted through the 'Modem Overview' interface.

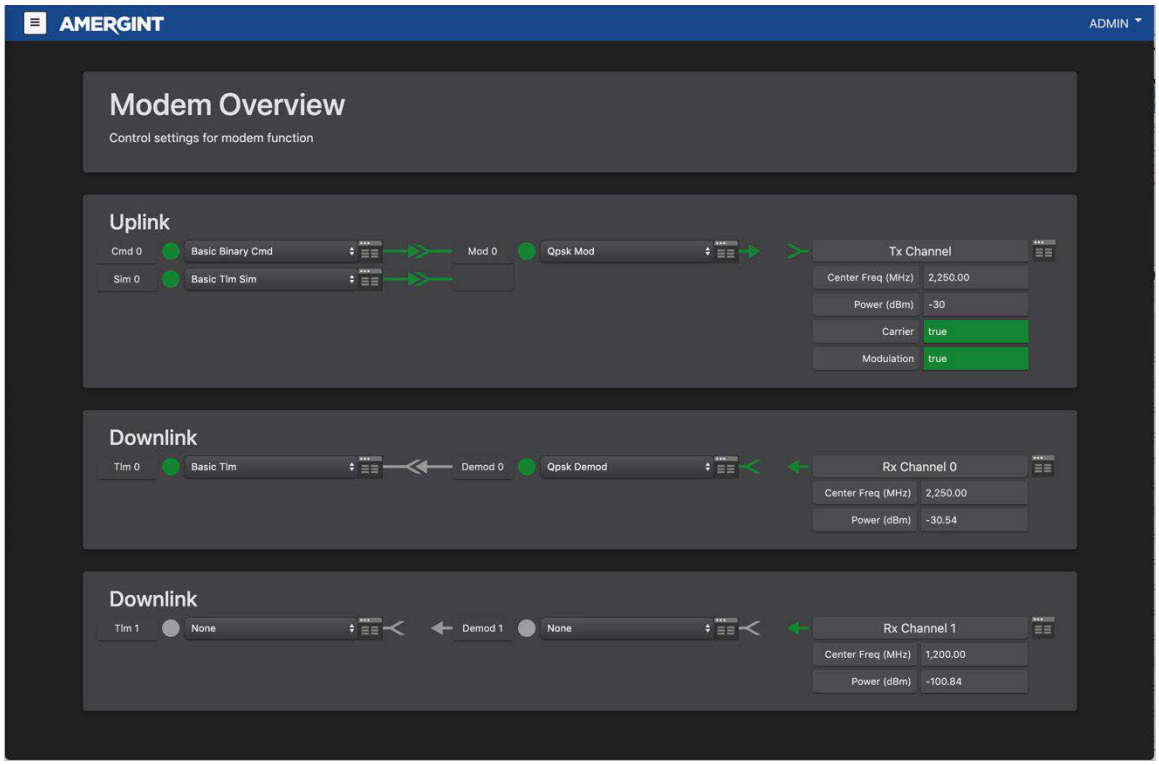

Figure 25. RUS-4 softFEP Modem Overview. Source: [22].

The rest of the editable SDR parameters are accessed through the ‘Software Devices (SwD) Overview’ module and are categorized and searchable by the name of the respective softFEP applications to which they apply, (i.e., satTRAC or Demod). A snapshot of the ‘SwD Overview’ module is pictured in Figure 26, which shows where different characteristics of the Received Bit Error Rate (RxBERT) module can be defined.

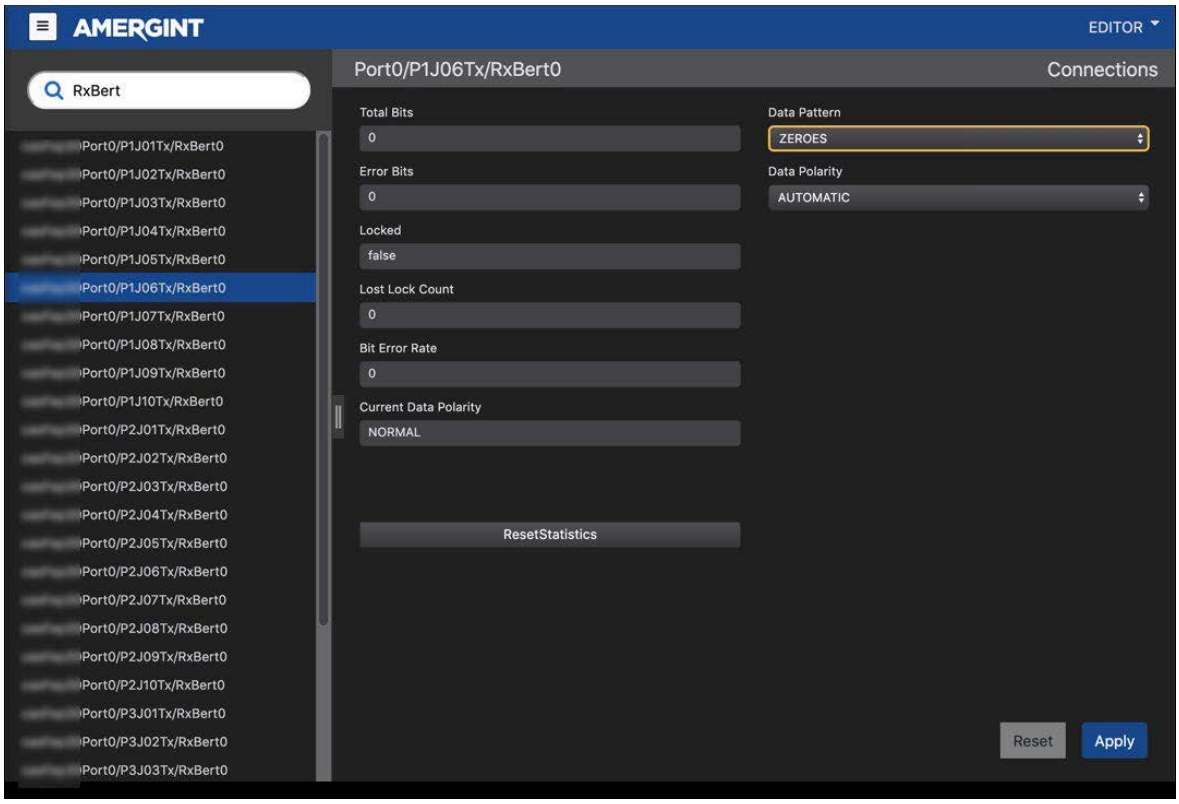

Figure 26. SwD Overview module window of the softFEP GUI. Source: [22].

Figure 27 is an overall block diagram showing how the various softFEP applications interface and combine to create the satTRAC SDR. The uplink or transmit chain on the top half of the diagram includes the applications for specifying a desired command or simulated telemetry message in bits. The ‘Modulator’ application is where the modulation type is selected, and the ‘Tx Out’ application is where the analog signal parameters are set and communicated to the Signal Converter for DAC and transmission. The receive chain on the bottom half of the diagram includes ‘Rx In’ applications which interface with each of the receive ports on the Signal Converter. As analog signals pass through the receive ports of the Signal Converter, they are mixed down to 70 MHz and digitally sampled. The digital data that represent the signals are communicated as Digital-IF through the ‘Rx In’ applications in the softFEP GUI, where the receiver tuning frequency is defined. The digital samples are then passed to a ‘Demod’ application where the modulation type and expected data rate are defined. After demodulation the bits are then passed to a ‘TLM’ application which further processes the baseband data. The ‘TLM’

application can be set to search for and sync onto a designated frame size with a designated marker. It can also decode a demodulated bit stream using one of the available coding schemes including the Consultative Committee for Space Data Systems (CCSDS) open-source protocol. The CCSDS encoding scheme is a popular format utilized by NASA and many other small-satellite operators [24]. A 'Spectrum Analyzer' module and 'IQ Constellation' are available to monitor the received signal and to assess how successfully the bits are being demodulated and decoded by the SDR. The 'Data Analysis' module allows bits to be captured and recorded at various points in the transmit and receive chains.

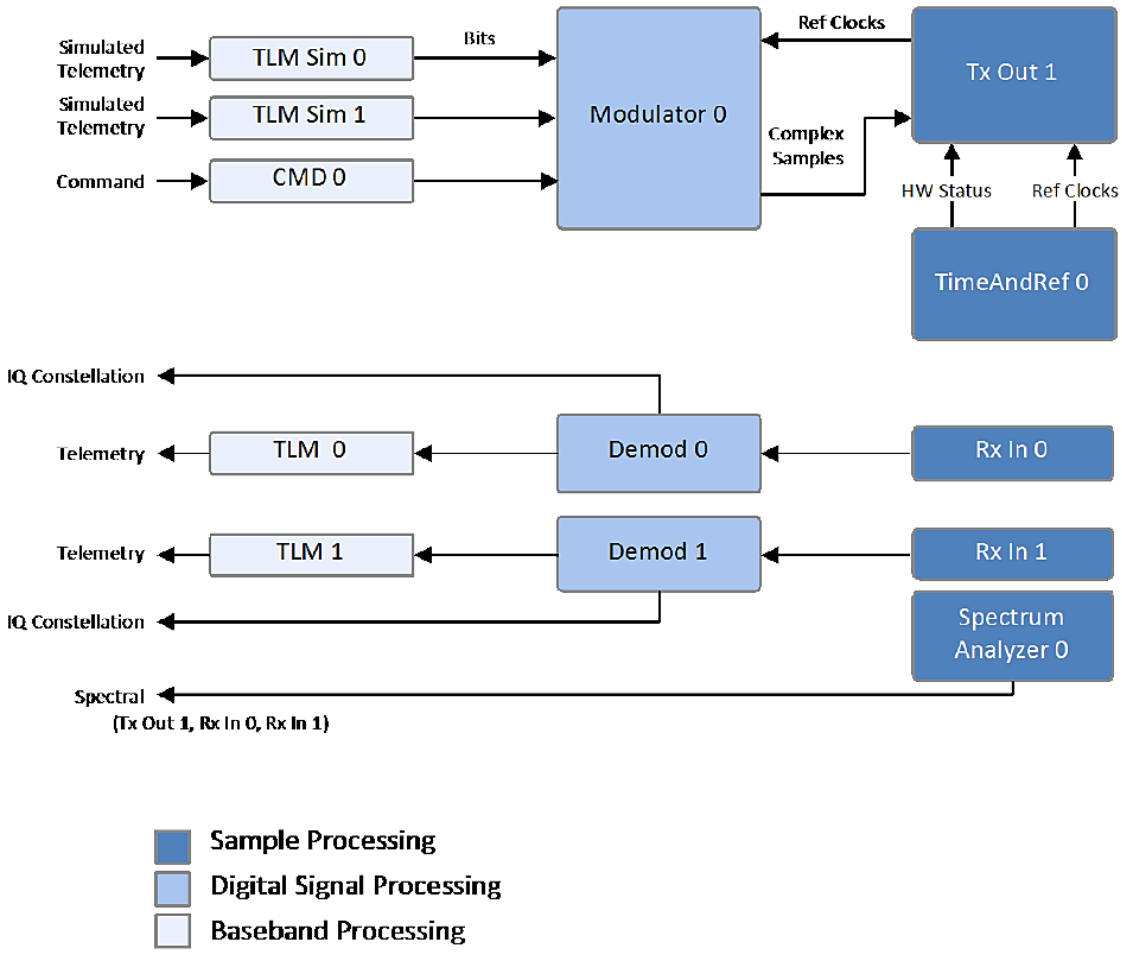

Figure 27. Diagram displaying the softFEP interface modules that connect to create the satTRAC SDR. Source: [22].

The AMERGINT satTRAC system is advertised to “connect at RF or IF frequency to support a wide range of satellite TT&C communications waveforms and signal processing functions” [23]. The technology employed inside RUS-4 is said to be heritage and utilized by many USG organizations, like NASA and the USAF, as well as industry partners like Raytheon, Lockheed Martin, and Northrop Grumman [25]. For this study, RUS-4 is categorized as a high-end commercial C2 system comparable to RUS-3 but with a heterodyne receiver architecture. The supposedly superior performance and operational characteristics of RUS-4 compared to the baseline USRP radios will be investigated and thoroughly evaluated through research and experimentation.

III. TEST OBJECTIVES, METHODOLOGY, AND EXPERIMENTATION

The purpose of this thesis research was to characterize the performance and parameters of the four RUS and evaluate their suitability for utilization in small satellite ground stations comparable to MC3 at NPS. Specifically, the performance of the two high-end commercial systems built by Kratos and AMERGINT was investigated and compared to the two baseline USRP systems. In order to accomplish this task, various tests and experiments were conducted to evaluate and compare the performance of each RUS. These experiments included test procedures designed to independently verify RF receiver parameters advertised in manufacturer specifications, as well as scenarios to evaluate other critical radio characteristics that were not explicitly documented or inherently transparent to potential customers and users. Some parameters and attributes were not successfully determined or verified, and these occurrences were noted. This evaluation also includes the assessment of the usability, effectiveness, flexibility, and support of each system's GUI, which are critical characteristics of controlling the parameters of the SDRs.

A. NOISE FIGURE

Noise figure is a quantification of the amount of internal noise generated by a system and is an indication of how much the receiver's electronic components degrade the SNR of an input signal of interest [9]. A receiver inside an ideal communication system would capture the signal of interest along with the ambient noise in the spectrum without adding internally generated noise during processing. In actuality, the internal electronic components used to receive, amplify, and capture RF signal create a quantifiable amount of energy that can be represented as the noise figure. Noise figure is a particularly important metric because the internal noise of a receiver is always present and physically unavoidable. A radio with a large noise figure will have difficulty detecting weak signals of interest in the received spectrum, and its amplifiers will continue to propagate the internally generated noise throughout the receiver chain.

Equation 3 describes how the noise figure (F) is defined as the ratio of the power of the input signal of interest (S_i) over the input noise (N_i) and the output signal (S_o) power over the output noise power (N_o) [19]. Noise figure expressed as a power ratio of input and output SNR is defined in Equation 3.

$$F = \frac{(S_i/N_i)}{(S_o/N_o)} \tag{3}$$

Equation 3. Noise Figure described as a ratio of input and output SNR [19].

The noise figure F can also be described as a relation of the noise temperature of the receiver, T_r, and a reference temperature T_0 which is the approximate noise temperature of Earth and equal to 290 Kelvin [1]. This definition of noise figure is expressed in Equation 4.

$$F = 1 + \frac{T_r}{T_0} \tag{4}$$

Equation 4. Noise Figure described as a ratio of the noise temperature of a receiver and the noise temperature of Earth from [1].

The noise figure experiments conducted during this thesis research were designed with the concepts of these equations in order to comparatively analyze the performance of the RUS as well as to independently verify their manufacturer-provided specifications.

1. Noise Figure Experiments

In order to determine the noise figure associated with the receivers of each of the four RUS, an experiment was designed to measure the amount of internal noise present in each system in a controlled environment. This was accomplished by capturing the energy of the complex baseband signal present at a receiver during a 'cold' or baseline condition, as well as during a 'hot' condition where a calibrated amount of noise was inserted into the DUT. The magnitude of the noise floor was measured during both the hot and cold conditions which were compared and from which a noise figure was calculated. Equation 5 describes the ratio of the hot and cold noise power values as in terms of the Y-factor [19].

$$Y = \frac{N_0^h}{N_0^c} \quad (5)$$

Equation 5. Definition of Y-factor term relating hot and cold noise power levels from [19].

After experimentation, the recorded files were analyzed with a MATLAB script written to compare the noise energy present during the cold and hot measurements and calculate noise figure in dB for the receivers of the RUS using the 'Y-factor' technique as described [19]. The noise figure measurements MATLAB script utilized can be found in Appendix A.

a. Baseband Sample Data Recording

During the noise figure experiments, a GNU Radio flowgraph was used to record files of the complex baseband sample data from the receivers of the baseline USRP systems RUS-1 and RUS-2. A snapshot of a portion of the SDR receiver model from GNU Radio Companion GUI is pictured in Figure 28. A depiction of the entire model can be found in Appendix B. The 'File Sink' block located at the end of the receiver chain enabled recording of the bit streams during experimentation.

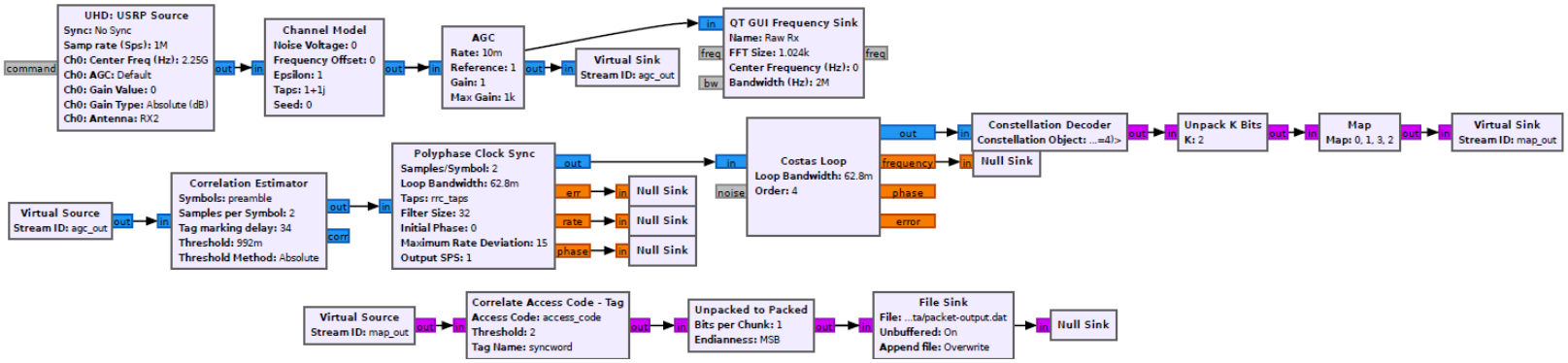

Figure 28. Snapshot of GNU Radio Companion receiver flowgraph used to operate RUS-1 and RUS-2 during experimentation.

The complex baseband samples from RUS-3 were captured utilizing the 'File Recorder' module inside the qRadio SDR GUI. Figure 29 is a snapshot of the module set to record data from the 'Digitizer' and save them onto the host computer as a '.dat' file. This directed the SDR to record a data file of the input receiver spectrum to the RFFE directly after digitization.

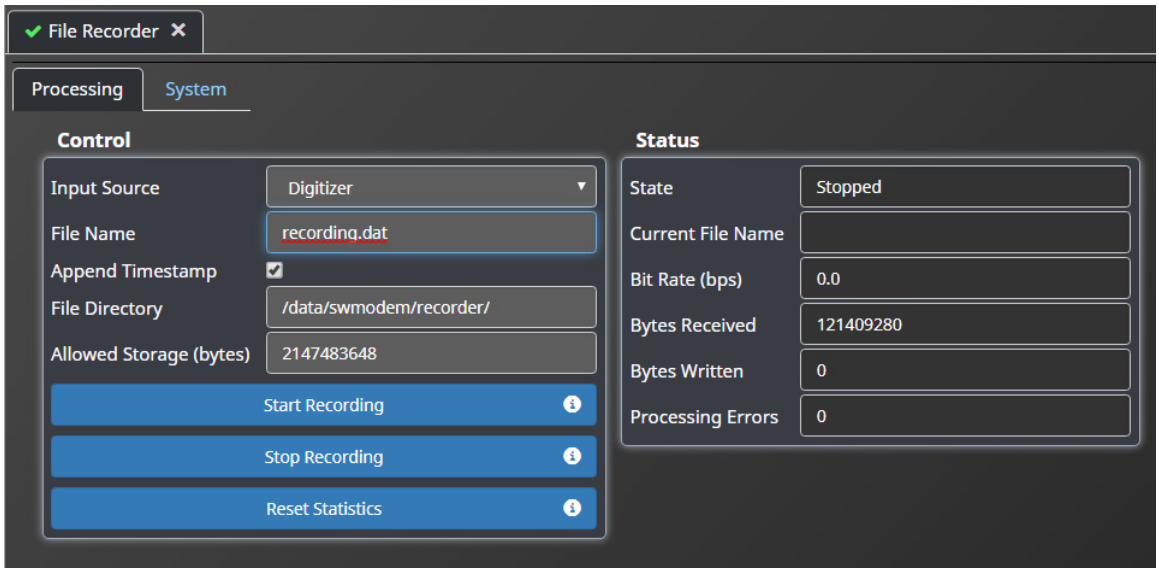

Figure 29. Snapshot of File Recorder module inside qRadio SDR GUI.

RUS-4 did not provide the capability to monitor or record baseband sample data as it passed through the radio, so it was unable to be evaluated during this experiment. The contractor AMERGINT noted that this capability could be acquired for an additional ~$20K.

b. Noise Figure Measurements

In order to accurately measure the amount of internal noise contributed by each system, the level of intentionally generated input noise during the hot conditions had to be consistent and quantifiable. This was accomplished through the employment of the HP 346B Noise Source pictured on the left of Figure 30, which was calibrated and measured with a FieldFox spectrum analyzer like one pictured on the right. When supplied with the

specified 28V of power, the HP 346B provided a consistent and repeatable level of noise energy into each device under test (DUT) during experimentation.

Figure 30. Picture of HP 346B Noise Source (left) and FieldFox Spectrum Analyzer (right) used during experimentation.

The output signal generated from the calibrated noise source was then fed through a cabled connection into an Amplifier Research LN1G11 low-noise preamplifier to raise the amplitude of the input noise signal to a level adequately above the cold condition noise floor. Figure 31 is a picture of this preamplifier hardware configured for the noise figure experimentation.

Figure 31. LN1G11 preamplifier used during noise figure measurements with HP 346B noise source attached.

Figure 32 is a block diagram illustration of the cable connected hardware in the lab setup used to conduct the noise figure experiments. This includes the equipment that was used to generate the calibrated level of noise and the RUS being evaluated during the current test, referred to as the DUT. The noise source was powered off for 'cold' measurements and powered on for 'hot' measurements. The DUT recorded data measurements of its receiver's input spectrum during the test.

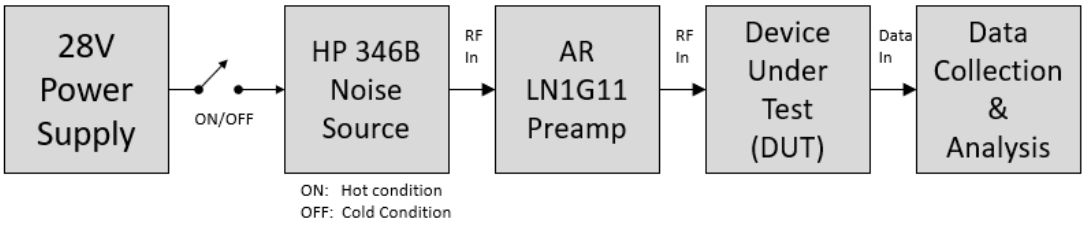

Figure 32. Diagram of noise figure measurements setup. Adapted from [19].

Cold measurements were recorded from RUS-1:3 with the HP 346B noise source connected but with the power supply off. These recorded data files captured the baseline reference noise temperatures and the respective noise floors of each system within the cold test configuration. Power was then supplied to the noise source and files were recorded

again while the test configuration remained the same. These collected data measurements represented the hot condition where the receivers' noise temperatures and respective noise floors now included internally generated noise in addition to the known amount of energy generated by the calibrated noise source. After experimentation, the collected data measurements were analyzed to calculate a noise figure value for each DUT. Results can be found in the corresponding Section A of Chapter IV.

B. PHASE NOISE

Phase noise is a phenomenon resulting from local oscillator instability referred to as time jitter inside a local oscillator [19]. The local oscillators provide the frequency reference used for RF mixing so any variability in their output will result in the production of signals that are out-of-phase. These phase differences culminate in the distortion of complex baseband signals called phase noise, which causes a spectral broadening or spreading effect on the signal of interest, which in turn increases noise distortion in the spectrum and reduces the receive SNR [19]. This spectral-broadening can also cause adjacent channel interference between out-of-band signals that can bleed into the receiver's band of interest [19]. Since an ideal local oscillator does not exist, phase noise is another unavoidable physical phenomenon experienced within any receiver.

1. Internally Generated Phase Noise Experiments

In an attempt to investigate the level to which internally generated phase noise degrades the performance of the four RUS, an experiment was developed to measure the effects of a test signal within a 1 Hz adjacent band [19]. This measurement quantifies the level of spectral broadening due to phase noise occurring at some frequency from the desired carrier frequency. This power is measured in dB below the carrier frequency of the signal of interest, or dBc and is depicted in Figure 33 located Δf from the center frequency.

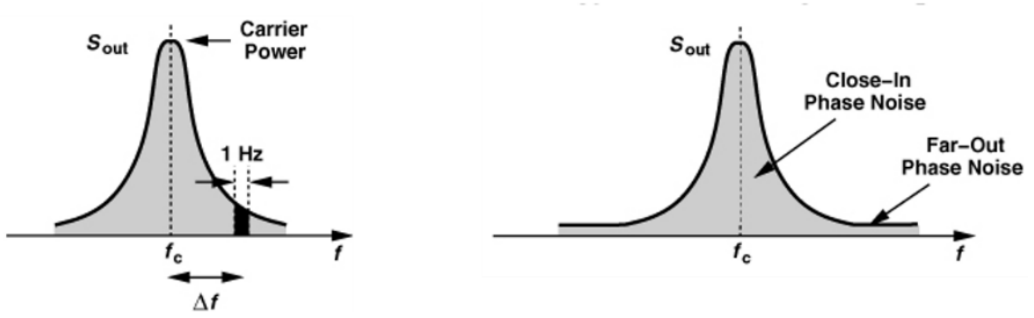

Figure 33. Phase noise measurement of 1 Hz band located Δf from signal of interest carrier frequency. Source: [19].

This phase noise measurement can be taken at various distances from the carrier frequency, and typical values are less than -100 dBc for a Δf equal to 1 MHz [19]. However, measuring the energy of a 1 Hz band is extremely difficult because no available RF instrumentation is specified with enough narrow-band resolution or accuracy that would result in useable measurements. In order to collect meaningful test data, the measurement band was widened to a level within the specification of the available RF instrumentation, recorded, and analyzed.

The designed experiments consisted of a pure sinusoidal signal, also referred to as a tone, located at 2250 MHz and generated by an Agilent, now owned by Keysight, 5171B signal generator like the one pictured in Figure 34. The center frequency was chosen to be 2250 MHz because that frequency is located in the center of the S-band downlink band utilized by MC3 ground stations and many others in the small satellite community.

Figure 34. Picture of signal generator comparable to the device used during experimentation. Source: [26].

The 2250 MHz tone was inserted at a power level of -50 dBm into the RF input ports of the four RUS during testing, the transceivers and SDR were tuned to receive the signal, and baseband sample data is recorded from each RUS. The baseband measurements recorded were analyzed to compare the total signal power of the spectrum compared to the power level of a test bandwidth located 1 MHz from the carrier frequency. The results of the test bandwidth were normalized to the specified 1-Hz test bandwidth to compute the phase noise in dBc and can be found in the corresponding Section B in Chapter IV [19].

2. Adjacent-Channel Phase Noise Experiments

Another experiment was constructed to investigate the effects of phase noise on a signal of interest resulting from a strong, adjacent-channel signal. This is a realistic scenario experienced by small-satellite operators that operate in a crowded frequency spectrum where many other adjacent channels may be present. The objective of the experiment was to incrementally degrade the link performance of an in-band signal of interest with the phase noise generated from another strong signal on the edge of the band of interest and observe the effects. The intent was such that, as the amplitude of the out-of-band tone was increased, the increased distortion would begin to overwhelm the reception of the signal of interest at a certain power level which could be measured and analyzed.

The signal of interest was chosen to be an unencoded 1 Mega-bit per second (1-Mbps) Quadrature Phase Shift Keying (QPSK) modulated PN11 bit sequence tuned to a center frequency of 2250 MHz and generated by RUS-3. The PN11 sequence is a well-known, repeating, pseudorandom-noise sequence of length 2047 bits that is recognizable by the RUS [19]. This signal was chosen because it represents a message that fits the parameters of a representative signal that should be able to be recognized and successfully detected by a small satellite ground station radio in an operational frequency band. RUS-3 was used as the standard signal generator for experimentation with the other three RUS and RUS-4 was used to replicate the experiment on RUS-3. RUS-4 was used to create the same test signal for RUS-3 during this experiment to eliminate any cross-contamination effects between the internal transmit and receive components of RUS-3. This deviation

from the signal source is deemed appropriate because both radios used the same 10 MHz reference clock to generate their transmitted signals.

A -30 dBm tone at 2250.5 MHz was produced with the 5175B signal generator to represent a strong adjacent-channel signal. The 1-Mbps QPSK signal of interest had a bandwidth of approximately 1 MHz so the tone represents an out-of-band signal that should be unaffected from filtering by the RFFE but attenuated by the baseband digital filter of the SDR [19]. The signal of interest and tone were combined with a Mini-Circuits ZX10-2-42-S+ RF coupler and fed into the receiver input of the four RUS during testing.

Figure 35. ZX10-2-42-S+ Mini-Circuits RF coupler used during experimentation. Source: [27].

In order to observe the effects of phase noise interference from the adjacent-channel tone, the input power was incrementally increased during the experiment to amplify the amplitude of the inserted signal. Figure 36 is an illustration of the described hardware and how it was connected for the experimentation.

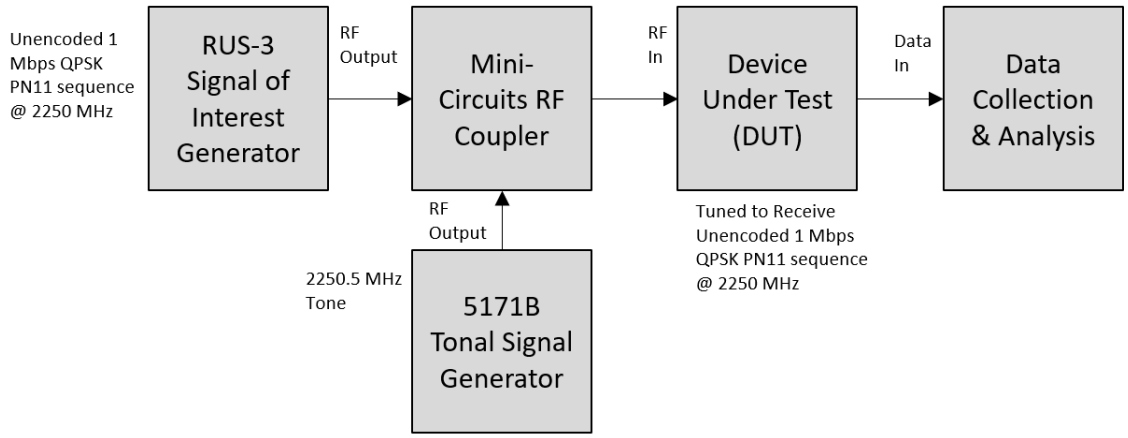

Figure 36. Diagram of adjacent-channel phase noise experimentation. Adapted from [19].

During experimentation, files of the received bits were recorded from the four RUS which were programmed to receive the signal of interest at 2250 MHz. BER at the RUS was calculated by analyzing the recorded files and counting the number of bit errors received from the expected 2047-bit PN11 sequence using a python script [19]. The script read the bits as they were received and recorded at the RUS and compared them to the known PN11 sequence being transmitted. RUS-3 and RUS-4 also provided IQ constellation plots and BER modules, as pictured in Figure 37. The plots were visually monitored during testing but were not used during analysis. These BER modules can be set to compare the received bits against a designated data pattern like PN11 and measure any errors.

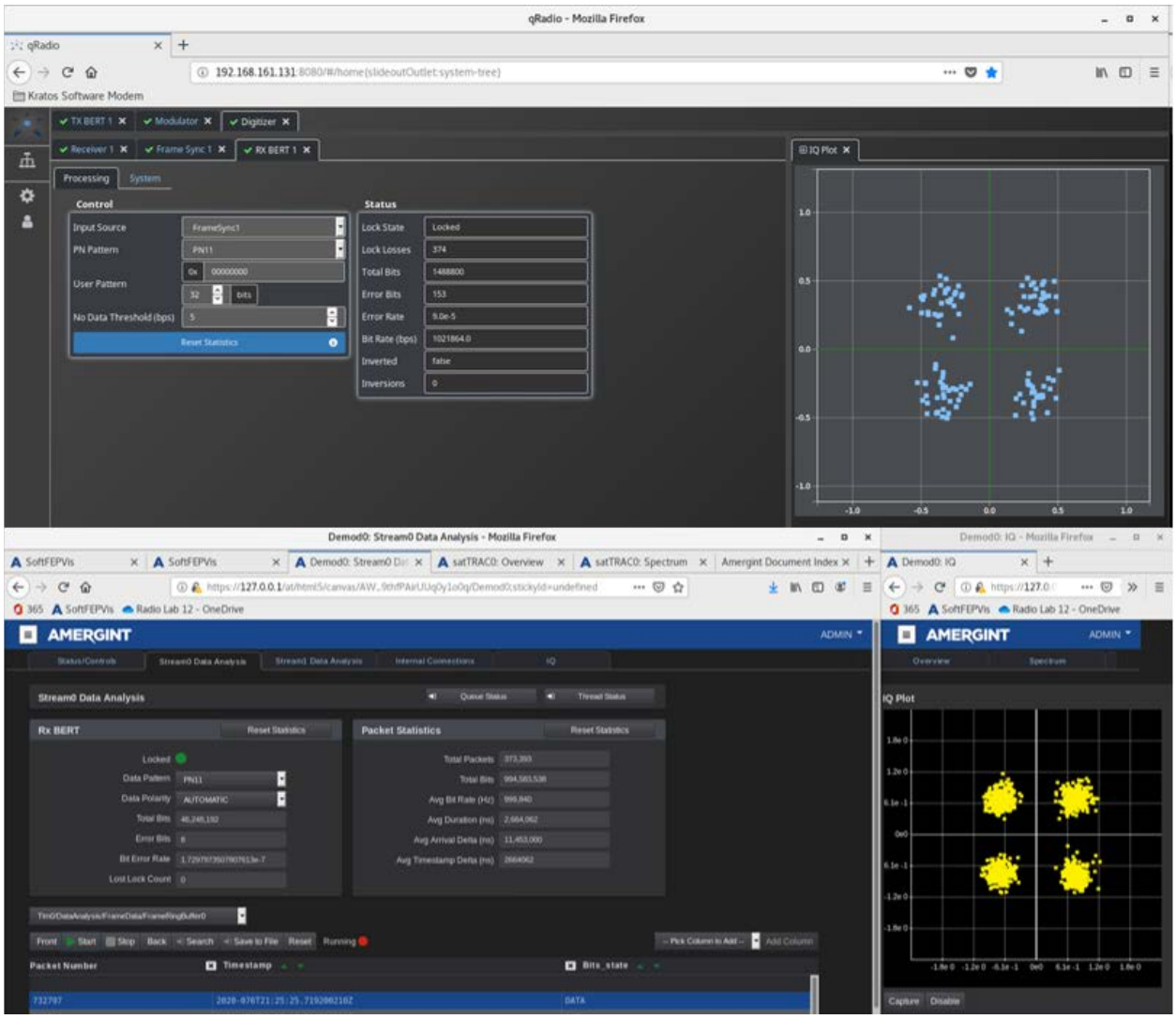

Figure 37. Snapshot of BER and IQ constellation plots provided by RUS-3 (top) and RUS-4 (bottom).

Results from adjacent-channel phase noise experimentation can be found in the corresponding Section B of Chapter IV.

C. IMAGE REJECTION

The process of receiving and digitally processing RF signals by SDR generally requires a mixing process to down-convert the incoming frequency to an IF. As discussed in Chapter II, there are multiple ways to execute this down-conversion process, including through a direct conversion radio architecture like RUS-1:3 or through a heterodyne radio

architecture like RUS-4. Both architectures involve the process of analog mixing which produces down-converted frequencies along with unwanted images that need to be removed before A/D conversion is performed.

A heterodyne receiver removes out-of-band energy from received signals with both a RF bandpass filter at the received spectrum before mixing down to an IF and filtering again with an IF bandpass filter before ADC [19]. This process is effective at removing sinusoidal images from the local oscillator but is still limited by interference from the image band. This image band created by the initial RF bandpass filter is centered at the frequency located at to double the IF (f_I) below the carrier (f_0) as described in Equation 6 [19].

$$f_{image} = f_0 - 2 f_I \tag{6}$$

A direct conversion receiver avoids the image banding effects experienced with heterodyne receivers, but instead includes unwanted contributions from the strong DC component from RF tuning and local oscillator imbalances that can interfere with SNR in the receive spectrum. These physical phenomena are expected given the selection of receiver architecture, but the magnitude of their effects on the RUS was investigated through experimentation.

1. Direct Conversion Receiver IQ Imbalance Measurements

As discussed in Chapter II, direct conversion receivers translate RF input signals immediately down to baseband by mixing the analog input with a complex sinusoid created by a local oscillator at the frequency of interest. The unavoidable existence of minute phase errors inside a local oscillator results in an imbalance between the quadrature components used to produce the baseband signals [19]. This effect, referred to as IQ imbalance, manifests as a reflection of the fundamental frequency in the negative frequency domain and is measured in dBc from the signal of interest [19]. Understanding the existence of this effect within the three direct conversion RUS, an experimental procedure was developed to compare the magnitude of IQ imbalance exhibited within each direct conversion radio receiver.

In the designed experiment, the receiver of the DUT was tuned to 2250 MHz and a real sinusoid tone was inserted with the 5171B signal generator at 2250.5 MHz, which in turn produced an IQ imbalance component in the received spectrum at 2249.5 MHz [19]. Figure 38 is an illustration of the how the hardware was connected for the experimentation.

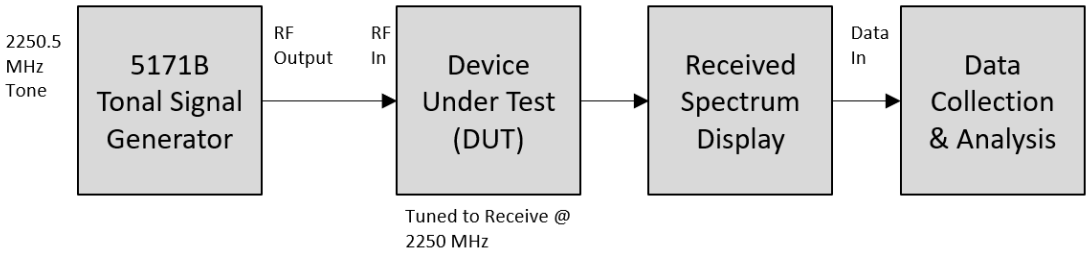

Figure 38. Diagram of IQ imbalance measurement experimentation. Adapted from [19].

The power of the tone from the signal generator was increased in 10 dB increments from -70 dBm to -20 dBm and measurements were recorded of the received spectrum at each step. The location of the IQ imbalance was noted at each step by observing the received spectrum and measured in dBc from the peak of the carrier frequency. These data points were analyzed to evaluate the magnitude of the IQ imbalance contribution over a range of amplitudes. The results of this experimentation can be found in Section C of Chapter IV.

2. Image Band Interference Measurements

An experiment was constructed to investigate the effects of image band interference on the received spectrum of the heterodyne receiver architecture of RUS-4. As described in Equation 6, the location of this image band is determined by the IF utilized during down-conversion, which is 70 MHz for RUS-4.

RUS-4 provides the user access to the down-converted analog IF through an 'IF In/Out' port located directly adjacent to the 'RF In' ports on the satTRAC Signal Converter. This allows the user to connect a spectrum analyzer to this port and view the IF of the

received spectrum that has been down-converted from RF after entering one of the receiver's input ports.

An experiment was designed to observe the amplitude of a test image in the IF domain created by an in-band tone from the 5171B signal generator. RUS-4 was tuned to receive a signal of interest at 2250 MHz, while a tone was inserted into the receiver at 2115 MHz, which is approximately equal to the expected carrier frequency minus twice the IF as described in Equation 6. The output power of the tone was varied, and the resulting image signal amplitude was observed at 70 MHz on a FieldFox Spectrum Analyzer tuned to receive from the IF domain. Figure 39 is an illustration of how the hardware was connected for the image band interference measurement experimentation.

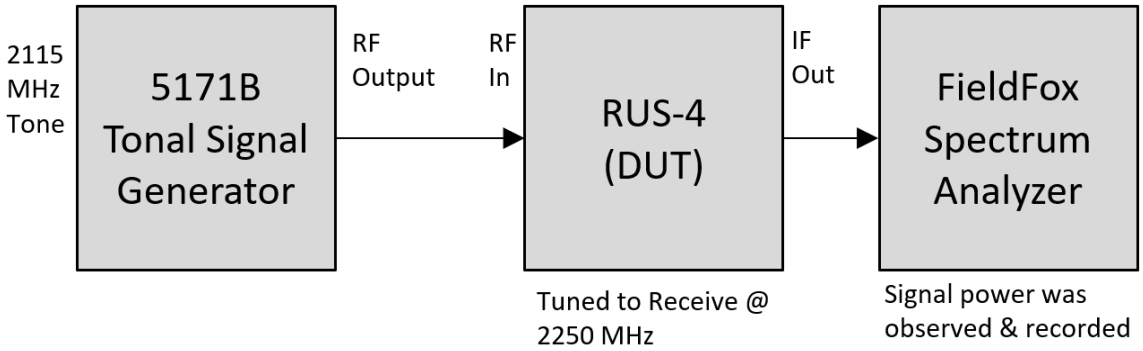

Figure 39. Diagram of image band interference measurement experimentation.

If the bandpass filter is operating effectively, the amplitude of the test image will be attenuated to a value much below the output power provided by the signal generator. The test signal was transmitted at a range of output powers and the resulting amplitudes were recorded to analyze the bandpass filter performance. The results and analysis of this experimentation can be found in Section C of Chapter IV.

D. RECEIVER SENSITIVITY

Receiver sensitivity is a measure of the ability of a receiver to detect a signal of interest in the presence of noise or other interfering signals. It can be defined as the

minimum required receive power P_r at an RFFE that produces a received SNR that culminates in a specified BER [19]. Receiver sensitivity is a characterization of how an SDR handles the combination of degrading effects like noise, non-linearity, and other interference when receiving a signal of interest. It is truly an end-to-end evaluation of how the SDR hardware and software performs signal detection. Receiver sensitivity is especially important for small satellite ground station receivers, which often are limited by low-gain antennas, weak incoming signals, and noisy receive spectra.

1. Receiver Sensitivity Measurements

An experiment was developed to excite the RUS receivers with a standard test signal over a range of decreasing input power in order to calculate an SNR and compare it to the measured BER at the receiver. A 1-Mbps QPSK modulated PN11 sequence at 2250 MHz was again used as the test signal because of the ability of the four RUS to easily recognize the well-known data pattern in the S-band frequency range. RUS-3 was used to generate the test signal for experimentation with RUS-1, RUS-2, and RUS-4; RUS-4 was used to generate the test signal for RUS-3. During experimentation the receive parameters of the DUT were programmed to receive the test signal and data files were recorded incrementally as the test signal was attenuated to calculate BER and evaluate receiver performance as the amplitude of the signal of interest decreased. The results of this experimentation can be found in the corresponding Section D of Chapter IV.

E. BER PERFORMANCE

Much like receiver sensitivity, BER is another end-to-end functional parameter that characterizes how well an SDR receives the information that has been transmitted from a desired source. Given that the power of a signal of interest is strong enough to be sensed and captured by a RFFE, BER also evaluates how well the analog signals have been demodulated and interpreted by the RFBE of the SDR. This process involves algorithms inside SDR that analyze demodulated bits and try to decipher which symbols they were intended to represent given the modulation and encoding scheme chosen at the transmitter of the source. A bit error can be the result of a bad decision made by one of these algorithms, mismatched signal parameters programmed into the SDR, or a manifestation

of the physical effects occurring in the transmission channel like noise or other interference. BER performance is agnostic to the cause of any bit errors and is instead a true measure of how well the bits of received message match what was transmitted from the transmission of the source.

1. BER Performance Measurements

An experiment was developed to transmit the standard test signal, an unencoded 1-Mbps, QPSK-modulated PN11 sequence, combined with noise energy from the HP 346B calibrated noise source over a range of input power into the DUT to comparatively measure the BER performance of the four RUS. The RUS receivers under test were programmed to receive the test signal and binary output files were recorded to independently calculate the measured BER.

The HP 346B calibrated noise source was used to generate approximately -59 dBm of noise when powered on and was combined with the test signal using a ZX10-2-42-S+ Mini-Circuits RF coupler. RUS-3 was used as the test signal generator for experimentation with the other three RUS, and RUS-4 was used to conduct experimentation on RUS-3. Figure 40 is an illustration of the hardware configuration used during the experimentation.

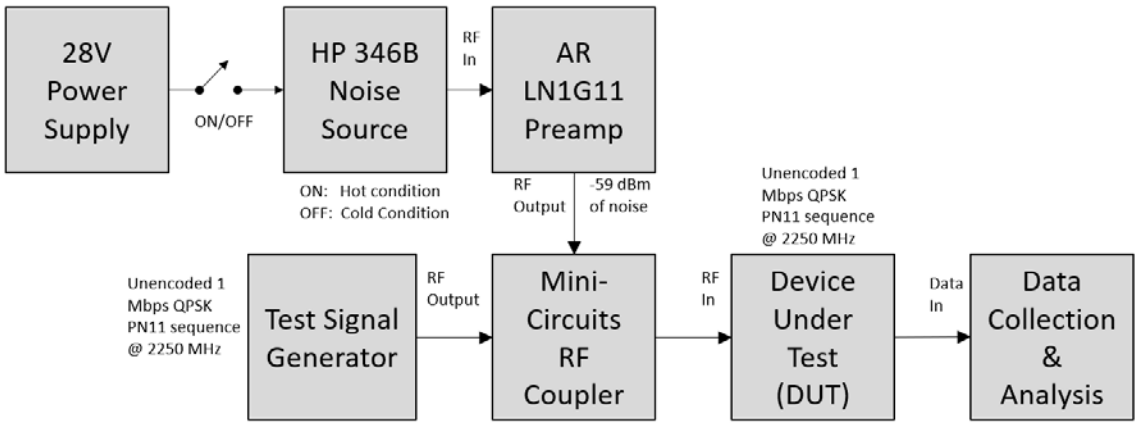

Figure 40. Diagram of BER performance measurement experimentation. Adapted from [19].

The intent of the designed experiment was to incrementally decrease the input power of the test signal while maintaining a constant level of input noise such that the SNR would also decrease incrementally to a level that would induce bit errors in the RUS. This effect could be measured and analyzed to compare the BER performance of the RUS. The results of this experimentation can be found in Section E of Chapter IV.

F. DYNAMIC RANGE

Dynamic range is a characteristic that describes the capacity of a receiver to perceive a small signal of interest in the presence of other large unwanted co-channel signals [11]. More specifically, dynamic range is a measure of a receiver's ability to maintain its linearity over a wide range of signal powers [9]. The spectrum captured by a radio receiver contains the signal of interest and potentially many other interfering signals that can be much stronger than the signal of interest [7]. A unique challenge for SDR receivers is the necessity to attempt to keep the input RF bandwidth as wide as possible while also preventing high power adjacent signals from interfering with narrow band channels [12]. This drives the requirement that the system's digitizer must have enough dynamic range to process both the strong and the weak signals that have been received [7]. The ideal digitizer would provide about 6 dB of dynamic range per bit of resolution in order to ensure an adequate SNR of the intended signal at the receiver [7]. All four RUS employ a digitizer with a resolution of 12 bits, but any deviations in performance between the various hardware components is unknown.

One quantification of this attribute is through the measurement of the magnitude of a radio's spurious free dynamic range (SFDR). SFDR represents the difference in power between the noise floor and the necessary signal power required to create a third-order distortion component above the noise [12]. This attribute was investigated with the four RUS through some preliminary experiments, but as reported with the phase noise experimentation, hardware components inside the radio receivers seemed to be hardwired to avoid non-linearity effects. This behavior created difficulties when attempting to consistently create the third-order distortion component necessary to measure the SFDR.

This characteristic is an important parameter for SDR and should be further investigated in future work.

G. GUI PERFORMANCE AND EXPERIENCE

Software functionality, usability, and supportability associated with the four RUS was analyzed through experience with the systems during experimentation for this research. The flexibility of each SDR was investigated and the ease-of-use was compared while learning about and operating each of the four RUS. Another aspect of the evaluation was the ability of each RUS to support various operational waveforms and coding schemes used by MC3 and other small-satellite operators across private industry and academia. The level of difficulty associated with manipulating the systems through their respective GUI was also compared.

Each of the RUS was accompanied by their own set of documentation detailing characteristics of the respective system and how to operate and change parameters within the GUI. The documentation was evaluated for its usefulness and used as reference material during test set-up and experimentation.

RUS-1 and RUS-2 were operated through the open-source GNU Radio software toolkit utilized by many in academia and the small-satellite community. RUS-2 and RUS-3 were operated with their own proprietary software applications which were provided with the hardware upon delivery of the systems.

H. MANUFACTURER SPECIFIED PARAMETERS

Table 2 is a compilation of the published specifications for the four RUS, some of which were evaluated through the experimentation of this thesis.

Table 2. Available SDR parameters as specified by manufacturer documentation.

Parameter	Units	RUS-1	RUS-2	RUS-3	RUS-4
Manufacturer	**N/A**	National Instruments	Ettus Research	Kratos (RT Logic)	AMERGINT
Hardware Device	**N/A**	USRP-2922	USRP B205mini-I	SpectralNet Lite Digitizer SpectralNet Server (Dell R440)	satTRAC Signal Converter satTRAC Server (Dell R740)
System Description	**N/A**	Baseline USRP Standard	Common RF System-on-Chip (RFSoC)	Unevaluated High-End Commercial System	Unevaluated High-End Commercial System
Software	**N/A**	GNU Radio	GNU Radio	SpectralNet (Digitizer) qRadio (Baseband SDR)	satTRAC (Signal Converter) softFEP (SDR)
Cost	**$**	3,182.00	942.00	26,600	82,300
Tx Frequency Range	**MHz**	400 – 4400	70 – 6000	50 – 2500	Test Loop: 1690 – 2400 L-Band: 1750 – 1850 S-Band: 2025 - 2120
Max Tx Power	**dBm**	20	20	-5	10
Tx Gain Range	**dB**	31	89.8	89	60
Tx Dynamic Range	**dB**	74	74	74	80
Tx Bandwidth	**MHz**	20 (16-bit)/ 40 (8-bit)	56	10	40
Output Spurious	**dBc**	*	*	-40	-65
Rx Architecture	**N/A**	Direct Conversion	Direct Conversion	Direct Conversion	Heterodyne
Rx Hardware Chip	**N/A**	SBX-40	AD9364	AD9364	Discrete Components
Rx Frequency Range	**MHz**	400 – 4400	70 – 6000	50 – 2500	Test Loop (S): 1690 – 2400 Test Loop (L): 950 – 1450 L-Band: 1150 – 1250 S-Band: 2200-2300
Rx Power	**dBm**	0 (max)	-15 (max)	-60 to 0	-100 to -23
Rx Bandwidth	**MHz**	20	56	10 (qRadio)	40
Noise Figure	**dB**	7	8	7	8
In-Band Spurious	**dBc**	*	*	-50	-59

THIS PAGE INTENTIONALLY LEFT BLANK

IV. RESULTS AND ANALYSIS

The research and experimentation accomplished during this thesis work culminated in the following results and analysis. The experiments described in Chapter III were designed to investigate critical RF and SDR system parameters and characteristics that could potentially affect the functional performance of conducting effective small-satellite C2 communications. This research also included the assessment of performance, functionality, and ease-of-use of the GUIs used to operate the RUS.

A. NOISE FIGURE MEASUREMENTS RESULTS

As described in Chapter III, data files were recorded from each SDR receiver with the connected noise source powered off to measure the noise temperature in a cold state. Data files were recorded again with the noise source powered on, which represented the noise temperature in a hot condition. These hot and cold measurements captured from the three RUS were compared and analyzed with the 'Noise_Figure_Measurements.m' MATLAB script, which can be found in Appendix A. The script read the recorded complex baseband data, measured the energy present during both states, and calculated a noise figure value in dB using the Y-factor method outlined in Equation 5.

Table 3 contains the noise figure values specified by the SDR manufacturers as well as the measured values obtained through the experimentation of this thesis. As stated previously, the noise figure of RUS-4 was not measured through this experimentation due to the lack of access to satTRAC baseband sample data.

Table 3. Specified and measured values of the noise figure of the four RUS.

RUS	Manufacturer	Receiver Component	System Description	Specified Noise Figure (dB)	Measured Noise Figure (dB)
RUS-1	National Instruments	SBX-40 RF Daughterboard	Baseline USRP Standard	7	5.55
RUS-2	Ettus Research	B205mini (AD9364 Chip)	Common RF System-on-Chip (Soc)	8	6.32
RUS-3	Kratos	SpectralNet Lite Digitizer (AD9364 Chip)	High-End Commercial System	7	5.6
RUS-4	AMERGINT	satTRAC Signal Converter (super-heterodyne)	High-End Commercial System	8	*

1. RUS Experimental Data

The following figures are snapshots of the MATLAB output code and plots from the script used to calculate the noise figure values for RUS-1:3. Tables 4:7 contain parameters set within each RUS during the experiments as well as some of the data collected.

a. RUS-1 Noise Figure Measurements Results

Figure 41 and Table 4 list the results from the noise figure measurements experimentation with RUS-1.

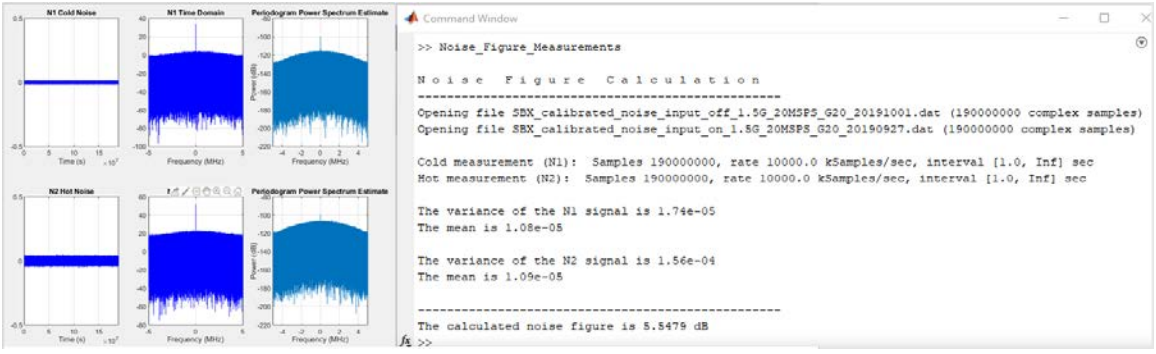

Figure 41. RUS-1 noise figure results from output of MATLAB Script.

Table 4. Programmed parameters and measured values from RUS-1 noise figure measurements. Adapted from [19].

Parameter	Symbol	Value	Notes
Tuning Frequency (MHz)	f_c	1500	Value chosen between UHF/S-Band Downlink Freq
Input Gain (dB)	G	20	
Sampling Rate (MS/sec)	f_s	20	Highest sampling rate for 1GbE connection
'Cold' State Noise Energy (J)	N_0^c	1.74×10^{-5}	Output noise energy with noise source powered off
'Cold' State File Name	SBX_Calibrated_noise_input_off_1.5G_20MSPS_G20_20191001.dat		
'Hot' State Noise Energy (J)	N_0^h	1.56×10^{-4}	Output noise energy with noise source powered on
'Hot' State File Name	SBX_Calibrated_noise_input_on_1.5G_20MSPS_G20_20190927.dat		
Y-Factor (unitless)	Y	8.97	$Y = N_0^h / N_0^c$
Noise Figure (dB)	F	5.5	From MATLAB script as pictured in Figure 31

b. RUS-2 Noise Figure Measurements Results

Figure 42 and Table 5 list the results from the noise figure measurements experimentation with RUS-2.

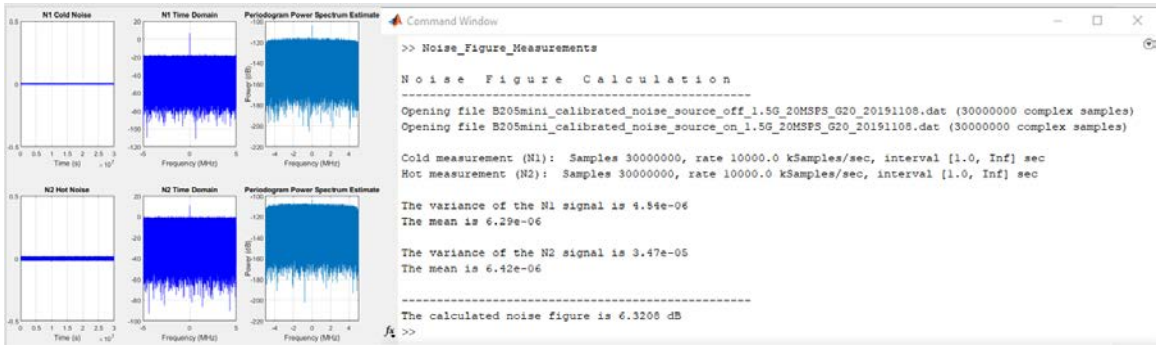

Figure 42. RUS-2 noise figure results from output of MATLAB Script.

Table 5. Programmed parameters and measured values from RUS-2 noise figure measurements. Adapted from [19].

Parameter	Symbol	Value	Notes
Tuning Frequency (MHz)	f_c	1500	Value chosen between UHF/S-Band Downlink Freq
Input Gain (dB)	G	20	
Sampling Rate (MS/sec)	f_s	20	Highest sampling rate for 1GbE connection
'Cold' State Noise Energy (J)	N_0^c	4.54×10^{-6}	Output noise energy with noise source powered off
'Cold' State File Name	B205mini_Calibrated_noise_input_off_1.5G_20MSPS_G20_20191108.dat		
'Hot' State Noise Energy (J)	N_0^h	3.47×10^{-5}	Output noise energy with noise source powered on
'Hot' State File Name	B205mini_Calibrated_noise_input_on_1.5G_20MSPS_G20_20191108.dat		
Y-Factor (unitless)	Y	7.64	$Y = N_0^h / N_0^c$
Noise Figure (dB)	F	6.32	From MATLAB script as pictured in Figure 32

c. RUS-3 Noise Figure Measurements Results

Figure 43 and Table 6 list the results from the noise figure measurements experimentation with RUS-3.

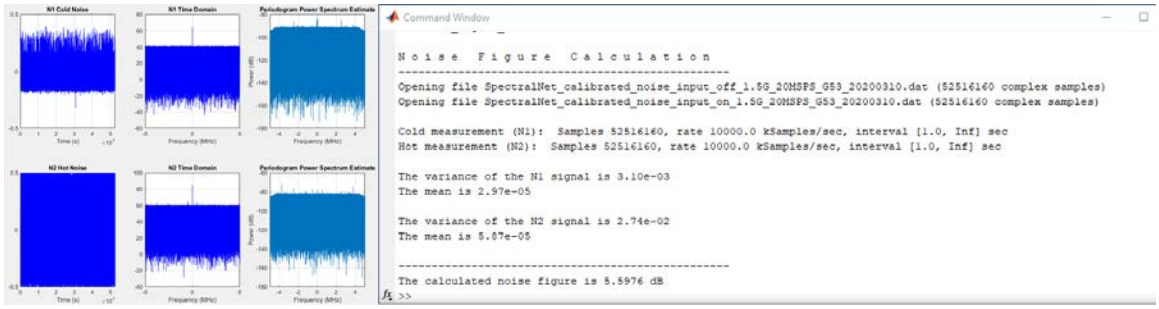

Figure 43. RUS-3 Noise Figure results from output of MATLAB Script.

Table 6. Programmed parameters and measured values from RUS-3 noise figure measurements. Adapted from [19].

Parameter	Symbol	Value	Notes
Tuning Frequency (MHz)	f_c	1500	Value chosen between UHF/S-Band Downlink Freq
Input Gain (dB)	G	53	Optimal value during cold state from SpectralNet
Sampling Rate (MS/sec)	f_s	20	Value set to mirror RUS-1/RUS-2 experiments
'Cold' State Noise Energy (J)	N_0^c	3.1×10^{-3}	Output noise energy with noise source powered off
'Cold' State File Name	B205mini_Calibrated_noise_input_off_1.5G_20MSPS_G20_20191108.dat		
'Hot' State Noise Energy (J)	N_0^h	2.74×10^{-2}	Output noise energy with noise source powered on
'Hot' State File Name	B205mini_Calibrated_noise_input_on_1.5G_20MSPS_G20_20191108.dat		
Y-Factor (unitless)	Y	8.84	$Y = N_0^h / N_0^c$
Noise Figure (dB)	F	5.6	From MATLAB script as pictured in Figure 33

2. Analysis of Noise Figure Measurements Results

Results from the noise figure measurement experimentation indicate that the all three of the evaluated RUS operate at, or better than, their manufacturer-specified values. As stated, the noise figure of RUS-4 was unable to be independently measured and verified against the contractor's provided specifications in the same manner as RUS-1:3. There was no evidence obtained through anecdotal experience operating RUS-4 that indicated it would not meet its specified value as well.

The results obtained through the experimentation uncovered no appreciable disparity in receiver performance in terms of noise figure. This fact may be true because the three RUS evaluated employ the same direct conversion receiver architecture and possibly use similar grade receiver components.

Data collection limitations with RUS-4 aside, it appears that all four RUS generate an acceptably low amount of internal noise, in line with industry standards, such that it does not significantly degrade the receive SNR or performance of the SDR. Nevertheless, each SDR's noise figure value must be considered when calculating the required link margin for a potential satellite operator.

B. PHASE NOISE MEASUREMENTS RESULTS

The phase noise measurements were not successfully completed due to time and laboratory access constraints resulting from the COVID-19 pandemic. These measurements should be obtained in future research and testing.

1. Internally Generated Phase Noise Measurements Results

The experiment described in Chapter III to measure internally generated phase noise was unable to be completed successfully. The experiment, which involves measuring the effects of a test signal within a 1 Hz adjacent band, should be included in future work to continue this research.

2. Adjacent-Channel Phase Noise Measurements Results

The objective of this experiment described in Chapter III was to observe the incremental degradation of the RUS receiver performance due to the presence of an increasing amount of phase noise interference. This effect was produced by raising the amplitude of a strong tone inserted into an adjacent-channel. It was expected that this interference would result in degradation that would be observed to be gradual and measurable. It was also expected that this gradual degradation would continue to a level at which the receiver would become completely overwhelmed by the phase noise interference. This varying BER performance and threshold would be observed, recorded, and compared between the four RUS.

As the amplitude of the adjacent-channel tone was increased, instead of observing a gradual drop-off of receiver performance in the form of increased BER, all four of the RUS received the signal of interest without bit errors. This behavior continued until the interfering tone was raised to an amplitude where the receiver broke lock and tried to demodulate the tone as opposed to the programmed signal of interest. As it turns out, the four RUS exhibited a similar behavior and seemingly decreased the level of input receiver gain automatically as the amplitude of the adjacent-channel tone was increased. This effect occurred even though the gain was manually set to a static value at the SDR of the four RUS.

This autonomous response is probably an artifact of the internal RF receiver hardware in the devices which were probably designed to prevent non-linearity effects and the generation of any appreciable phase noise. This is another indication that the four RUS likely contain RF components of comparable quality that perform similarly.

Because of this behavior, no meaningful data was collected to quantify the phase noise contributions in each RUS. Although phase noise is inherently present within the four systems under test, it did not appear to significantly affect the overall performance of the radios to a level that was able to be measured and analyzed through the experimentation of this thesis.

C. IMAGE REJECTION MEASUREMENTS RESULTS

The image rejection performance of the four RUS was evaluated through experimentation while considering the different receiver architectures utilized by the four RUS. Direct conversion and super-heterodyne architectures differ in how they handle the unavoidable effects of unwanted images created during analog mixing, and the effects and performance were investigated.

1. IQ Imbalance Measurements Results

During experimentation the amplitude of IQ imbalance was measured in units of dBc from the peak of the test tone inserted at 2250.5 MHz. The input power was increased from -70 to -20 dBm in 10 dB steps. The receiver input gain was also varied to observe any effects. The noise floor of the DUT was also recorded during testing as a reference data point. The results from the three direct conversion RUS receivers that were evaluated are listed in Tables 7:9.

a. RUS-1 IQ Imbalance Results

Table 7 lists the results from the IQ imbalance experimentation with RUS-1.

Table 7. RUS-1 recorded measurements from IQ imbalance experimentation. Adapted from [19].

Input Power (dBm)	Receiver Gain (dB)	Noise Floor (dB)	IQ Imbalance (dBc)
-70	0	-127.0	-37
-70	10	-125.2	-37
-70	20	-124.4	-38.8
-60	0	-127.0	-39.2
-60	10	-125.2	-39.2
-60	20	-124.4	-40.4
-50	0	-127.0	-39.9
-50	10	-125.2	-39.9
-50	20	-124.4	-40.5
-40	0	-127.0	-40.9
-40	10	-125.2	-40.9
-40	20	-124.4	-40.7
-30	0	-127.0	-40.5
-30	10	-125.2	-40.5
-30	20	-124.4	-40.3
-20	0	-127.0	-40
-20	10	-125.2	-40
-20	20	-124.4	-40.9

Results show that the IQ imbalance experienced by RUS-1, which utilizes the SBX RF daughterboard, is consistently measured to be approximately -40 dBc, regardless of the values of input power or receiver gain [19]. This observation implies that the algorithms employed by RUS-1 resulted in a consistent magnitude of IQ imbalance during operation.

b. RUS-2 IQ Imbalance Results

Table 8 lists the results from the IQ imbalance experimentation with RUS-2.

Table 8. RUS-2 recorded measurements from IQ imbalance experimentation. Adapted from [19].

Input Power (dBm)	Receiver Gain (dB)	Noise Floor (dB)	IQ Imbalance (dBc)
-70	70	-82.7	-37.6
-60	70	-84.3	-63.4
-60	60	-94.4	-70.5
-50	60	-94.4	-29.2
-60	50	-103.2	-77.5
-60	40	-111	-89.5
-50	40	-106	-21.5
-50	30	-110.6	-93.5
-50	30	-110.6	-71.0

Results show that the IQ imbalance experienced by RUS-2, which utilizes the AD9364 transceiver chip, fluctuates between -29.2 to -89.5 dBc in a seemingly random manner. Most of the IQ imbalance measurements are more than -60 dBc, which implies that the AD9364 chip inside RUS-2 employs an algorithm to compensate or correct for the presence of the interference. This algorithm seems to fail when stressed into certain, and unforeseeable, conditions, resulting in IQ imbalance measurements much closer in magnitude to the test signal.

c. RUS-3 IQ Imbalance Results

Table 9 lists the results from the IQ imbalance experimentation with RUS-3.

Table 9. RUS-3 recorded measurements from IQ imbalance experimentation. Adapted from [19].

Input Power (dBm)	Receiver Gain (dB)	Noise Floor (dB)	IQ Imbalance (dBc)
-70 to -20	0	-75	unmeasurable
-70 to -20	10	-85	unmeasurable
-70 to -20	20	-95	unmeasurable
-70 to -20	30	-105	unmeasurable
-70 to -20	40	-108	unmeasurable
-70 to -20	50	-112	unmeasurable

Results show that the IQ imbalance experienced by RUS-3, which also utilizes the AD9364 transceiver chip, is suppressed and unmeasurable at all input power and gain values during experimentation. Although RUS-3 employs the same AD9364 as RUS-2, it appears that the qRadio SDR utilizes additional algorithms inside the RFBE to compensate for any IQ imbalance interference in the received spectrum.

2. Analysis of IQ Imbalance Measurements Results

Results from the three direct conversion RUS receivers evaluated during experimentation were unique and uncovered interesting information about each SDR device. RUS-1 seems to perform consistently with an IQ imbalance measured to be approximately -40 dBc. RUS-2 greatly exceeded the performance of RUS-1 during most of the experimentation, but the internal algorithms that compensate for the IQ imbalance were seemingly ineffective in certain, unpredictable conditions. RUS-3 exhibited superior performance through the implementation of effective algorithms that seemingly eliminate the IQ imbalance contributions altogether. The elimination of this IQ imbalance interference with RUS-3 is a significant achievement that negates one of the major performance drawbacks accepted while utilizing a direct conversion receiver architecture [19].

3. Image Band Interference Measurements Results and Analysis

The power of the test image at IF created by the in-band tone was recorded by observing the IF domain with the FieldFox spectrum analyzer. This power level was recorded at three different increments of output power from the 5171B signal generator. The programmed and recorded values appear in Table 10.

Table 10. Programmed and recorded values during image band interference measurements experimentation with RUS-4.

Output Power (dBm)	IF Power (dBm)	Delta (dBm)
-20	-69.1	49.1
-30	-77.2	47.2
-40	-87.3	47.3

As illustrated in Table 10, the amplitude of the IF test signal was consistently measured to be at least 47 dBm below the power of the generated output. This indicates that the bandpass filter inside the RFFE of RUS-4 effectively attenuates the image signal generated during the experimentation. The results from this experimentation imply that the receiver performance of the heterodyne hardware inside RUS-4 is not limited by interference in the image band created during down-conversion of RF signals.

D. RECEIVER SENSITIVITY MEASUREMENTS RESULTS

Binary data files were recorded from the four RUS during the receiver sensitivity measurements to capture the demodulated bits as they were interpreted by the DUT during experimentation. These data files were analyzed with a MATLAB script to compare the received bits sequentially against the transmitted PN11 data pattern to measure any bit errors and estimate a corresponding BER. A target BER of 10^{-5} was chosen for this experimentation and the minimum received power results from all four RUS can be found in Table 11. The BER results were plotted against the measured received power by the RUS and plotted in Figure 44.

1. RUS-1:4 Receiver Sensitivity Measurement Results and Analysis

Table 11 and Figure 44 contain the results from the receiver sensitivity experimentation with the four RUS.

Table 11. Receiver sensitivity results in terms of minimum received power required to achieve designated BER. Adapted from [19].

Target BER	RUS-1 P_r (dBm)	RUS-2 P_r (dBm)	RUS-3 P_r (dBm)	RUS-4 P_r (dBm)
10^{-5}	-94.5	-90.5	-89	-96

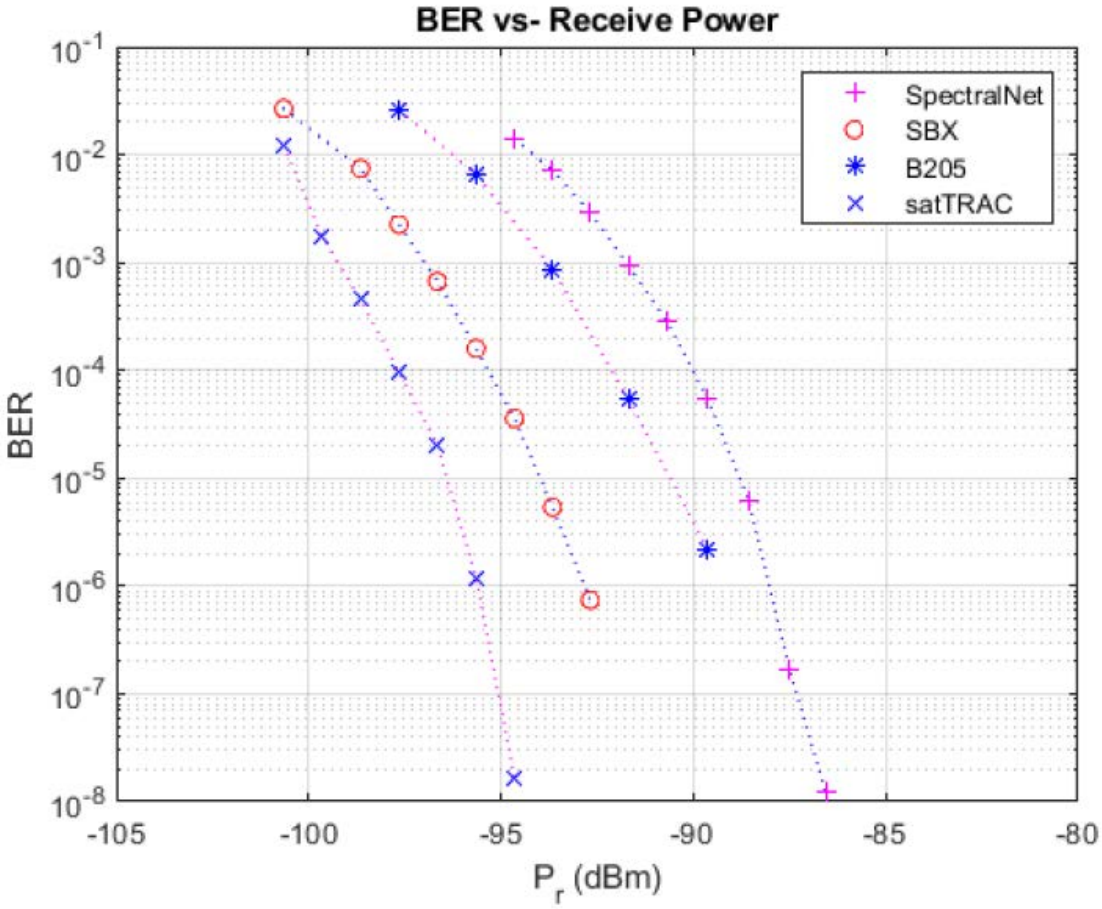

Figure 44. Receiver sensitivity measurements results for RUS-1 (SBX), RUS-2 (B205), RUS-3 (SpectralNet), and RUS-4 (satTRAC). Source: [19].

Results from the receiver sensitivity measurements experimentation yielded some interesting information about the four RUS. As expected, the super-heterodyne receiver inside RUS-4 exhibited superior receiver sensitivity performance over the three direct conversion receivers. This performance is reflected in Figure 44 as well as in Table 11, with RUS-4 exhibiting the lowest minimum received power value in of -96 dBm required

to achieve target BER of 10^{-5}. The baseline USRP device RUS-1, which contains the SBX RF daughterboard, also proved to contain a more sensitive receiver than the two newer RUS which contain the AD9364 transceiver chip. The recorded minimum required received power level of -94 dBm in Table 10 is very close to the performance of RUS-4 and nearly 5 dBm better than the other two RUS. The recorded values of RUS-2 and RUS-3 in Table 11 are similar as expected due to the common AD9364 transceiver RFFE component. All four RUS performed consistently across the range of experimentation and provided comparable but distinguishable results.

It should be noted that although receiver sensitivity is an important parameter for a radio receiver, a small satellite ground station could compensate for any deficit in received power to the SDR by utilizing a larger antenna or a higher-gain LNA to amplify the signal into the receiver.

E. BER PERFORMANCE MEASUREMENTS RESULTS

Much like with the receiver sensitivity measurements, binary data files were recorded from each DUT during the BER performance measurements. The data files recorded during experimentation were analyzed afterwards with a MATLAB script which counted discrepancies from the expected PN11 to calculate an estimated BER. The transmit gain of the RF output from the test signal generator was incrementally attenuated in 1 dB steps while the input noise power remained constant at -59 dBm throughout experimentation. The programmed parameters and calculated BER values of the four RUS can be found in Table 11 and are plotted together against the ideal BER curve in Figure 45 as reference.

1. RUS-1:4 BER Performance Measurements Results and Analysis

Only the relevant test points that resulted in measurable BER values appear in Table 12. It was observed during experimentation that RF output attenuation greater than 58 dB made the test signal too weak to be received and resulted in a catastrophic BER for all DUT. Also, RF output attenuation below 49 dB made the test signal significantly stronger than the noise and produced an SNR such that essentially no bit errors were measured from the data files recorded from the DUT.

Table 12. BER performance measurements results of all four RUS. Adapted from [19].

RF Output Attenuation (dB)	RUS-1 BER USRP-2922	RUS-2 BER B205mini	RUS-3 BER SpectralNet/qRadio	RUS-4 BER satTRAC
49	2.1×10^{-7}	~0	~0	8×10^{-8}
50	5.4×10^{-6}	1.1×10^{-6}	8.9×10^{-8}	1.8×10^{-6}
51	1.7×10^{-5}	1×10^{-5}	2.3×10^{-6}	1.8×10^{-5}
52	1.4×10^{-4}	6.3×10^{-5}	4.1×10^{-5}	2.1×10^{-5}
53	3.7×10^{-4}	2.9×10^{-4}	1.9×10^{-4}	1.1×10^{-4}
54	1.2×10^{-3}	unmeasurable	1×10^{-3}	4.7×10^{-4}
55	4.4×10^{-3}	unmeasurable	3.6×10^{-3}	unmeasurable
56	1.1×10^{-2}	7.4×10^{-3}	1×10^{-2}	9.1×10^{-3}
57	unmeasurable	unmeasurable	unmeasurable	1.8×10^{-2}
58	unmeasurable	unmeasurable	unmeasurable	3.2×10^{-2}

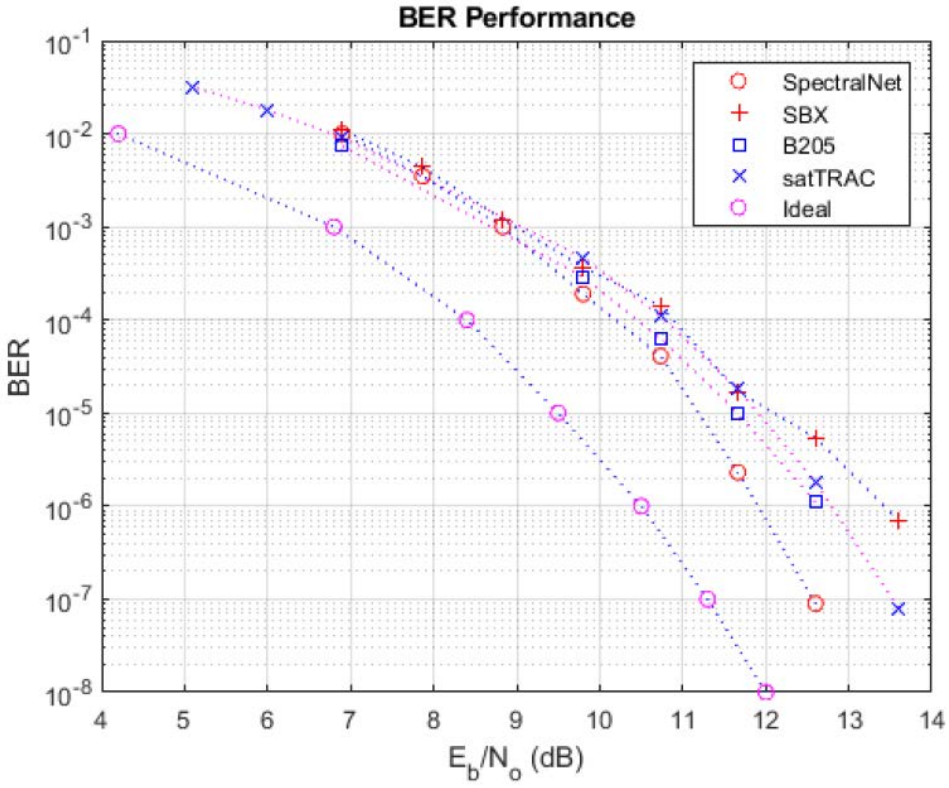

Figure 45. BER performance measurements results for RUS-1 (SBX), RUS-2 (B205), RUS-3 (SpectralNet), and RUS-4 (satTRAC). Source: [19].

Results recorded from the BER performance measurements with each DUT did not indicate superior performance by any of the four RUS. This is reflected in Figure 45 BER performance plot, with all four traces nearly on top of each other. This observation may have been the result of a deficiency in the test design, a lack in fidelity of the BER calculations, or the true performance of the four RUS.

Comparative measurements of receiver BER performance in low-SNR regimes were challenging to obtain due to the functionality of some software components of the RUS. RFBE elements seemingly caused the RUS to fail signal reception entirely before theoretically predicted, resulting in dramatic drop-offs in performance. However, data obtained through experimentation of BER performance seem to be comparable between the low and high-end SDR systems in this evaluation.

F. DYNAMIC RANGE MEASUREMENTS RESULTS

The SFDR measurements described in Chapter III were not successfully obtained due to difficulties with consistently creating third-order linearity effects in the RUS receivers. This is possibly a result of the hardware components in all four systems that are hardwired to avoid this phenomenon. This behavior should be researched further in future experimentation. Other ways to successfully investigate and evaluate dynamic range should be considered.

G. GUI PERFORMANCE AND EXPERIENCE RESULTS

As described in Chapter III, RUS-1 and RUS-2 were programmed and controlled with the open-source GNU Radio software which is common to MC3 and much of the small satellite community. Because the GNU Radio software suite is a known commodity that is supported by an unaffiliated online community as opposed to a commercial contractor, its evaluation was not focused on during this research. The experience with GNU Radio and the USRP devices was used as a baseline when assessing the software performance and functionality of the two high-end commercial systems and their associated proprietary software.

1. RUS-3 GUI Performance and Experience Results

RUS-3 was operated through the SpectralNet Digitizer GUI and the qRadio SDR GUI provided by Kratos. Both interfaces were user-friendly, accessible through a web browser, and were accompanied by associated documentation including a user guide and interface control document (ICD). The documentation was helpful when learning how to operate the system and while troubleshooting any errors encountered during experimentation. The contractor was normally responsive when contacted for help with specific questions or issues that were uncovered.

a. Test Signal Generation from RUS-3

During experimentation RUS-3 was utilized as the test signal generator for many of the experiments described in Chapter III. The creation of a standard unencoded 1-Mbps QPSK PN11 test signal was accomplished by defining waveform parameters inside the qRadio SDR GUI and setting the carrier frequency and power through the SpectralNet Digitizer GUI.

The PN11 data sequence was selected from a drop-down menu inside the TX BERT module, where the desired output bit rate was defined as 1,000,000 bps. QPSK modulation was designated in the Modulator module, which was programmed to digitally modulate the PN11 sequence generated from the TX BERT module. Finally, the Modulator was chosen as the desired input source inside the Digitizer module, which reported the output sample rate as well as the bandwidth of the transmitted signal. These qRadio SDR parameters, which were utilized to generate the standard test signal from RUS-3 during experimentation, are pictured in Figure 46.

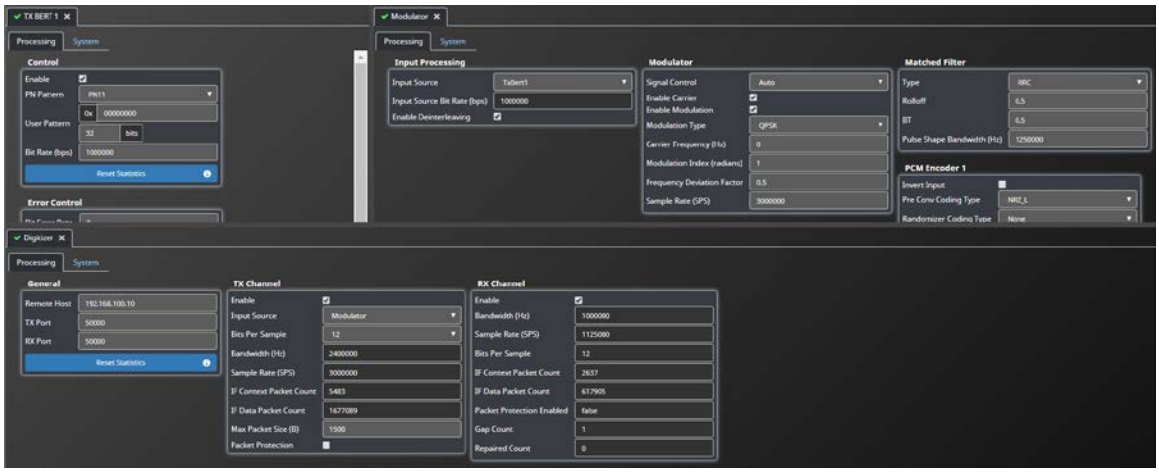

Figure 46. qRadio SDR GUI programmed to transmit the standard test signal used during experimentation.

The desired output frequency of 2250 MHz was entered into the Manual Frequency field inside the RF Output tab of the SpectralNet Digitizer GUI. The GUI provided a checkbox for users to quickly enable or disable RF output from the digitizer which proved to be useful during experimentation. The text-field attenuation control was also a useful mechanism to incrementally adjust the output power of the transmitted signal instantaneously in dB steps during testing. These parameters, as they appeared inside the SpectralNet GUI during test signal generation, are pictured in Figure 47.

Figure 47. SpectralNet GUI programmed to transmit the standard test signal used during experimentation.

Both RUS-3 interfaces were consistent, professional, and intuitive to the user. They provided useful tools like spectrum displays and real-time output metrics to monitor the status of RF output during transmission.

b. Test Signal Reception by RUS-3

As stated in Chapter III, during the experiments where RUS-3 was the DUT, RUS-4 was used to generate the standard unencoded 1-Mbps QPSK PN11 test signal. In order to receive the generated test signal, the expected waveform parameters were defined inside the qRadio SDR GUI and the tuning frequency was set in the SpectralNet Digitizer GUI.

Inside the qRadio SDR GUI, the Receiver module was programmed to demodulate the test signal by selecting the Digitizer as the Input Source, setting the Modulation Type to QPSK, and entering the expected bit rate as 1,000,000 bps. The Frame Sync module was programmed to locate frames of data inside the raw information that was demodulated by the Receiver module. This was accomplished by selecting the Receiver module as the Input Source and defining the Frame Length in bits to match the 2047-bit PN11 sequence. The qRadio SDR GUI programmed to receive the test signal generated during testing is pictured

in Figure 48. Data was collected with the File Recorder module set to record the demodulated information stream from the Receiver module.

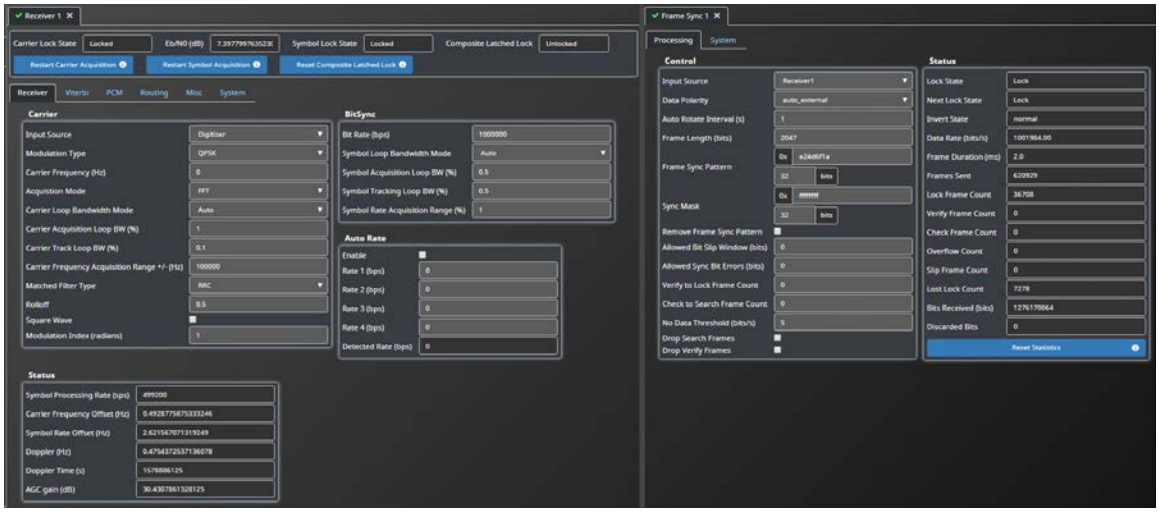

Figure 48. qRadio SDR GUI programmed to receive the standard test signal used during experimentation.

Inside the SpectralNet Digitizer GUI, the tuning frequency was set to the desired 2250 MHz on the RF Input tab as pictured in Figure 49. The input gain of the receive spectrum was adjusted in the Power and Gain settings, where the user could enter a static gain value or utilize the system's AGC.

Figure 49. SpectralNet GUI programmed to receive the standard test signal used during experimentation.

Programming RUS-3 to receive a signal of interest through its interfaces was also intuitive and straightforward. Input spectrum display, IQ plot, real-time output metrics, and BER modules were useful tools to monitor RF input and demodulation during signal reception and testing.

2. RUS-4 GUI Performance and Experience Results

RUS-4 was operated through the AMERGINT satTRAC softFEP GUI and applications which were accessible through a web browser on the satTRAC server. The softFEP applications contain adaptive documentation accessible through the GUI, but as the contractor noted, the documentation was written by a computer engineer and was often non-intuitive. A user guide document was also provided with the delivery of the system, but it was largely a top-level description that did not explain many of the parameters of the GUI. Many issues were encountered during experimentation and normal operation of the system, and the contractor provided limited support when contacted.

The softFEP application was also buggy, often getting hung up when switching between modules and required refreshing of browser window. Some of the critical SDR parameters were hidden inside SwD Overview interface which was hard to navigate and

often non-intuitive. The GUI performance was communicated to the contractor AMERGINT who provided limited resolution to the problems experienced. However, some of these issues should be resolved for future acquisitions because the contractor recently ported their entire system to a new operating system and delivered their system to MC3 before conducting exhaustive testing. Potential customers should always take software maturity into account when acquiring SDR systems and weigh the benefits of adopting nascent and unproven architectures against the required schedule to integrate and robustly test them in an operational architecture.

c. Test Signal Generation from RUS-4

When conducting experimentation with RUS-3 as the DUT, RUS-4 was used to generate the standard unencoded 1-Mbps QPSK PN11 test signal. This was accomplished by programming the SDR parameters inside various modules accessed through the Modem Overview window of satTRAC softFEP GUI pictured in Figure 25. The test signal parameters were input into the Uplink applications which generated the digital-IF which was delivered through the satTRAC application to the Signal Converter for DAC and transmission as analog RF.

The PN11 sequence was selected as the desired data pattern from a drop-down menu inside the Basic TLM Sim application pictured in Figure 50. The output Data Bit Rate was set to 1,000,000 Hz which matches the desired 1 Mbps and the Frame Length was set to 2047 bits like the standard PN11 sequence. Data Output was turned on and the number of Transmit Packets and Transmit Bytes fields incremented indicating successful data generation. The Enable Viterbi, G2 Invert, and G2 Before G1 options were all set to off because these options were not applicable for the desired test signal.

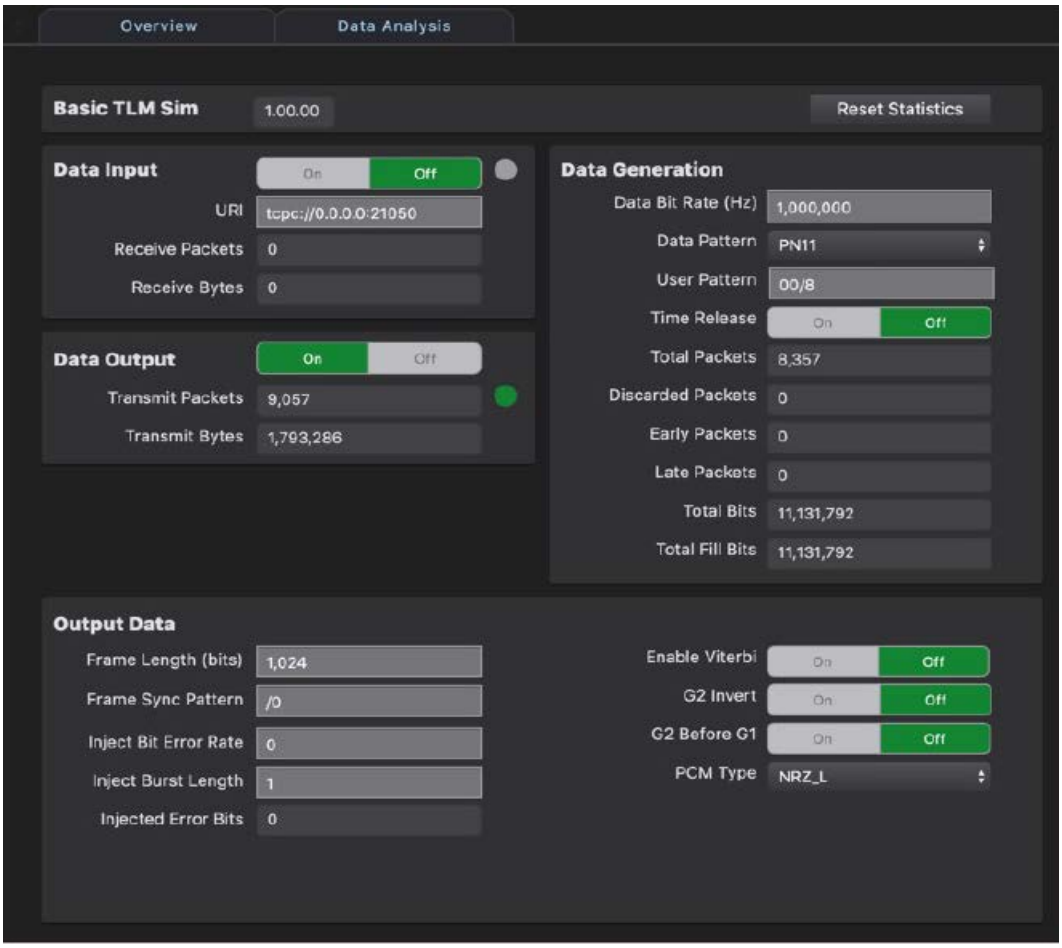

Figure 50. Basic TLM Sim application widow inside satTRAC softFEP GUI. Source: [22].

The QPSK Mod application, pictured in Figure 51, was then selected and programmed to digitally modulate the 1-Mbps PN11 data sequence generated by the Basic TLM Sim application. With Basic TLM Sim as the selected input, the TLM Sim Input was turned on, the Pulse Shape Type was set to Raised Root Cosine to match the test signal generated with RUS-3, and all other settings were left as their default values. When programmed correctly, the numbers in the Total Bits and Total Packets fields would increment indicating successful digital modulation of the data input.

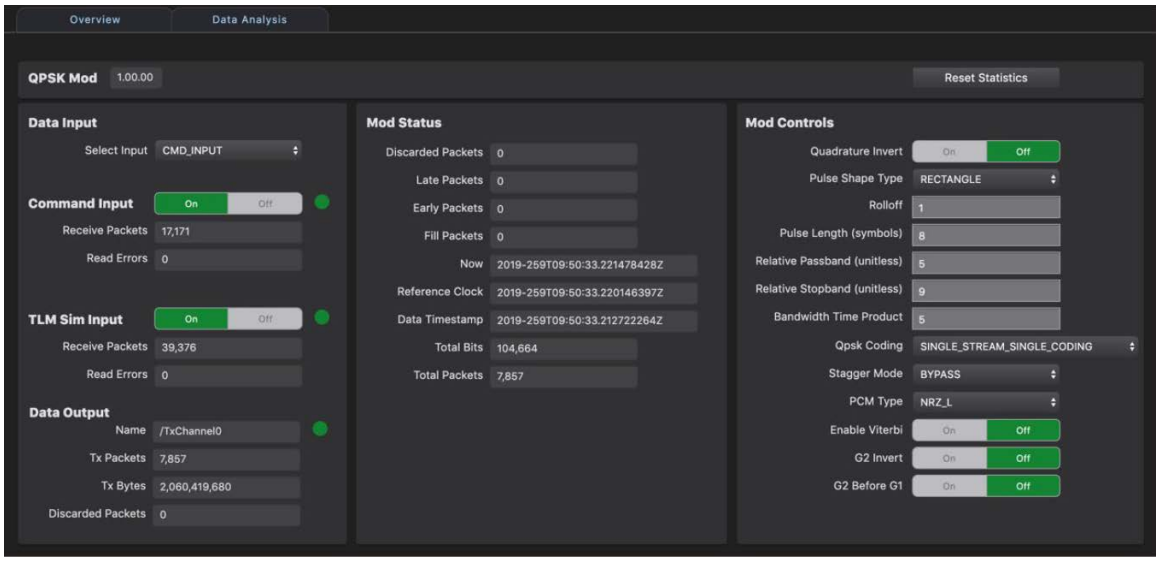

Figure 51. QPSK Mod application window inside satTRAC softFEP GUI. Source: [22].

Finally, the satTRAC application was utilized to set the desired carrier frequency, output signal power, and to select which output port on the Signal Converter from which RF was generated. An example of the Uplink parameters adjustable through the satTRAC application appears in Figure 52. RF generation from the Signal Converter was initiated and disabled by checking and unchecking the Enable Carrier and Enable Modulation boxes as they appear in Figure 52. During experimentation the S-Band output port was selected as the RF Signal Source of the 2250 MHz test signal.

Figure 52. Uplink parameters programmed into satTRAC application window inside satTRAC softFEP GUI. Source: [22].

The process of programming the standard test signal inside RUS-4 was generally straightforward and required the use of only one interface as opposed to RUS-3. Fewer output metrics were available to the user, but more settings could be accessed through the SwD Overview interface described in Chapter III and pictured in Figure 26. It was uncovered through experimentation and troubleshooting that many parameters were accessible only through the SwD Overview and were often difficult to locate by the user intuitively.

d. Test Signal Reception by RUS-4

When RUS-4 was the DUT during experimentation, the satTRAC softFEP GUI was programmed to receive the test signal generated from RUS-3. This was accomplished by defining the expected signal parameters through the Downlink applications pictured on the bottom half of Figure 25 after tuning the satTRAC Signal Converter appropriately inside the satTRAC application. Figure 53 depicts example Downlink parameters programmed into the satTRAC application, where the RF Signal Source of the Signal Converter is selected and the desired center frequency is entered in MHz.

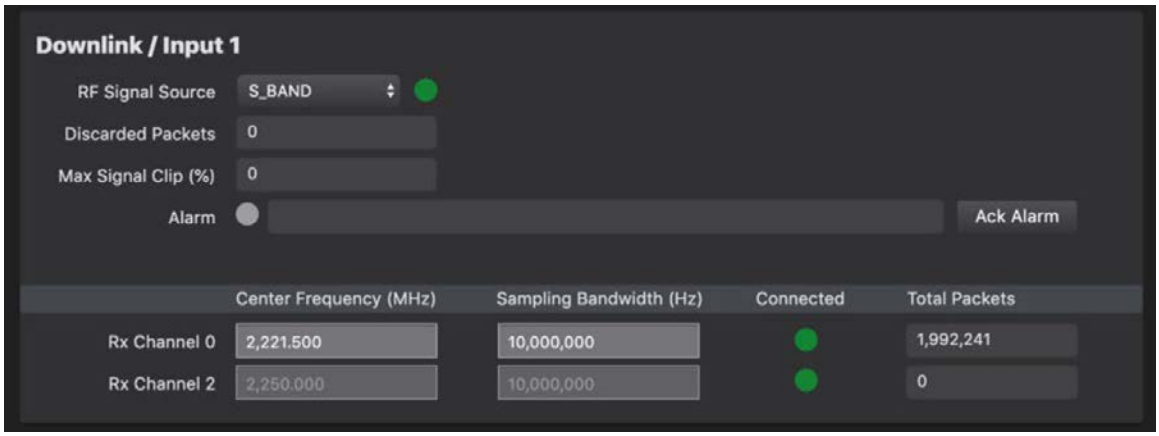

Figure 53. Downlink parameters programmed into satTRAC application window inside satTRAC softFEP GUI. Source: [22].

The QPSK modulation type and data rate parameters of the expected test signal were programmed through the QPSK Demod application pictured in Figure 54.

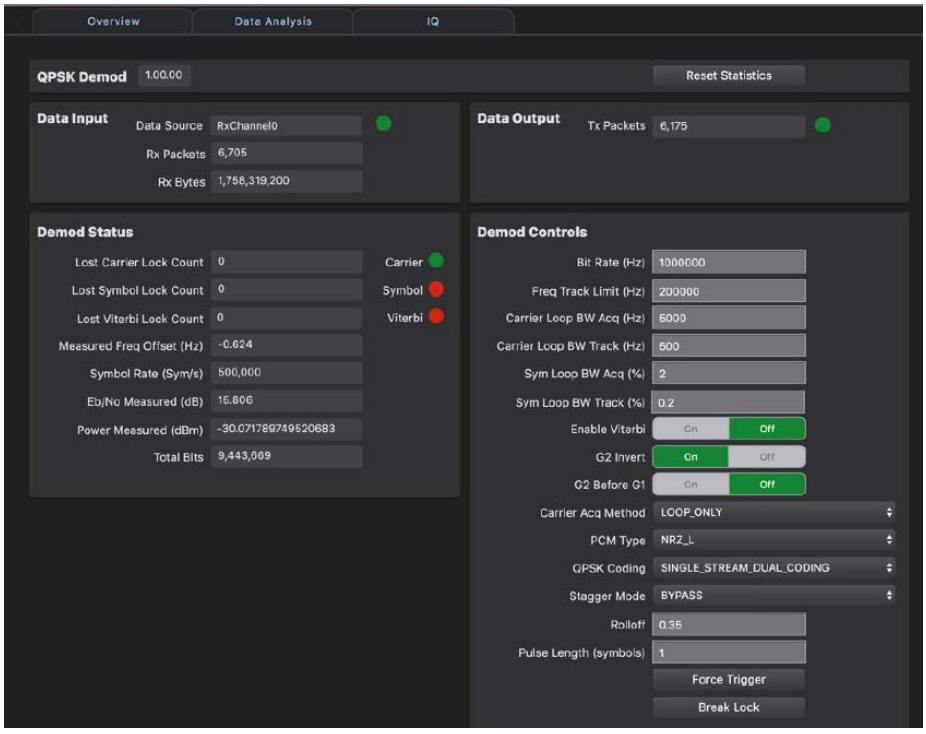

Figure 54. QPSK Demod application inside satTRAC softFEP GUI. Source: [22].

An IQ diagram is also accessible through the IQ tab inside the application which displays the symbol decisions produced by the demodulator and was useful to monitor during testing [22].

The Data Analysis tab inside the QPSK Demod application was utilized to record demodulated bits from the SDR that were saved as binary files during experimentation. This interface, pictured in Figure 55, also contained an Rx BERT module that could be programmed to compare the demodulated bits against certain data patterns and measure any received bit errors.

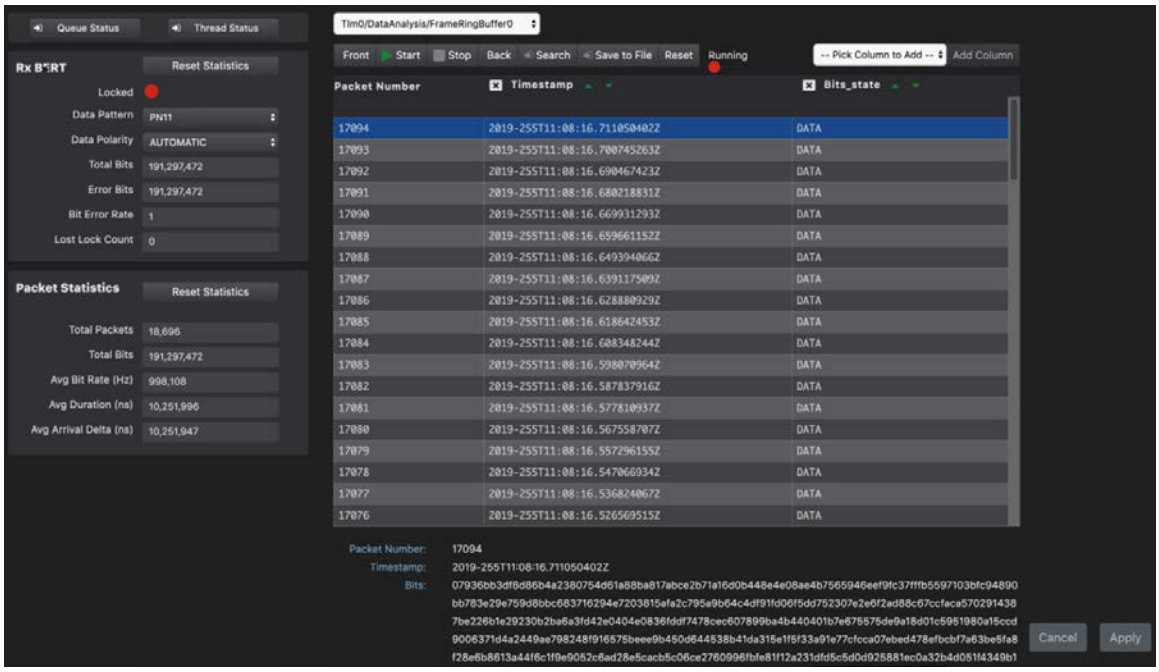

Figure 55. Data Analysis tab inside QPSK Demod application inside satTRAC softFEP GUI. Source: [22].

The last application pictured in the Downlink section of the Modem Overview page is the Basic TLM module which was programmed to search for and sync onto a specified frame length and sync pattern. This application was programmed to match the parameters of the PN11 test signal during experimentation as a sanity check, but all BER calculations were measured from independently analyzing bits that were recorded from the demodulator.

3. Analysis of RUS GUI Performance and Experience

The software and GUI platforms of RUS-3 and RUS-4 both provide the user with vastly different experiences than with the GNU Radio software used to operate the baseline USRP devices. While GNU Radio and the associated software is an extremely flexible and modular platform, it requires the user to have significant knowledge of digital signal processing, python and/or C++ coding languages, and familiarity with the toolkit utilized to create custom transmit and receive models. There is an existing library of 'blocks' to build an SDR model from, but they may not support some of the complex waveforms utilized by many satellite operators. The flexibility of the GNU Radio platform provides an educated user the potential to create custom SDR models to transmit or receive any variations in signal waveform parameters definable within the platform. However, the accuracy and fidelity of the custom SDR model falls completely on the user and the open source community with little or no validation from a centralized quality assurance apparatus.

While there is a large online community that uses the open source software and contributes to troubleshooting any bugs or any difficulties experienced by posting in online forums, there is no contractor support or official documentation to assist users. The informal documentation included with some of the GNU Radio blocks is inconsistent in the level of detail and, due to the fact there is no quality assurance associated with the platform, may contain errors. Small-satellite operators and other SDR users may not possess the skillset to effectively utilize a platform like GNU Radio and may prefer a more plug-and-play solution that is accompanied with associated training, system documentation, and contractor troubleshooting support.

The proprietary software associated with RUS-3 and RUS-4 provide more structured interfaces to construct transmit and receive chains with potential small-satellite waveforms. Both RUS are preloaded with common modulation types, encoding schemes, and common data sequences that are accessible through drop-down menus with intuitive controls editable with text fields and buttons. Both systems also allow the user to save configurations such that a user with no background knowledge of the specific waveform could load previously created configurations and operate the systems seamlessly.

The structured nature of the interfaces used with RUS-3 and RUS-4 does lead to a limitation in flexibility when the user wants to create atypical or testing configurations that may not be comparable to an operational waveform. The user is limited in some regards by the options available in the GUI when trying to create unique waveforms unlike with GNU Radio. For example, if a new small satellite utilized a new waveform that employs an atypical modulation type or encoding scheme not provided by RUS-3 and RUS-4, the user would have to write their own code to support C2 communications outside of the interfaces or pay the contractor to support the new formatting. This could be costly and time consuming depending on the level of change and the willingness of the contractor to take on additional work to design software for the unsupported waveform.

V. CONCLUSIONS

A. SUMMARY

This thesis work set out to characterize the performance of the four RUS and assess their functionality for application in the MC3 ground station network and other comparable endeavors in the small satellite community and the USG. The experimentation and evaluation focused on the receiver performance, GUI functionality, usability, and the cost associated with each RUS. It was discovered that SDR performance was often difficult to evaluate without first understanding how the underlying software features operate and learning the techniques necessary to create the desired effects of the user. This would have been an insurmountable task without the cooperation of the vendors, a fact that highlights the deficiencies of their published specifications and user documentation. A significant amount of time was invested in familiarization with the two high-end commercial RUS in order to confidently operate the systems during experimentation. Ultimately, the research, testing, and analysis conducted during this thesis resulted in many interesting findings that will inform potential consumers about the benefits and shortfalls associated with these systems.

In terms of receiver performance, it was determined that the two baseline USRP devices performed similarly to the two high-end commercial systems that were investigated during this study. The super-heterodyne receiver architecture employed inside RUS-4 resulted in marginally better receiver sensitivity measurements, but all four RUS seemed to produce comparable noise figure measurements, phase noise contributions, image rejection characteristics, and BER performance measurements, which are a good end-to-end evaluation of an SDR system. The experimentation and analysis conducted for this thesis highlighted the ability of powerful SDR algorithms to compensate for any deficiency in receiver hardware. Under the conditions investigated during this research, the receiver performance of all four systems would be acceptable for conducting C2 communications in most small satellite ground station applications, and any variances in capability could be accounted for with in-line attenuation between an antenna and the ground station SDR to increase the SNR. However, special mission users like those conducting signal intelligence

acquisitions which require more sensitive receivers may prefer the performance of RUS-4 over the other three RUS.

In terms of GUI functionality and system usability by a user, the two baseline USRP devices operated through GNU Radio provide a vastly different experience than the two high-end commercial systems which utilize proprietary software. The GNU Radio software platform is a flexible and powerful toolkit in the hands of the knowledgeable user, but the RFBE software platforms provided by RUS-3 and RUS-4 provide the user with a structured, plug-and-play solution capable of supporting operational small-satellite waveforms. The proprietary software and GUI's may not be as flexible as the open-source software associated with the baseline RUS-1 and RUS-2 systems, but they do come with contractor support and documentation that would enable successful small-satellite C2 operations without the need for personnel with expertise in digital signal processing and coding. Ultimately, the GNU Radio software and the proprietary software of RUS-3 and RUS-4 function comparably for application with small-satellite operations, but the suitability of each system depends on the intended mission and the personnel available to support the operations. Between the two high-end commercial systems, RUS-3 provided a superior GUI experience with professional documentation and contractor support that preferable to the product that was provided with RUS-4.

In terms of cost, the two baseline USRP devices are priced well below the two high-end commercial systems. RUS-1, which is the baseline SDR device utilized in MC3 ground stations, is priced about three times more than RUS-2, even though the performance of the two systems was very comparable. As stated in Table 2, RUS-2 operates with the same RFBE as RUS-1 over a larger frequency range, provides more gain and bandwidth, and is a smaller form factor device. The USB 3.0 connection utilized with RUS-2 may present data rate and ground station cable routing limitations for some users not encountered with the 1GbE connection of RUS-1, but in its smaller form factor allows integration into tighter, or weight-sensitive spaces, and potentially closer to downstream RF components minimizing cable loss and noise. RUS-2 is also cheaper and requires less power while providing similar overall performance to RUS-1. The high-end commercial systems provide the user with a different experience, reliability, and supportability than the two

baseline USRP devices, but also differ greatly in cost. RUS-4 is priced more than three times more than RUS-3 and provides similar performance and user experience. It is concluded from the analysis of this thesis that in most small-satellite applications RUS-2 provides the most value to the user wishing to employ a baseline USRP device with a custom GNU Radio RFBE, while RUS-3 provides the most value as a high-end commercial SDR with predefined operational small-satellite waveforms, documentation, and contractor supportability.

B. FUTURE WORK

Some areas for continued investigation and research have been identified to be pursued through future work. These items include additional lab testing to further evaluate RF parameters, operational testing with on-orbit satellites, and the documentation of integration activities with the SATRN platform utilized by the MC3 network.

1. Additional Lab Testing

As noted in Chapter IV, some of the identified RF parameters were not evaluated successfully either due to time constraints, unforeseen behaviors exhibited by the RUS, or the absence of a well-designed experiment to investigate the desired attribute. Further research should expand upon the experimentation that was conducted and explore additional ways to evaluate the parameters that were not investigated completely. This work could include a better assessment of the effects from co-channel and adjacent-channel phase noise, a characterization of the functional dynamic range of each RUS, and a more in-depth evaluation of non-linear effects. BER performance should also be re-evaluated with and without a 10 MHz synchronization source signal in order to highlight the importance of a good external synchronization source during operation. Other attributes like the performance of any Doppler compensation functionality should also be explored.

2. Satellite Pass Analysis

One activity that unfortunately was not included in this thesis was a comparative analysis of the functional performance of each RUS conducting TT&C communications to and from an operational satellite. This could be accomplished by recording a satellite pass

in MC3 and playing it back to the four RUS, or real-time by connecting the RUS to the MC3 dish antenna at NPS. The four SDR devices could be programmed to receive the same signal relatively easily and fed the same satellite pass recording. This could be accomplished with a real satellite pass by splitting the received signal four ways at some point downstream of the receive antenna. This could be an enormously beneficial activity that would provide a side-by-side comparison of functional performance in a realistic, operational setting.

3. SATRN Integration Testing and Analysis

The C2 communications to and from MC3 ground station networked ground stations are managed through SATRN software platform identified in Chapter 1. The tasks required to integrate these SDR devices and their software interfaces into an operational MC3 ground station should be researched. Execution and documentation of this integration, to include the SATRN software, would an extremely valuable activity to accomplish.

APPENDIX A. NOISE FIGURE MEASUREMENTS MATLAB CODE

```
%--------------------------------------------------------------------------
%Read_Complex_Capture_File_Function Script%
%
%Dr. M.B. Matthews and Capt Sam Wood
%Naval Postgraduate School
%Oct 2019
%--------------------------------------------------------------------------
function data = Read_Complex_Capture_File(filename, start, stop)
if nargin < 2, start = 1; end
if nargin < 3, stop = inf; end
len = stop;
localName = ['./' filename];
if (exist(localName) == 0)
fprintf ('Read_Complex_Capture_File: file %s not found\n',
filename);
data = [];
return;
end
fprintf('Opening file %s ', filename);
fid = fopen (filename, 'r');
data = fread (fid, 2*len, 'float');
data = data(1:2:end) + 1i*data(2:2:end);
data = data(start:end);
fprintf('(%d complex samples)\n', length(data));
fclose(fid);
return;
```

```
%-------------------------------------------------------------------------
%Noise Factor Measurement Script%
%
%Dr. M.B. Matthews and Capt Sam Wood
%Naval Postgraduate School
%Oct 2019
%-------------------------------------------------------------------------
function [bits,detect] = Noise_Figure_Measurements(file, len, tstart,
tstop)
close all;
fprintf('\nN o i s e F i g u r e C a l c u l a t i o n\n');
fprintf('-------------------------------------------------\n');
% default file
%N1 Cold Measurement
default_file1
= 'SBX_calibrated_noise_input_off_1.5G_20MSPS_G20_20191001.dat';
% default_file1 =
'B205mini_calibrated_noise_source_off_1.5G_20MSPS_G20_20191108.dat';
% default_file1 =
'SpectralNet_calibrated_noise_input_off_1.5G_20MSPS_G53_20200310.dat';
%N2 Hot Measurement
default_file2
= 'SBX_calibrated_noise_input_on_1.5G_20MSPS_G20_20190927.dat';
% default_file2 =
'B205mini_calibrated_noise_source_on_1.5G_20MSPS_G20_20191108.dat';
% default_file2 =
'SpectralNet_calibrated_noise_input_on_1.5G_20MSPS_G53_20200310.dat';
% input argument processing
if nargin < 1, file1 = default_file1; file2 = default_file2; end
if nargin < 2, len = inf; end
if nargin < 3, tstart = 1; end
if nargin < 4, tstop = inf; end
% parameters
fs = 10.0e6; T = 1/fs; % initial sampling rate
% fprintf('Time interval [%.1f, %.1f] sec\n', tstart, tstop);
start = floor(fs*tstart)+1; stop = floor(fs*tstop);
x1 = Read_Complex_Capture_File(file1, start, stop); % read file,
complex data
x2 = Read_Complex_Capture_File(file2, start, stop);
N1 = length(x1);
N2 = length(x2);
fprintf('\nCold measurement (N1): Samples %d, rate %.1f kSamples/sec,
interval [%.1f, %.1f] sec\n', ...
N1, fs/1000, tstart, tstop);
fprintf('Hot measurement (N2): Samples %d, rate %.1f kSamples/sec,
interval [%.1f, %.1f] sec\n\n', ...
1
N2, fs/1000, tstart, tstop);
% remove intentional offset
fo1 = 0.0e6; % tuning offset on N1 Cold Measurement
fo2 = 0.0e6; % tuning offset on N2 Hot Measurment
fd1 = 0;
fd2 = 0;
t1 = (0:T:T*N1-T)';
t2 = (0:T:T*N2-T)';
```

```
% fprintf('N1: Frequency shifting %.0f kHz\n', fo1+fd1/1.0e3);
y1 = x1 .* exp(-1i*2*pi*(fo1+fd1)*t1);
% fprintf('N2: Frequency shifting %.0f kHz\n', fo2+fd2/1.0e3);
y2 = x2 .* exp(-1i*2*pi*(fo2+fd2)*t2);
fig1=figure('Position',[0.2000 289 1.0048e+03 829.6000]);
subplot(2,3,1); plot(real(y1),'b'); grid;
axis([0 length(y1) -0.5 0.5]);
xlabel('Time (s)');
title('N1 Cold Noise');
subplot(2,3,4); plot(real(y2),'b'); grid;
axis([0 length(y2) -0.5 0.5]);
title('N2 Hot Noise');
xlabel('Time (s)');
% spectral plot
% fprintf('N1 Spectrum display\n');
NFFT1 = N1;
Y1 = fftshift(fft(y1(1:NFFT1).^2));
df1 = fs/N1; f1 = (-fs/2:fs/N1:fs/2-df1);
subplot(2,3,2); plot(f1/1e6, 20*log10(abs(Y1)), 'b');
% Ymax1=max(20*log10(abs(Y1)));
% axis([min(f1) max(f1) -20 100]);
title('N1 Time Domain');
xlabel('Frequency (MHz)');
grid;
% fprintf('N2 Spectrum display\n\n');
NFFT2 = N2;
Y2 = fftshift(fft(y2(1:NFFT2).^2));
df2 = fs/N2; f2 = (-fs/2:fs/N2:fs/2-df2);
subplot(2,3,5); plot(f2/1e6, 20*log10(abs(Y2)), 'b');
% Ymax2=max(20*log10(abs(Y2)));
% axis([min(f2) max(f2) -20 100]);
title('N2 Time Domain');
xlabel('Frequency (MHz)');
grid;
% Periodogram
% periodogram(y,[],'psd',NFFT,fs,'centered')
subplot(2,3,3); periodogram(y1,[],'power',NFFT1,fs,'centered')
subplot(2,3,6); periodogram(y2,[],'power',NFFT2,fs,'centered')
yb1=abs(mean(y1)); %mean of the N1 signal
sigmay1=var(y1); %variance of N1 signal
yb2=abs(mean(y2)); %mean of the N2 signal
sigmay2=var(y2); %variance of N2 signal
2
yfactor=sigmay2/sigmay1;
ENR=14.54; %dB
E=10^(ENR/10);
F=E/(yfactor-1); %Noise Factor
FdB=10*log10(F); %dB Noise Figure
fprintf('The variance of the N1 signal is %.2e\nThe mean is %.2e\n
\n',sigmay1,yb1)
fprintf('The variance of the N2 signal is %.2e\nThe mean is %.2e\n
\n',sigmay2,yb2)
fprintf('-------------------------------------------------\n');
fprintf('The calculated noise figure is %.4f dB\n',FdB)
end
```

THIS PAGE INTENTIONALLY LEFT BLANK

APPENDIX B. GNU RADIO RECEIVER MODEL

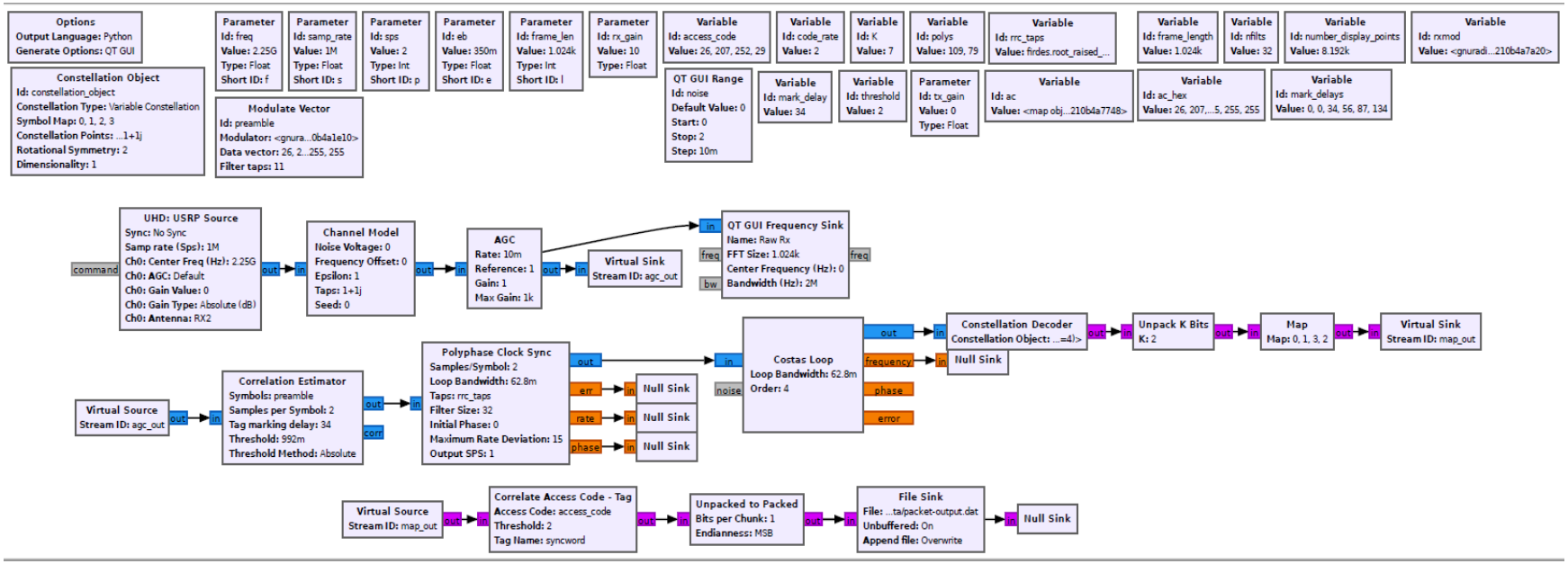

THIS PAGE INTENTIONALLY LEFT BLANK

APPENDIX C. VITA 49 RADIO TRANSPORT (VRT) SDR PROTOCOL

VITA 49 is the Digital-IF protocol utilized by RUS-3 and RUS-4. It is described as "an open standard offering a consistent protocol for the interconnection between proprietary interfaces to improve interoperability, maintain ability, and upgradability" [28]. Figures 56 and 57 illustrate how this protocol is utilized by SDR devices to transfer digital data.

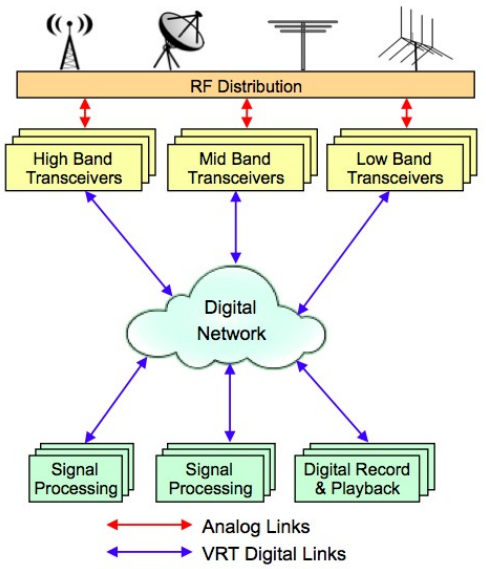

Figure 56. VRT-enabled software radio. Source: [28].

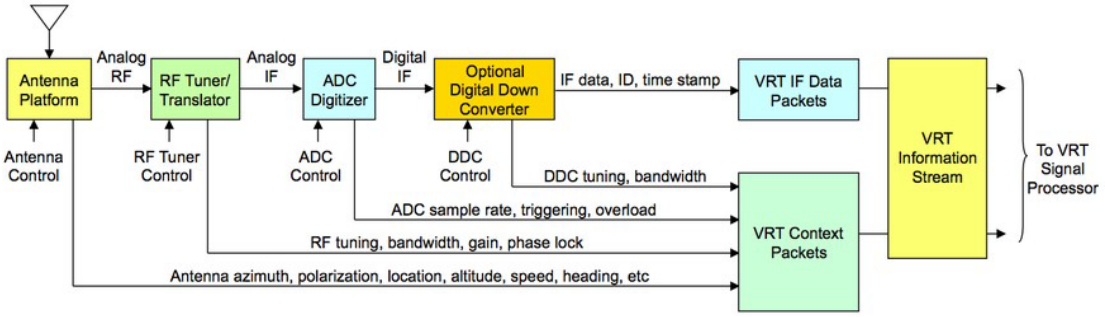

Figure 57. VRT-enabled SDR delivering VITA 49 IF data and context packets. Source [28].

THIS PAGE INTENTIONALLY LEFT BLANK

APPENDIX D. HARDWARE SPECIFICATIONS

A. RUS-1 SPECIFICATIONS

Section A contains RUS-1 specifications provided by the manufacturer in [15].

Transmitter

Frequency range	400 MHz to 4.4 GHz
Frequency step	<1 kHz
Maximum output power (P_{out})	50 mW to 100 mW (17 dBm to 20 dBm)
Gain range[1]	0 dB to 31 dB
Gain step	0.5 dB
Frequency accuracy[2]	2.5 ppm
Maximum instantaneous real-time bandwidth[3]	
16-bit sample width	20 MHz
8-bit sample width	40 MHz
Maximum I/Q sampling rate[4]	
16-bit sample width	25 MS/s
8-bit sample width	50 MS/s
DAC	2 channels, 400 MS/s, 16 bit
DAC spurious-free dynamic range (sFDR)	80 dB

Receiver

Frequency range	400 MHz to 4.4 GHz
Frequency step	<1 kHz
Gain range[5]	0 dB to 31.5 dB
Gain step	0.5 dB
Maximum input power (P_{in})	0 dBm
Noise figure	5 dB to 7 dB

[1] The output power resulting from the gain setting varies over the frequency band and among devices.

[2] *Frequency accuracy* is based on temperature-compensated crystal oscillator (TCXO) vendor specifications and is not measured. Alternatively, you can incorporate an external reference source to provide a more precise frequency Reference Clock and to achieve better frequency accuracy.

[3] Instantaneous bandwidth depends on many factors including, but not limited to, network configuration and host computer performance. Actual data throughput may be chipset dependent.

[4] I/Q sampling rate depends on many factors including, but not limited to, network configuration and host computer performance. Actual data throughput may be chipset dependent.

[5] The received signal amplitude resulting from the gain setting varies over the frequency band and among devices.

Frequency accuracy[6]	2.5 ppm
Maximum instantaneous real-time bandwidth[7]	
16-bit sample width	20 MHz
8-bit sample width	40 MHz
Maximum I/Q sample rate[8]	
16-bit sample width	25 MS/s
8-bit sample width	50 MS/s
Analog-to-digital converter (ADC)	2 channels, 100 MS/s, 14 bit
ADC sFDR	88 dB

Power

Caution The protection provided by this product may be impaired if it is used in a manner not described in this document.

Total power, typical operation	
Typical	12 W to 15 W
Maximum	18 W
Power requirement	Accepts a 6 V, 3 A external DC power connector

Note You must use either the power supply provided in the shipping kit, or another UL listed ITE power supply marked *LPS*, with the USRP-2922.

Physical Characteristics

If you need to clean the module, wipe it with a dry towel.

Physical dimensions	
(L × W × H)	15.875 cm × 4.826 cm × 21.209 cm (6.25 in. × 1.9 in. × 8.35 in.)
Weight	1.193 kg (2.63 lb)

[6] *Frequency accuracy* is based on temperature-compensated crystal oscillator (TCXO) vendor specifications and is not measured. Alternatively, you can incorporate an external reference source to provide a more precise frequency Reference Clock and to achieve better frequency accuracy.

[7] Instantaneous bandwidth depends on many factors including, but not limited to, network configuration and host computer performance. Actual data throughput may be chipset dependent.

[8] I/Q sample rate depends on many factors including, but not limited to, network configuration and host computer performance. Actual data throughput may be chipset dependent.

B. RUS-2 SPECIFICATIONS

Section B contains RUS-2 specifications provided by the manufacturer in [18].

Specifications[2]

Specification	Typical	Unit
RF Performance[3]		
IIP3 (at typical NF)	-20	dBm
Power Output	> 10	dBm
Receive Noise Figure	< 8	dB
Conversion Performance and Clocks[3]		
ADC Sample Rate (Max.)	61.44	MS/s
ADC Resolution	12	bits
DAC Sample Rate (Max.)	61.44	MS/s
DAC Resolution	12	bits
Host Sample Rate (16b)	61.44	MS/s
Frequency Accuracy	±2.0	ppm

Specification	Typical	Unit
Power		
USB Power	5	V
Physical		
Dimensions	83.3 x 50.8 x 8.4	mm
Weight	24.0	g
Operating Temperature Range		
B200mini	0 – 40	°C
B200mini-i	0 – 45	°C
B205mini-i	0 – 45	°C

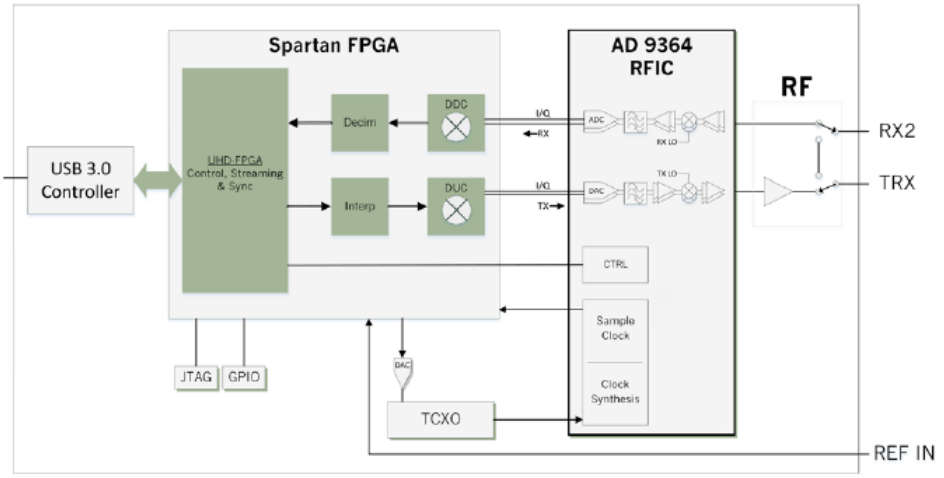

[2] All specifications are subject to change without notice.

[3] Additional RF and digitizer specifications can be found on the ADI 9364 data sheet. http://www.analog.com/media/en/technical-documentation/data-sheets/AD9364.pdf

About Ettus Research

Ettus Research™, a National Instruments company, is the world's leading supplier of software defined radio platforms, including the USRP™ (Universal Software Radio Peripheral) family of products. The USRP platform supports multiple development environments on an expansive portfolio of high performance RF hardware, and enables algorithm design, exploration, prototyping, and deployment of next generation wireless technologies across a wide variety of applications spanning DC to 6 GHz such as cognitive radio, spectrum monitoring and analysis, remote sensing, advanced wireless prototyping, mobile radio, public safety, broadcast TV, satellite communication, and navigation.

Ettus Research
A National Instruments Company

C. RUS-3 SPECIFICATIONS

Section C contains RUS-3 specifications provided by the manufacturer pertaining to the SpectralNet Digitizer Lite front-end and qRadio SDR in [20] and [21].

10 System Specifications

Signal Levels and Data Interfaces

Frequency Tuning Range	50 – 2500 MHz.
Instantaneous Bandwidth	10 kHz to 54 MHz.
RF Input Levels	-60 to 0 dBm. Absolute max: +5 dBm damage level.
RF Output Levels	-40 to -5 dBm operating.
A/D resolution	Selectable from 4 through 12 bits. AGC or manual gain control.
Network Transport	1 Gb Ethernet, 2 RJ45 connectors for Management and Data ports.
Network Data Format	ANSI VITA-49.0 IF data and context packets.

Environmental

Storage Temperature	-20 °C to +70 °C.
Operating Temperature	0 °C to 50 °C.
Relative Humidity	0% to 90% RH. Atmosphere must be non-condensing.
Maximum Altitude	Operating: 3048 m (10,000 ft). Storage: 12,000 m (39370 ft).
Dust	Air must be free of conductive or corrosive dust or other conductive particles.

2. BLOCK DIAGRAMS

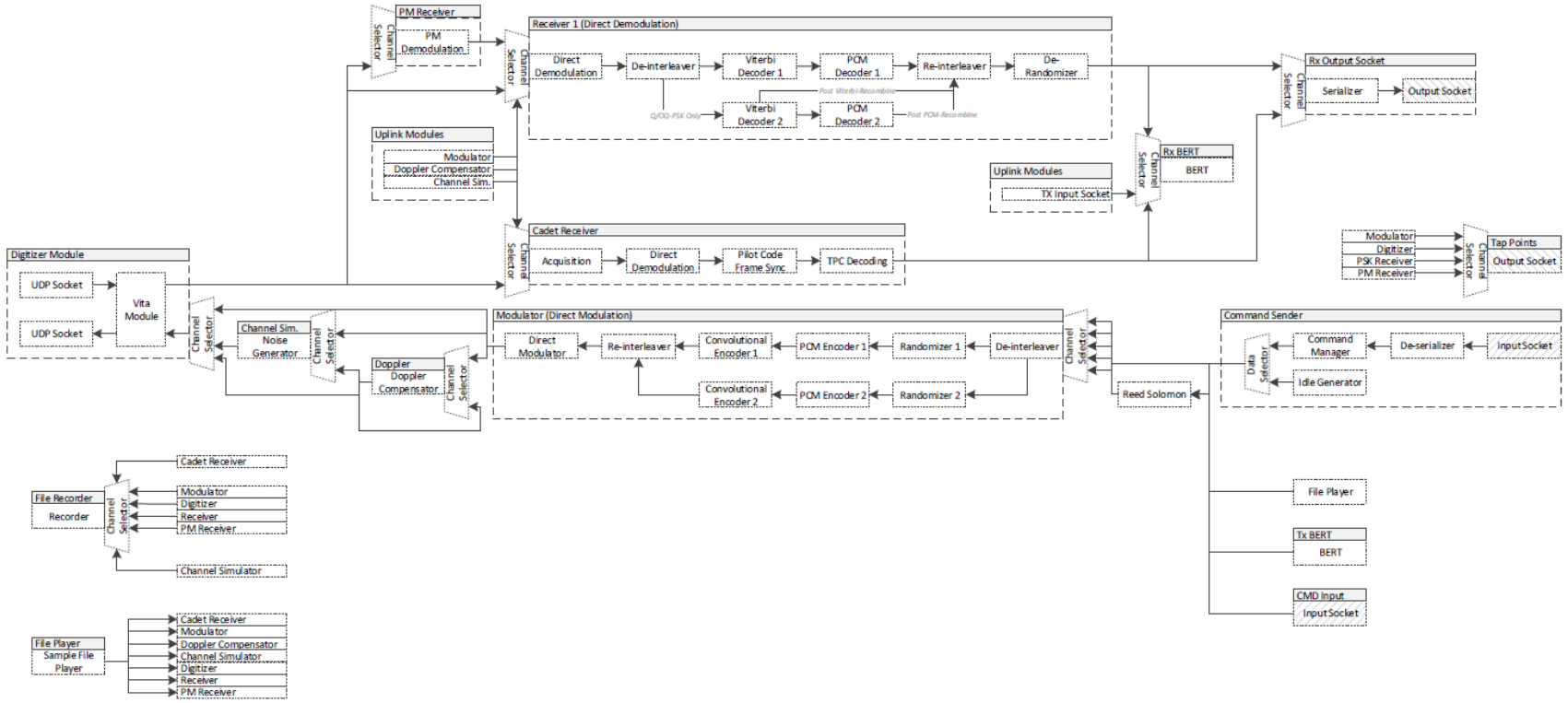

3. UPLINK (COMMANDING)

3.1 ANALOG INTERFACES

Description	Specification
RF Frequency Range:	50 MHz to 2500 MHz
RF Tuning Step Size:	0.1 Hz
RF Output Power Levels:	-40 dBm to -5 dBm
RF Connector Type:	SMA
D/A Resolution	Selectable from 4 through 12 bits.
Instantaneous Bandwidth:	125 kHz to 10 MHz[1]
Number of Transmit Channels:	1

3.2 MODULATOR SPECIFICATIONS

Description	Specification
Number of Transmit Channels:	1
Direct Modulation Types:	BPSK QPSK DQPSK (Normal / Alternate) OQPSK 8PSK FSK MSK GMSK SOQPSK_TG PCM PM PCM FM
Symbol Rate:	7 sps to 5 Msps[2]
Mod Index (PM):	0.0 to 3.0 Radians
Frequency Deviation (FM):	0 to 4 MHz
Match Filter:	None

[1] The instantaneous bandwidth of the SpectralNet Lite device for *RF transport* is 54 MHz. The quantumRadio supports processing a maximum of 10 MHz of instantaneous bandwidth. When using the SpectralNet Lite as the front end for quantumRadio, the instantaneous bandwidth is limited to quantumRadio's maximum instantaneous bandwidth (10 MHz.).

[2] Max rate assumes a bandwidth of 10MHz > 5 Msps @ 8PSK > 15 Mbps and that they data is unencoded.

	Raised Cosine Root Raised Cosine Bandpass Gauss	
Match Filter Rolloffs:	User Defined from 0% to 100%	
PCM Coding:	NRZ-L,M,S BIϕ-L,M,S D-BIϕ-L,M,S	
Dual PCM Encoders:	Supported	
Convolutional Encoding	Rate = ½, ¾ (K=7) CCSDS Polynomial - G1=1111001 - G2=1011011 G1 / G2 Invert Support Reverse order mode (G1 / G2 output order is reversed) Bypass mode supported	
Dual Convolutional Encoders:	Supported	
Randomizer Coding Type:	Polynomial ($x^{17} + x^{12} + 1$)	
Doppler Compensation[3]:	Shift: Rate:	+/- 1 MHz +/- 100 kHz/sec
Fill (Continuous Carrier)	Supported	
Idle Pattern:	User Defined	
Data Source(s):	Internal BERT Network File Player	
Command Sender:	User definable: - Idle Pattern - Fill Command - Command Gap - Carrier Rise / Fall time - Subcarrier Rise / Fall time - On/Off (Burst) Commanding - Preamble - Barker Code	
Frame Sync:	User definable; - Frame Length - Sync Pattern - Allowable Bit Slips - Allowable Bit Errors	

[3] Not currently shown in block diagram.

	- Sync Pattern Removal - Fixed/Auto polarity - Auto-rotate of IQ constellation
Reed Solomon:	Reed Solomon Encoding (223, 255) and (239, 255) - Virtual Fill up to 7 bits per frame - Block Interleaving (CCSDS compliant) - Viterbi Decoding can be concatenated with Reed Solomon Decoding. - Decoder Output data can have VCDU only or VCDU w/ ASM re-appended - Check Symbol Removal - ASM Removal
Carrier Sweep:	Supported modes include; - Continuous Rising - Continuous Falling - One Shot Rising - One Shot Rising Return to Zero - One Shot Falling - One Shot Falling Return to Zero
HDLC Encoder:	Bitwise Data reflection FCS reflection & swap FCS Modes - Off - 16 bit CCITT - 16 bit 8408 (Reflected 1021)

4. DOWNLINK (TELEMETRY)

4.1 ANALOG INTERFACES

Description	Specification
RF Frequency Range:	50 MHz to 2500 MHz
RF Tuning Step Size:	0.1 Hz
RF Input Power Levels:	-60 dBm to 0 dBm
RF Connector Type:	SMA
A/D Resolution	Selectable from 4 through 12 bits.

Instantaneous Bandwidth:	125 kHz to 10 MHz[4]
Number of Receive Channels:	1

4.2 RECEIVER SPECIFICATIONS

Description	Specification
Number of Receive Channels:	1
Direct Demodulation Types:	BPSK QPSK DQPSK (Normal / Alternate) OQPSK 8PSK FSK MSK GMSK SOQPSK_TG PCM PM PCM FM
Symbol Rate:	7 sps to 5 Msps[5]
Mod Index (PM):	0.0 to 3.0 Radians
Frequency Deviation (FM):	0 to 4 MHz
Match Filter:	None Raised Cosine Root Raised Cosine
Match Filter Rolloffs:	User Defined from 0% to 100%
Number of Subcarrier Channels:	2
Subcarrier Types:	Sine Square
Subcarrier Minimum IF/RF Freq.:	1 kHz
Subcarrier Maximum IF/RF Freq.:	Limited by bandwidth
PCM Decoding:	NRZ-L,M,S Biϕ-L,M,S D-Biϕ-L,M,S
Dual PCM Decoders:	Supported

[4] The instantaneous bandwidth of the SpectralNet Lite device for *RF transport* is 54 MHz. The quantumRadio supports processing a maximum of 10 MHz of instantaneous bandwidth. When using the SpectralNet Lite as the front end for quantumRadio, the instantaneous bandwidth is limited to quantumRadio's maximum instantaneous bandwidth (10 MHz.).

[5] Max rate assumes a bandwidth of 10MHz > 5 Msps @ 8PSK > 15 Mbps and that they data is unencoded.

Viterbi Decoding	Rate = ½, ¾ (K=7) CCSDS Polynomial - G1=1111001 - G2=1011011 G1 / G2 Invert Support Reverse order mode (G1 / G2 output order is reversed) Bypass mode supported
Dual Viterbi Decoders:	Supported
De-Randomizer Coding Type:	Polynomial ($x^{17} + x^{12} + 1$)
Cadet Radio:	Support includes; • TPC with/without Parity • Whitener • User definable Frame Sync
Data Source(s):	Internal BERT Network File Player
Auto Rate Detect:	Support for up to 4 bit rates[6]

5. MISC.

5.1 SPECTRALNET LITE

5.1.1 Network

Description	Specification
Network Transport:	2 RJ45 connectors (1 Gb Ethernet) • (1) for Management Port • (1) for Data Port
Network Data Format:	ANSI VITA-49.0 IF data and context packets

5.1.2 Reference Signals

Description	Specification
Reference Signals:[7]	IRIG-B 1PPS 10MHz
Reference Connector Type:	BNC
Reference signals required	No

[6] Does not support rates which are multiples of one another (i.e. 10kbps, 100kbps, etc.).
[7] Reference signals are inputs. The quantum system does not have the ability to generated reference signals.

D. RUS-4 SPECIFICATIONS

Section D contains RUS-4 specifications provided by the manufacturer in [22].

AMERGINT

satTRAC SL/1200 Hardware Specifications

RF Output	Specification
Number of Output Channels	1
Frequency Ranges:	
SGLS Up	1750 to 1850 MHz
USB Up	2025 to 2120 MHz
1200 MHz	1150 to 1250 MHz
Test (unfiltered)[1]	1690 to 2400 MHz or 950 to 1450 MHz
Output Power Range	-30 to +10 dBm
P1dB	+26 dBm (S/L) +16 dBm (1200 MHz)
Output Power Accuracy	+/-0.5 dB
Instantaneous Dynamic Range	80 dB
Noise Power Density	-135 dBm/Hz max (S/L) -123 dBm/Hz max (1200 MHz)
Output VSWR	1.3: 1
Output Impedance (nominal)	50 Ohms
Gain Adjustment	60 dB in 0.1 dB Steps
Instantaneous Bandwidth	> 40 MHz (at S/L) > 100 MHz (at 1200 MHz)
Tuning Step Size	< 1 µHz
Output Spurious	< -65 dBc with output power -15 to +10 dBm
Output Spurious with Analog Video I/O Enabled	< -55 dBc with output power -15 to +10 dBm
Frequency Stability and Aging (using internal reference)	+/- 5 ppb over operating temp range, < +/- 100 ppb/yr
Amplitude Response (Flatness)	+/- 0.2dB over 4 MHz
Phase Noise	
10 Hz	-60 dBc/Hz
100 Hz	-80 dBc/Hz
1 kHz	-90 dBc/Hz
10 kHz	-95 dBc/Hz
100 kHz	-97 dBc/Hz
1 MHz	-115 dBc/Hz
10 MHz	-124 dBc/Hz
100 MHz	-136 dBc/Hz

[1] Unfiltered outputs do not meet the output spurious, VSWR and flatness performance specifications.

RF Input	Specification
Number of Input Channels	2
Frequency Ranges:	
SGLS/USB Down	2200 to 2300 MHz
1200 MHz	1150 to 1250 MHz
Test/Echo (unfiltered)[1]	1690 to 2400 MHz or 950 to 1450 MHz
Operational Input Power Range	-100 to -23 dBm
Maximum Input Signal (damage)	+18 dBm
Instantaneous Dynamic Range	> 74 dB
Noise Figure (at max gain)	< 4 dB typical, 8 dB max
Input VSWR	1.3: 1
Input Impedance (nominal)	50 Ohms
AGC (50 dB range) Time Constant	0.001 to 1 seconds
Instantaneous Bandwidth	> 40 MHz (at S/L) > 100 MHz (at 1200 MHz)
Tuning Step Size	< 1 µHz
In-Band Spurious	< -59 dBc
Amplitude Response (flatness)	+/- 0.2dB over 4MHz

Timing and Reference Signals	Specification
Frequency Reference	10 MHz
Internal Frequency Reference Accuracy	< 0.1 ppm
External Frequency Reference Input	
Level Range	-10 to +10 dBm
Impedance	50 Ohms
Phase-Lock Frequency Range	+/-5 Hz
Spurious	-60 dBc max
Phase Noise at Offset ≥ 10 Hz	-86 dBc/Hz max
Time References Supported	IRIG-B, 1PPS, NTP
Time Reference Voltage Levels (for IRIG and 1PPS)	0.3 to 5 V peak-to-peak
Time Reference Impedance (for IRIG and 1PPS)	10K Ohms

Analog Video I/O	Specification
Video Input & Output Channels	2 In, 2 Out
Video Bandwidth	7.5 MHz
Input/Output Impedance	50 Ohms

Environmental Information	Specification
Server Temperature (Operating)	-5°C to 40°C
Server Temperature (Storage)	-40°C to 65°C
Server Relative Humidity	5% to 95% non-condensing
satTRAC-SL Temperature (Operating)	-5°C to 45°C
satTRAC-SL Temperature (Storage)	-40°C to 65°C
satTRAC-SL Relative Humidity	5% to 90% non-condensing

Physical Information	Specification
Weight	< 65 lbs
Server Dimensions	3.4 H x 19 W x 25.5 D (in)
satTRAC Dimensions	1.75 H x 17.1 W x 15 D (in)
Power Requirements	+12 V DC at 6 Amps max

- **Spectral Purity:** High compression points and multi-rate digital filtering insure NTIA compliance. That means < -65 dBc.
- **Noise Figure (Receiver):** The noise figure targets high performance test and measurement applications, exceeding most ground station needs.
- **Implementation Loss (BER):** The measured implementation loss for satTRAC is well below 0.7 dB across a typical Eb/N0 range, often within 0.25 dB of theory.
- **Output Power Range:** satTRAC's outputs have an accuracy of better than 0.5 dB over the output power range and over the specified temperature range.
- **Dynamic Range:** An instantaneous dynamic range of 80 dB enables multi-carrier reception on a single RF/IF input.

E. HP 346B NOISE SOURCE SPECIFICATIONS

Section E contains specifications regarding the HP 346B calibrated noise source provided by the manufacturer in [29].

General Specifications

Specifications

The specifications in Table 3-1 are performance standards or limits against which the noise source may be tested. These specifications for the noise source when used with a Noise Figure Analyzer are ONLY valid if the analyzer has been allowed to meet its specified warm up time of 60 minutes.

ENR expanded uncertainty analysis and supplemental characteristics are not specifications but are typical characteristics included as additional information.

Table 3-1 346A/B/C specifications

Specification	346A	346B	346C
Frequency range	10 MHz to 18 GHz	10 MHz to 18 GHz	10 MHz to 26.5 GHz
Operating temperature	0 °C to 55 °C	0 °C to 55 °C	0 °C to 55 °C
Excess Noise Ratio (ENR) range[a]	4.5 to 6.5 dB	14 to 16 dB	12 to 17 dB
Maximum Standing Wave Ratio (SWR) [for source ON/OFF states]	<1.3:1 (0.01 to 0.03 GHz) <1.15:1 (0.03 to 5.0 GHz) <1.25:1 (5.0 to 18.0 GHz)	<1.3:1 (0.01 to 0.03 GHz) <1.15:1 (0.03 to 5.0 GHz) <1.25:1 (5.0 to 18.0 GHz)	<1.25:1 (0.01 to 18.0 GHz) <1.35:1 (18.0 to 26.5 GHz)
Reflection Coefficient (Rho) (r) [for source ON/OFF states][b]	0.13 (0.01 to 0.03 GHz) 0.07 (0.03 to 5.0 GHz) 0.11 (5.0 to 18.0 GHz)	0.13 (0.01 to 0.03 GHz) 0.07 (0.03 to 5.0 GHz) 0.11 (5.0 to 18.0 GHz)	0.11 (0.01 to 18.0 GHz) 0.15 (18.0 to 26.5 GHz)
Impedance	50 Ω nominal	50 Ω nominal	50 Ω nominal
Maximum reverse power	1 watt	1 watt	1 watt
Power required	28 ±1 V (60 mA peak, 30 mA average for source ON)	28 ±1 V (60 mA peak, 30 mA average for source ON)	28 ±1 V (45 mA)
Connectors[c]	Output: APC-3.5 (male) standard[d] Input: Bias: BNC (f)	Output: APC-3.5 (male) standard[d] Input: Bias: BNC (f)	Output: APC-3.5 (male) standard[d] Input: Bias: BNC (f)

F. AMPLIFIER RESEARCH LN1G11 LOW NOISE PRE-AMPLIFIER SPECIFICATION

Section F contains specifications regarding the LN1G11 Low Noise Pre-amplifier provided by the manufacturer in [30].

rf/microwave instrumentation

Model LN1G11,
M1 through M3
Low Noise Pre-Amp
1GHz–11GHz

The Model LN1G11 is a broadband, self-contained linear amplifier for laboratory applications requiring instantaneous bandwidth and low noise.

The LN1G11 is useful for amplifying low level signals to more useful levels for driving power amplifiers and other similar applications. In addition, with its low noise figure it can be used to increase the sensitivity of receivers with relatively high noise figures.

The LN1G11 contains an internal power supply which automatically adjusts for the AC input voltage. The AC input connector is an IEC 320 type located on the rear panel

The LN1G11 can be supplied in a benchtop cabinet with the RF connectors located on the front panel or the rear panel. The LN1G11 can also be supplied without the cabinet for rack mounting, front or rear RF connectors.

SPECIFICATIONS

POWER OUTPUT.....+10 dBm at less than 1 dB gain compression

FREQUENCY RESPONSE.....1.0–11.0 GHz

INPUT FOR RATED OUTPUT .....–16 dBm maximum

GAIN.....27 dB minimum

GAIN FLATNESS.....±1.5 dB

NOISE FIGURE.....6.5 dB typical

INPUT IMPEDANCE .....50 ohms, VSWR 2.5:1 maximum

OUTPUT IMPEDANCE.....50 ohms, VSWR 2.5:1 maximum

MISMATCH TOLERANCE .....100%, will operate without damage, foldback or oscillation with any magnitude and phase of source and load impedance.

MODULATION CAPABILITY .....Will faithfully reproduce AM, FM, or pulse modulation appearing on the input signal

HARMONIC DISTORTION .....–20 dBc maximum at +10 dBm output

THIRD ORDER INTERCEPT POINT.....+20 dBm typical

PRIMARY POWER (selected automatically) .....100–240 VAC, 50/60 Hz with an IEC 320 AC input connector

MODEL CONFIGURATIONS

MODEL	CONNECTORS	STYLE	SIZE (W x H x D)	WEIGHT
LN1G11	N Front	Benchtop	26.0 x 11.7 x 21.6 cm 10.3 x 4.6 x 8.5 in	4.5 kg, 10.0 lbs
LN1G11M1	N Rear	Benchtop	26.0 x 11.7 x 21.6 cm 10.3 x 4.6 x 8.5 in	4.5 kg, 10.0 lbs
LN1G11M2	N Front	Rack mount	24.1 x 8.9 x 20.3 cm 9.5 x 3.5 x 8.0 in	1.8 kg, 4.0 lbs
LN1G11M3	N Rear	Rack mount	24.1 x 8.9 x 20.3 cm 9.5 x 3.5 x 8.0 in	1.8 kg, 4.0 lbs

G. MINI-CIRCUITS ZX10-2-42-S+ POWER SPLITTER/COMBINER SPECIFICATIONS

Section G contains specifications regarding the ZX10-2-42-S+ power splitter/combiner provided by the manufacturer in [27].

Outline Dimensions (inch / mm)

A	B	C	D	E	F	G
.74	.90	.54	.50	.04	.16	.29
18.80	22.86	13.72	12.70	1.02	4.06	7.37

H	J	K	L	M	N	wt
.37	--	.122	.496	.106	.122	grams
9.40	--	3.10	12.60	2.69	3.10	20.0

2040.00	3.42	3.44	0.02	13.42	0.71	1.71	1.09	1.08
2180.00	3.37	3.38	0.01	14.64	0.74	1.62	1.10	1.09
2460.00	3.26	3.26	0.01	17.92	0.91	1.47	1.09	1.08
2600.00	3.19	3.19	0.00	20.16	1.05	1.39	1.08	1.08
2760.00	3.19	3.18	0.01	23.86	1.02	1.26	1.05	1.05
2920.00	3.10	3.12	0.02	27.75	1.18	1.14	1.02	1.03
3240.00	3.11	3.11	0.00	23.53	1.50	1.07	1.03	1.02
3400.00	3.13	3.16	0.03	20.10	1.54	1.19	1.05	1.10
3540.00	3.23	3.27	0.04	17.91	1.30	1.31	1.07	1.05
3680.00	3.26	3.29	0.03	16.12	1.55	1.40	1.07	1.08
3820.00	3.31	3.36	0.05	14.58	1.52	1.51	1.09	1.08
4100.00	3.48	3.52	0.03	12.21	1.48	1.78	1.15	1.15
4150.00	3.54	3.58	0.04	11.90	1.37	1.83	1.16	1.16
4200.00	3.52	3.55	0.03	11.51	1.50	1.87	1.17	1.18

1. Total Loss = Insertion Loss + 3dB splitter loss.

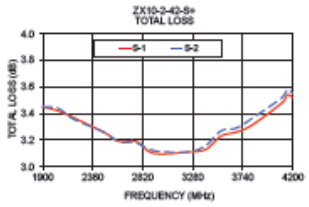

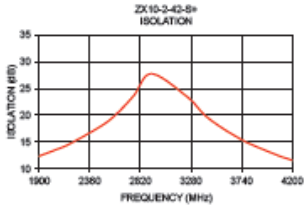

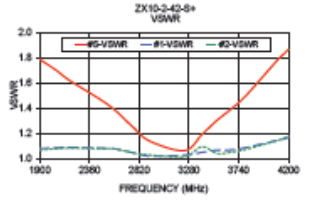

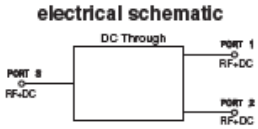

Notes
A. Performance and quality attributes and conditions not expressly stated in this specification document are intended to be excluded and do not form a part of this specification document.
B. Electrical specifications and performance data contained in this specification document are based on Mini-Circuit's applicable established test performance criteria and measurement instructions.
C. The parts covered by this specification document are subject to Mini-Circuits standard limited warranty and terms and conditions (collectively, "Standard Terms"); Purchasers of this part are entitled to the rights and benefits contained therein. For a full statement of the Standard Terms and the exclusive rights and remedies thereunder, please visit Mini-Circuits' website at www.minicircuits.com/MCLStore/terms.jsp

Mini-Circuits®
www.minicircuits.com P.O. Box 350166, Brooklyn, NY 11235-0003 (718) 934-4500 sales@minicircuits.com

REV.M
M171494
ZX10-2-42-S+
ED-10281/2
HY/RS/CP/AM
161217
Page 1 of 1

LIST OF REFERENCES

[1] J. R. Wertz, D. F. Everett and J. J. Puschell, *Space Mission Engineering: The New SMAD*, Hawthorne, CA: Microcosm Press, 2011.

[2] E. Mabrouk, "What are SmallSats and CubeSats?", NASA, 2017. Accessed September 24, 2019. [Online]. Available: https://www.nasa.gov/content/what-are-smallsats-and-cubesats

[3] J. Heyman, "FOCUS: CubeSats—A costing pricing challenge," *SatMagazine*, Oct-2009. Accessed November 22, 2019. [Online]. Available: http://www.satmagazine.com/story.php?number=602922274

[4] Under Secretary of Defense, Acquisition, Technology, and Logistics, "Performance of the Defense Acquisition System, 2016 annual report," Washington, DC, USA, United States, 2016. [Online]. Available: https://apps.dtic.mil/dtic/tr/fulltext/u2/1019605.pdf

[5] G. Minelli, L. Magallanes, N. Weitz, D. Rigmaiden, J. Horning and J. Newman, "The mobile cubeSat command and control (MC3) ground station network: An overview and look ahead", presented at the 33rd Annual AIAA/USU Conference on Small Satellites, Logan, UT, USA, 7 Aug 2019.

[6] *Nomenclature of the Frequency and Wavelength Bands Used in Telecommunications*," ITU-R Recommendation V.431-8, August 2015. [Online]. Available: https://www.itu.int/dms_pubrec/itu-r/rec/v/R-REC-V.431-8-201508-I!!PDF-E.pdf

[7] E. Grayver, *Implementing Software Defined Radio*, 2013th ed., New York, NY, USA: Springer, 2013.

[8] C. J. Prust, "Laboratory 1: introduction to software-defined radio communications systems laboratory,"Electrical Engineering and Computer Science Department, Milwaukee School of Engineering, Milwaukee, WI, USA September 2019. [Online]. Available: https://faculty-web.msoe.edu/prust/EE4022/Lab01.pdf

[9] A. B. Carlson, *Communication Systems: An Introduction to Signals and Noise in Electrical Communication.* 2nd ed. New York, NY, USA: McGraw-Hill, 1975.

[10] J. G. Proakis, *Digital Communications*, 4th ed., Boston, MA, USA: McGraw-Hill, 2001.

[11] R. Keim, A. White, O. Hoilett, and Texas Instruments, "Active components in RF circuits," *All About Circuits*, 2017. Accessed October 3, 2019. [Online]. Available: https://www.allaboutcircuits.com/textbook/radio-frequency-analysis-design/rf-principles-components/active-components-in-rf-circuits/

[12] W. H. W. Tuttlebee, *Software Defined Radio: Enabling Technologies.* New York, NY, USA: J. Wiley & Sons, 2002.

[13] T. F. Collins, R. Getz, D. Pu, and A. M. Wyglinski, *Software-defined radio for engineers*. Norwood, MA, USA: Artech House, 2018.

[14] D. L. Adamy, *EW 102: A Second Course in Electronic Warfare*, Boston, MA, USA: Artech House, 2006.

[15] National Instruments, *USRP-2922 Specifications,* 2017. [Online]. Available: https://www.ni.com/pdf/manuals/375868c.pdf

[16] GNU Radio Project, "About GNU Radio". Accessed March 30, 2020 [Online]. Available: https://www.gnuradio.org/about/

[17] National Instruments, *USRP Software Defined Radios,* 2019. [Online]. Available: http://www.ni.com/pdf/product-flyers/usrp-software-defined-radio.pdf

[18] Ettus Research, *USRP B205mini-i,* 2020. [Online]. Available: https://www.ettus.com/

[19] M. B. Matthews, "Laboratory 12 – radio study", Space Systems Academic Group, Naval Postgraduate School, Monterey, CA, USA, 2020.

[20] Kratos Defense and Security Solutions, *quantum quickStart Guide*, Version 2.0, Real Time Logic Corporation, June 2018.

[21] Kratos, *Software Modem quantumRadio*, DS-274. [Online]. Available: https://www.kratosdefense.com/-/media/datasheets/rtl-dst_qradio.pdf

[22] AMERGINT Technologies., *Modem/Baseband Unit User Guide*, Delivered media, Document Number: AT-satTRAC-F0507-USR-AT-19-AT-1586, Version: 1.0, October 2019.

[23] AMERGINT Technologies, *Signal, Network, and Data Processing*, 2019. [Online]. Available: https://www.amergint.com/products/

[24] J. Wilmot, "Using CCSDS Standards to Reduce Mission Costs," in 31st Annual AIAA/USU Small Satellite Conference 2017, Aug. 5, 2017. [Online]. doi: https://ntrs.nasa.gov/archive/nasa/casi.ntrs.nasa.gov/20170007440.pdf

[25] AMERGINT Technologies, *AMERGINT WANFEC Ground Technology and Info to Meet Laser Communications Requirements*, 2017 [Online]. Available: https://www.nasa.gov/sites/default/files/atoms/files/06_amergint_ground_technology_for_laser_comm_requirements.pdf

[26] TestWorld, *Keysight (Agilent) N5171B RF Analog Signal Generator, up to 6 GHz*, [Online]. Available: https://testworld.com/used-electronic-test-equipment/manufacturers/keysight-agilent/keysight-agilent-signal-generators/exg-series/keysight-agilent-n5171b-rf-analog-signal-generator-6-ghz.

[27] Mini-Circuits, *ZX10-2-42-S+*, 2017. [Online]. Available: https://www.minicircuits.com/WebStore/dashboard.html?model=ZX10-2-42-S%2B

[28] R. Hosking, "VITA 49 Radio Transport: The new software radio protocol," Accessed May 12, 2020. [Online]. Available: http://vita.mil-embedded.com/articles/vita-radio-software-radio-protocol/

[29] Agilent, *Agilent 346A/B/C noise source*, 2018. [Online]. Available: https://literature.cdn.keysight.com/litweb/pdf/00346-90148.pdf

[30] Amplifier Research, *Model LN1G11, M1 through M3 Low Noise Pre-Amp 1GHz–11GHz*. [Online]. Available https://www.arworld.us/post/LN1G11.pdf

THIS PAGE INTENTIONALLY LEFT BLANK

INITIAL DISTRIBUTION LIST

1. Defense Technical Information Center
   Ft. Belvoir, Virginia

2. Dudley Knox Library
   Naval Postgraduate School
   Monterey, California